Technische Universität München
Fakultät für Medizin

Microtubule-associated protein tau gene as risk factor for the sporadic
Parkinson syndrome
- A postmortem brain study in Parkinson´s disease and control

Christina Victoria Isabella Tauber

Vollständiger Abdruck der von der Fakultät für Medizin der Technischen
Universität München zur Erlangung einer Doktorin der Medizinischen
Wissenschaft (Dr. med. sci.) genehmigten Dissertation.

Vorsitz: Prof. Dr. Angelika Harbauer

Prüfer der Dissertation:

1. Prof. Dr. Stefan Lichtenthaler

2. Prof. Dr. Paul Lingor

Die Dissertation wurde am 18.01.2023 bei der Technischen Universität
München eingereicht und durch die Fakultät für Medizin am 14.06.2023
angenommen.

Abstract

Background: "The *MAPT* gene, encoding the microtubule-associated protein tau, is part of a 952 kb haplotype block on chromosome 17q21.31, which is subject to an inversion polymorphism, leading to two allelic variants, called H1 and H2 haplotypes. Homozygosity for the more common haplotype H1 is associated with an increased risk for several tauopathies, but also for the synucleinopathy Parkinson's disease (PD). The present study aimed to clarify whether the *MAPT* haplotype influences gene expression of tau on mRNA and protein levels in postmortem brains of PD patients and controls. We also investigated mRNA expression levels of several other *MAPT* haplotype-encoded genes. Additionally, we assessed the expression of *SNCA* on chromosome 4, endoding the protein α-synuclein (α-syn).

Methods: Postmortem tissues from cortex of fusiform gyrus (ctx-fg) and of the cerebellar hemisphere (ctx-cbl) of neuropathologically confirmed PD patients (n = 14) and age- and sex-matched controls (n = 12) without neurodegenerative diseases were genotyped for the *MAPT* haplotype to identify cases homozygous for either H1 or H2. Relative expression of genes within the *MAPT* inversion region was quantified using real-time RT-qPCR. Soluble and insoluble protein levels of tau and α-syn were determined by Western blotting.

Results: H1 homozygosity was associated with increased *total MAPT* mRNA expression in ctx-fg in both PD and controls. H2 homozygosity was associated with increased expression of *MAPT-AS1* in the ctx-cbl, as well as incresesd *KANSL1* and *KANSL1-AS1* mRNA in both brain regions. PD patients had higher levels of insoluble 0N3R and 1N4R tau isoforms and also of insoluble α-syn in the gyrus fusiformis, regardless of the *MAPT* genotype.

Conclusion: The increased presence of insoluble α-syn protein in PD donors in gyrus fusiformis validated the selected postmortem brain tissue. Our findings in this small, but well controlled cohort of PD and controls demonstrated that patients also had higher insoluble 0N3R and 1N4R tau levels in the ctx-fg, supporting a putatibe biological relevance of tau in PD. The total *MAPT* mRNA expression was increased in the disease-predisposing H1/H1 condition, regardless of the actual disease status. Associated with disease-protective H2/H2 condition, the long non-coding antisense *MAPT-AS1* was increased, and thus, might to be an interesting candidate for future therapeutic or preventive concepts" [1].

Table of contents

List of figures

List of tables

Abbreviations

α-syn	α-synuclein
AD	Alzheimer's disease
bp	Base pairs
CBD	Corticobasal degeneration
cDNA	Complementary DNA
CERAD	The Consortium to Establish a Register for Alzheimer´s Disease
DEPC water	Diethyl pyrocarbonate treated water
DNA	Deoxyribonucleic acid
EDTA	Ethylendiamintetraacetat
g	Gravity
gDNA	Genomic DNA
LB	Lewy Bodies
L-Dopa	Levodopa
Luhmes cells	Lund human mesencephalic cells
min	Minute
PCR	Polymerase chain reaction
PD	Parkinson´s disease
PMI	Postmortem interval
PSP	Progressive supranuclear palsy
qPCR	Quantitative polymerase chain reaction
RIN	RNA Integrity Number
RIPA	Radioimmunoprecipitation Assay
RT	Room temperature
s	Seconds
SDS	Sodium dodecyl sulfate
SN	Substantia nigra
SNPs	Single nucleotide polymorphism

Declaration and publication

Partial results of the presented thesis have been submitted for publication:

Christina V. Tauber, Sigrid C. Schwarz, Thomas W. Rösler, Thomas Arzberger, Steve Gentleman, Günter U. Höglinger, et al. (2022). Different *MAPT* haplotyes influence expression of total *MAPT* in postmortem human brain.

Submission as original article at Acta neuropathologica communications (24th December 2022). Revision with minor changes (10th February 2023).

It is hereby noted that sections of this thesis have been taken from the submitted publication (i.e., in the chapters Introduction, Materials and Methods, Tables, Figures, Results, and Discussion). The relevant passages have been correctly cited and referenced.

Introduction

1.1 The sporadic Parkinson syndrome

1.1.1 Epidemiology

Parkinson's disease (PD) is the second most common neurodegenerative disease after Alzheimer's disease (AD) [1, 2]. With an estimated prevalence rate from 100 to 200 per 100.000 inhabitants, PD affects worldwide more than 6 million people [3]. Due to population ageing and improved survival under therapy, the number of patients is expected to double over the next 30 years [4]. Regarding the increasing global burden of the disease and limited therapy options, PD is in the spotlight of present medical research.

1.1.2 Classification

Parkinsonism is classified in four etiologies: sporadic, genetic, secondary and atypical Parkinson syndromes. The vast majority of cases occur sporadically without apparent family history primarily in elderly people with unknown etiology [5]. Monogenic mutations with autosomal dominant and recessive forms often lead to symptoms at a younger age and explain only 5-10% of all cases [6]. Culprits for secondary Parkinson syndromes are dopamine antagonizing medications (i.e. classic neuroleptics, lithium, antiemetics), toxins, or inflammatory pathologies. The term atypical Parkinson syndrome describes several neurodegenerative conditions which all have in common to present with a spectrum of Parkinsonism signs without responding well to standard dopamine drug treatment [7].

1.1.3 Clinical features and diagnosis

For the clinical diagnosis of Parkinsonism, the presence of bradykinesia is required along with one of the cardinal signs rigidity, resting tremor or postural instability [8]. On examination, further signs may be present like a masked face, reduced arm swing, short stepped gait or pill-rolling tremor. Typically, symptoms start and progress asymmetrically with affecting gait and balance in later disease stages [9]. Based on the presented symptoms, different phenotypes of PD can be classified of which the tremor-dominant form is beneficial for disease progression and survival rate [10]. In addition, a variety of non-motor symptoms can occur which manifest as sensory disorder (pain, anosmia), autonomic dysfunction (bladder dysfunction, orthostatic hypotension), sleep disorder or neuropsychiatric symptoms. Especially depression, anosmia and rapid eye movement sleep behavior can precede the disease onset as prodromal symptoms by several years [11, 12]. In the long term, patients face severe disability, dementia in 80% of cases [13], and a decreased life expectancy compared to the general population [14, 15].

Surrogate biomarkers will contribute to an early diagnosis, prediction of disease progress and differential diagnosis [16] So far, numerous candidate biomarkers were identified related to abnormal protein accumulation, oxidative stress or neuroinflammatory reaction [17-20]. However to date, a definite confirmation of Parkinsonism remains to be obtained postmortem through neuropathology assessment. Studies revealed that up to 20 percent of patients diagnosed with PD during their lifetime suffered from a Parkinson syndrome other than sporadic PD [21]. This highlights the importance of the neuropathology assessment for an accurate etiologic classification.

1.1.4   Neuropathology

The major neuropathological hallmarks of PD are the loss of dopaminergic neurons in the pars compacta of substantia nigra (SN) and the accumulation of cytoplasmic inclusions, so-called Lewy Bodies (LB). LB are found diffusely throughout the brain in cell somata and are composed primarily of the protein α-synuclein (α-syn) [22]. Inclusion bodies located in neuronal cell processes are termed Lewy neurites [23, 24]. According to the systematic histopathological studies by Braak [25], PD can be divided into six stages. Each stage is defined by a characteristic distribution of structural and pathological changes: Before the appearance of clinically manifest motor symptoms (stages 1 and 2), the pathological changes are limited to the autonomic nervous system, the medulla oblongata and the bulbus olfactorius. In stages 3 and 4, the classic motor symptoms manifest themselves, whereby the substantia nigra and other core regions of the midbrain, and the basal forebrain, are now additionally affected. In stages 5 and 6, large parts of the telencephalon are pathologically altered and there are multiple impairments of higher brain functions. There is strong evidence that the disease may begin in the peripheral autonomic nervous system [26-29]. According to the gut-brain-axis hypothesis, an external trigger induces LB pathology which spreads through cell-to-cell-transmission via the vagus nerve and olfactory bulb to the upper central nervous system [30, 31].

1.1.5   Synucleinopathy and α-syn

Neurodegenerative diseases associated with aggregation and deposition of the protein α-synuclein are termed synucleinopathies. PD is the synucleinopathy with the highest prevalence. [32] α-syn is an abundant protein expressed mainly in presynaptic terminals of neurons of most types. The physiological function of α-syn is not fully understood and appears to be very diverse. Described cellular functions of α-syn include for instance neurotransmitter release, dopamine homeostasis and vesicle transport [33]. The secondary structure of a-synuclein is variable. Under physiological conditions dissolved and membrane-bound α-syn is balanced in an equilibrium [34]. Under pathological conditions α-syn adopts a ß-sheet structure [35] forming aggregates that are classified into oligomers,

fibrils and LB based on their structure and size [36]. It is assumed that the neurotoxic properties of α-syn are based on these structural changes. Due to its capacity of spreading from cell to cell, it has been hypothesized that PD pathology can propagate in a prion-like manner to surrounding cells in the form of α-syn seeds [37]. However, it is still under debate whether LB itself cause cell death or are the result of means of cell protection [9, 23, 38, 39]. Besides α-syn accumulation, various impairments in cell components have been detected in PD pathology such as mitochondrial dysfunction [37].

1.1.6   Pathophysiology

The core pathophysiology of PD is explained by the dopaminergic neurotransmitter deficiency in the SN (pars compacta) and the subsequent dysfunction of the basal ganglia. At the time of clinical manifestation up to 30-70% of dopaminergic cells in the nigro-striatal system are estimated to be lost [40]. The basal ganglia contain several nuclei in the diencephalon (nucleus subthalamicus), telencephalon (corpus striatum) and mesencephalon (SN pars compacta and reticularis). As functional unit, the basal ganglia are decisive for the modulation of movement. In general, movement is initiated in the primary motor cortex with involvement of supplementary motor cortex areas. After several circuitry loops for fine adjustment by the basal ganglia, the executive neuronal output is projected to several spinal tracts to address muscle groups respectively [9]. Due to the loss of nigrostriatal projections the basal ganglia tend to inhibit cortically generated movements which explain the clinically observed motor symptoms [41]. Additionally, the loss of non-dopaminergic pathways leads to the development of non-motor symptoms [42, 43].

1.1.7   Therapy

To this day, therapies are restricted to symptomatic treatment only and can not stop the disease progression. The basic principle is to compensate for the deficit of dopamine through substitution, dopamine receptor agonists and degradation inhibitors [44]. Standard therapy for the replacement of dopamine is the administration of its precursor Levodopa (L-Dopa) capable of passing the blood-brain-barrier. After 5-10 years on average, severe side effects such as wearing off, on-off-phases or dyskinesia occur [2]. If the medical treatment failed, some patients benefit from invasive therapies [45]. With less dopaminergic neurons in the SN, other brain regions like the nucleus subthalamicus become relatively overactive. The procedure of deep brain stimulation corrects this imbalance through implanted pacemakers using high-frequency electrical currents. However, only 1% of PD patients are suitable for this treatment due to stimulus-based side effects [46]. Of great importance is also the treatment of non - motor symptoms as they can impair quality of life more than the motor symptoms itself in some patients [9].

1.1.8   Environmental and genetic risk factors

It is assumed that a combination of environmental and genetic factors lead to the manifestation of sporadic PD [47]. The largest risk factors are age, followed by family history and sex. In a retrospective cohort study, having at least one first-degree relative with PD is associated with a 2.8-times higher risk for the disease [48]. A recent longitudinal twin study prompted a modest heritability for PD [49]. Prevalence in men is higher than in women with a ratio of 1.5 to 1.0 [2]. There is conflicting data about the prevalence of PD among different ethnicities, but PD seems to be less frequent in people of African or Asian descent [2, 50]. Considering environmental factors, exposure to toxins (pesticides, herbicides or metals) increase the risk for PD, while smoking and drinking coffee are associated with reduced risk [51].

In the past two decades, genome-wide association studies (GWAS) have identified genetic susceptibility loci that confer the risk for sporadic PD [5]. In general, genes contain common variations which are defined as single-nucleotide-polymorphisms (SNPs), if their frequencies are > 1% in a population [52]. The effects of several risk variations in different gene loci with minor to moderate influence might combine leading to the development of sporadic PD. The strongest genetic associations are common variations at the SNCA gene, encoding α-syn -syn, followed by variations at *MAPT*, encoding for the microtubule-associated protein tau [53-58].

1.2   The gene *MAPT* as risk factor for the sporadic Parkinson syndrome

1.2.1   The tau protein

Tau is primarily expressed in the central nervous system stabilizing the neuronal cytoskeleton and regulating axonal transport processes [59-62]. Six tau isoforms are present in the human brain, which differ by expression of either 3 or 4 microtubule binding repeat domains (termed 3R or 4R isoforms) and the number of N-terminal inserts (termed 0N, 1N, 2N isoforms) (**Fig 1**) [1, 63]. Tau isoforms emerge either through cassette splicing of exon 2 and 3 (N-terminal) or alternative splicing of exon 10 (R-terminal).

Post-translational modifications such as hyperphosphorylation lower the binding affinity of tau to microtubule. The subsequently increased aggregation property leads to pathologic tau inclusions which are able to propagate throughout the brain trans-synaptically [64, 65]. Pathologic aggregates containing hyperphosphorylated tau protein do occur within the brain in a variety of neurodegenerative diseases, including AD, corticobasal degeneration (CBD) or progressive supranuclear palsy (PSP), which are therefore jointly referred to as tauopathies [1, 66]. The latter diseases CBD and PSP are clinically

referred to as atypical Parkinson syndromes [67]. Levels of 3R and 4R tau are regulated in the adult human brain with a ratio of 1:1. Whereas in many neurodegenerative conditions, tau appears insoluble and assembled with 3R and 4R tau levels out of balance [63, 68]. Through an excess of 4R tau PSP and CBD are labelled as 4R tauopathy, Pick´s disease as 3R tauopathy, whereas AD is characterized by a balanced ratio [69, 70].

The N-terminal region of tau has been shown to be involved in solubility and folding by inhibiting tau polymerization [71], and stabilizing tau in a folded state [72]. It is fundamental to note that the number of microtubule-binding repeat domains in the carboxy-terminal of tau have distinct properties. Compared to 3R tau, 4R tau regulates microtubule dynamics more efficient, binds to microtubule with a greater affinity [73] and is more prone to aggregation [66]. Recently, it has been suggested that tau isoform imbalance itself might be detrimental regardless which R-isoform is overexpressed [74]. Still, the involvement of the N-terminus and R- terminus in tau function are complex and more studies will be required to understand the effect of differential expression of tau isoforms on tau- protein itself, microtubule stabilization and potential interaction with α-syn.
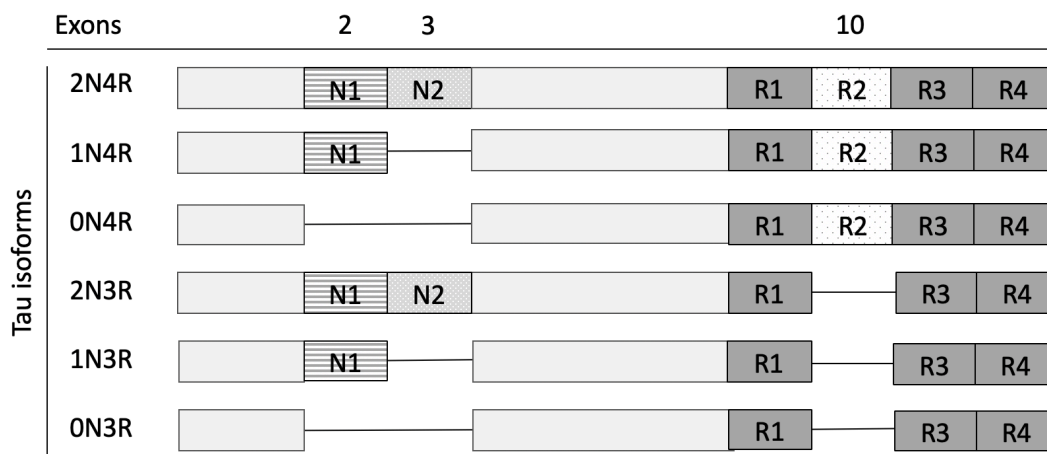
Figure 1. The six tau isoforms after splicing of exon 2,3 and exon 10. Modified from Park,2016.

1.2.2 The gene *MAPT* and its haplotypes

"The *MAPT* gene encoding tau is located within a 952 kb haplotype bloc on chromosome 17q21.31, which is subject to an inversion polymorphism, leading to two allelic variants, called H1 and H2 haplotypes [75, 76] (**Fig 2**) " [1]. The haplotypes differ through 14 SNPs which are specific for the H1 clade, while the H2/H2 haplotype is mainly preserved [77]. Above that, a variety of SNPs mark specific subhaplotypes of H1/H1 [78]. The *MAPT* haplotypes have been associated with different neurodegenerative conditions. Inherited mutations in *MAPT* are linked to frontotemporal dementia and Parkinsonsim linked to chromosome 17 [79].

"H1 homozygosity (H1/H1) is more common, with varying frequency across human populations [80], and associated with an increased risk for neurodegenerative tauopathies AD, PSP and CBD [81-85], but

surprisingly also for the synucleinopathy PD [55, 57, 77, 86-88]. In contrast, H2 homozygosity (H2/H2) is considered to be protective against tauopathies [26-30] as well as PD [31]" [1]. The inversion haplotype H2/H2 is found with a frequency of 5 – 37.5% in Europeans, merely 6% in Africans and < 1% in Asians [76, 89]. Apart from that, certain mutations in H2/H2 are associated with the 17q21.31 microdeletion syndrome, which is characterized by developmental delay and typical facial features [90].
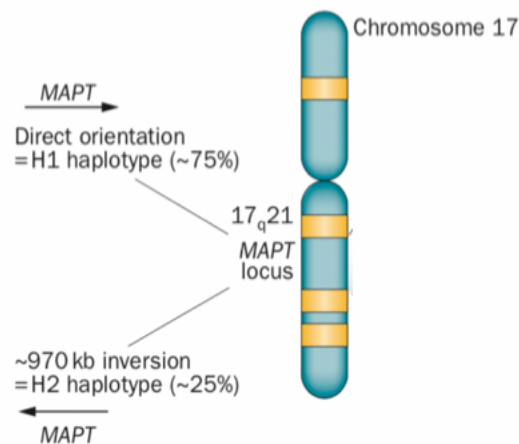
Figure 2. Illustration of the polymorphism of the *MAPT* gene. The *MAPT* gene is located on chromosome 17 and marked by a large inversion region with two allelic variants: H1 and H2. The rare H2/H2 haplotype is inversely orientated. The allelic variants differ through several single-nucleotide polymorphisms. Adapted from Wade-Martins et al., 2012. kb, kilobase.

1.2.3 Involvement of *MAPT* and tau protein in the sporadic Parkinson syndrome

At present, it is unclear how exactly the H1/H1 haplotype confers a higher risk for developing PD and other neurodegenerative diseases. Haplotype-specific properties may increase the risk for PD by affecting gene expression levels or splicing processes of the transcript [54, 91] or lead to an altered proportion of tau isoforms through mis-splicing [69, 92]. In recent years, a multitude of findings highlighted the involvement of *MAPT* in PD.

"Studies on postmortem brain and human neural cells suggested that H1 homozygosity is associated with an increased *MAPT* expression and different expression patterns of *MAPT* transcripts on mRNA level [93, 94]. Increased mRNA levels of 4R *MAPT* [95], but lower levels of 2N *MAPT* transcripts, have been described for H1/H1 compared to H2/H2 in 10 different postmortem brain regions of 134 healthy subjects [96]. The mRNA ratio of 4R to 3R *MAPT* was found to be increased in cerebellum of PD cases not genotyped for *MAPT* haplotype [63]. These findings imply that haplotype- and disease-specific expression and splicing of *MAPT* may contribute to the association of H1-homozygosity with sporadic PD. Vice versa, It is hypothesized that the protective association of the H2/H2 haplotype towards PD

might be explained by this haplotype-specific expression since the inclusion of exon 3 decreases the aggregation property of tau [95, 96]" [1].

Regarding tau protein in human brain only few studies exist which have used different lysis buffers and examined different brain regions. Among five different brain regions, protein levels of total tau and 0N3R were overall lower in the cerebellum of healthy donors (*n* = 12) stratified for *MAPT* H1/H1 and H2/H2 [96]. Another study, conducted in three brain regions, found a decrease of soluble levels of tau in the SN in PD compared to controls (Lei 2012). They also reported a higher ratio of 4R to 3R tau in PD cases in frontal cortex and cerebellum compared to controls. However, no *MAPT* haplotyping was performed [97].

In relation to the clinical manifestation of PD, some H1/H1 sub-haplotypes have been associated with distinct motor phenotypes [59]. Interestingly in PD, hyperphosphorylated tau can also be found colocalized in LB, the aggregates mainly composed of α-syn in postmortem brain [98-100]. The ability to mutually promote their aggregation of tau and α-syn was shown by *in-vitro* studies [101, 102]. It is of interest that the phosphorylation status of tau is highly modified in PD, similar to AD [103]. Nonetheless, the interaction between α-syn and tau and the mechanisms by which both contribute to onset, progression or neuronal cell death in PD are still under investigation.

1.2.4 Encoded genes in the *MAPT* polymorphism region

"Noteworthy, the *MAPT* haplotype block comprised not only the *MAPT* gene, but 19 other nucleotide sequences (**Table 1**). Among these, a number of transcripts have been shown to be associated with PD, such as *MAPT-AS1, KANSL1, KANSL1-AS1, NSF and STH* which so far have only been partially explored in this context" [1].

The *MAPT-Antisense 1* (*MAPT-AS1*) is a long non-coding RNA which partially overlaps with the promotor and 5´untranslated region of *MAPT* [64]. It generates various RNA molecules, termed natural antisense transcripts, of which some potently suppress tau translation both in vitro and in vivo [104]. *MAPT-AS1* impacts gene expression by direct interaction with key regulators of DNA methylation [105]. Overexpression of *MAPT-AS1* had an inhibitory effect on *MAPT* promotor activity in human striatal progenitor cells [106]. In postmortem studies, *MAPT-AS1* was lower expressed in PD compared to controls in SN and other brain regions [106].

The gene KAT8 regulatory NSL Complex Subunit 1 (*KANSL1)* encodes a nuclear protein product affecting gene expression through histone acetylation. Certain mutations of this gene were found causative for the 17q21.1 microdeletion syndrome [107] and *KANSL1* was also identified as risk loci for AD [108]. In terms of PD, *KANSL1* was identified as a risk factor by GWAS studies [109] and found upregulated in substantia nigra [110]. In large-scale GWAS data in temporal cortex [111] and studies

conducted in prenatal human brain [112], the *MAPT* H1/H1 haplotype was associated with a decreased *KANSL1* expression. At present, there is no data on the functional role of *KANSL1* in PD. The regulation between *KANSL1* and its corresponding non-coding antisense (*KANSL1-AS1*) is currently not known as long non-coding RNAs can act either activating or repressing gene expression of its counterpart [113]. Saitohin (*STH*) is an intronless gene located in intron 9 of *MAPT* itself with unkown funkction, However, it has been demonstrated that STH may regulate splicing of *3R* and *4R MAPT* [114]. Further evidence proved a postmortem brain study in which not only a higher expression of STH was detected in PD patients, but also a strongly positive correlation with higher expression of both *3R* and *4R MAPT* transcripts [63].

For other transcripts on the *MAPT* locus, like *PLEKHM1* and *NSF* no association with PD has been found to date. The gene pleckstrin homology domain containing, family M (with RUN domain) member 1 (*PLEKHM1*) is affecting vesicular transport, engaging in osteoblast-osteoclast interaction and thus osteopetrosis [115]. Expression of *PLEKHM1* was found increased in the cerebellum of healthy *MAPT* H1/H1 carriers compared to H2/H2 carriers [93].

The gene N-ethylmaleimide sensitive factor, vesicle fusing ATPase (*NSF*) is a widespread protein expressed from colon to brain. Its protein product contributes to intracellular membrane fusion in the SNARE complex which might be linked to α-syn [116]. In transcriptome studies *NSF* was identified as candidate risk gene for PD [117, 118]. Currently there is no functional data for the role of *NSF* in PD.

Table 1. Genes encoded in the *MAPT* polymorphism region.

Abbreviation	Gene
PLEKHM1	Pleckstrin homology domain containing, family M (with RUN domain) member 1
CRHR1	Corticotropin releasing hormone receptor 1
SPPL2C	Signal peptide peptidase like 2C
MAPT-AS1	*MAPT* Antisense RNA1
MAPT-IT1	*MAPT* intronic transcript 1
MAPT	Microtubule-associated protein tau
SRP68	Metazoan signal recognition particle RNA
SRP68P1	Metazoan signal recognition particle RNA pseudogene 1
SRP68P2	Metazoan signal recognition particle RNA pseudogene 2
SRP68P3	Metazoan signal recognition particle RNA pseudogene 3
STH	Saitohin
KANSL1	KAT8 regulatorx NSL complex subunit 1
KANSL1-AS	KAT8 regulatorx NSL complex subunit 1-Antisense
ARL17B	ADP-ribosylation factor-like 17B
yRNA	yRNA

LRRC37A	Leucine rich repeat containing 37A
RN7SL656P	RNA, 7SL, cytoplasmic 656, pseudogene
RN7SL199P	RN7SL199P RNA, 7SL, cytoplasmic 199, pseudogene
FAM215B	FAM215B family with sequence similiarity 215, member B (non-protein-coding)
NSF1	N-ethylmaleimide-sensitive-factor

Highlighted genes were selected as genes of interest in this study. In addition, *NRF2* and synuclein *genes SNCA, SNCB, SNCG* which are located on different chromosomes were included. Gene information derive from the NCBI gene database.

1.2.5 Other genes of interest in Parkinson´s disease - *NRF2* and synuclein genes

In addition, genes not located within the *MAPT* inversion region but of interest in the context of PD were examined in this study.

The gene nuclear factor, erythroid 2 like 2 (*NRF2*) is located on chromosome 2q31.2 and encodes for a transcription factor belonging to the family of basic leucine zipper proteins. Main task of *NRF2* is the regulation of over 250 genes which are involved in cell response to injury and inflammation by producing free radicals. Notably, oxidative stress is considered to play a major role in disease pathogenesis of PD [119]. *NRF2* is a promising pharmalogical target in order to control cellular oxidative stress and inflammation [120].

The synuclein genes are located on chr 4q22.1(*SNCA),* on chr 5q35.2 (*SNCB*) and on chr 10q32.2 (*SNCG*). The genes *SNCB* and *SNCG* belong to the synuclein family together with *SNCA,* although both are no susceptibility genes for PD [121]. *SNCB* encodes β-synuclein which is of particular interest because of its ability to inhibit α-syn aggregation and toxicity in vitro and in vivo [122]. However, as fibrillation of β-syn itself was observed its interaction with α-syn remains controversial [123]. Regarding expression profiles in synucleinopathies, a decrease of β-syn was observed in postmortem brain tissue with diffuse LB pathology [124]. The proteins α- and β-Synuclein (β-syn) have a broad expression pattern throughout the brain. Meanwhile, γ-synuclein encoded in *SNCG* is expressed mainly in the peripheral nervous system and some forms of breast carcinoma [125]. In contrast to α-syn, the related β-and γ-syn possess no propensity for aggregation due to the lack of the hydrophobic NAC (non-amyloid component) region and are not found in LB [35]. With regard to synuclein protein, differences have been described in PD and LB Dementia compared to control subjects in different brain regions, but no consistent trend is available due to different methods [100, 126-129]. The expression of *SNCB* and *SNCG* on mRNA and protein level in postmortem tissue have so far not been examined in the context of PD.

1.2.6 Aims of this study

The underlying hypothesis of this work is that polymorphism in *MAPT* may be responsible for differences in gene expression and protein levels which might lead to the association of the H1/H1 *MAPT* haplotype and PD. "Prior studies described differences in gene expression at the *MAPT* locus in human brains, but never in the context of PD and *MAPT* haplotype simultaneously. Some publications compared *MAPT* haplotypes of healthy donors [93-96], others only PD vs controls without haplotype differentiation [63]" [1]. The overall objective of this matched postmortem brain study of PD and control cases was to explore the effect of *MAPT* haplotype and disease on the following parameters:

1) To examine the expression of *MAPT* and its transcripts

2) To examine the expression of selected genes located in the *MAPT* inversion region 17q21.23

3) To investigate the associated protein level of total tau and its isoforms in different solubilities

4) To investigate the protein level of α-Syn in different solubilities

"Therefore, this study investigated both the influence of both the *MAPT* haplotype and the PD disease status on mRNA expression levels of genes within the *MAPT* locus (*MAPT, MAPT-AS1, KANSL1, KANSL1-AS1, STH, PLEKHM1, NSF)* as well as *NRF2*, the alpha-, beta-, gamma-synuclein genes *SNCA, SNCB, SNCG.* In addition, protein levels of soluble and insoluble tau and α-syn were examined under the same paradigm. The analysis was performed in *MAPT* genotyped human postmortem samples of the cortex of fusiform gyrus (ctx-fg), a brain region affected typically by α-syn pathology in PD, and the cortex of cerebellum (ctx-cbl), a region whithout α-syn pathology in PD" [1].

Targeting these aspects might identify potential PD relevant gene transcripts within the *MAPT* loci and provide novel insights on the role of *MAPT* and tau in PD

2 Materials and Methods

2.1 Materials

2.1.1 Consumables

Standard Materials were purchased from Sigma Aldrich, Starlab or Sarstedt.

Table 2. Consumables.

Consumables	Manufacturer (City, Country)
DNA LoBind Tube 2 ml	Eppendorf (Hamburg, Germany)
Ethanol liquid ≥ 99.9%, 1 L	Honeywell Chemicals (Charlotte, USA)
MaXtract™ High Density Tubes 2 ml	Qiagen (Venlo, The Netherlands)
Micro tube, 2 ml	Sarstedt (Nuermbrecht, Germany)
MicroAmp Fast Optical 96-well plate	Applied Biosystems (Waltham, USA)
MicroAmp™ Optical Adhesive Film PCR	Applied Biosystems
PCR tube 0.2 ml	Nerbe plus (Winsen, Germany)
Petri Dish 140x20	Thermo Scientific (Waltham, USA)
RNase Zap™	Sigma Aldrich (St. Louis, USA)
TPD (One Touch)	Sorenson BioScience (Salt Lake City, USA)
TPD (Ultra Point Graduate Filter)	Starlab (Hamburg, Germany)
Ultrapure™ DEPC Treated Water	Invitrogen (Carlsbad, USA)

2.1.2 Enzymes

Table 3. Enzymes.

Enzymes (trade name)	Manufacturer (City, Country)
Invitrogen Taq DNA Polymerase, recombinant	Thermo Scientific
iScript™ cDNA Synthesis Kit	Bio-Rad Laboratories, Inc. (Hercules, USA)
Turbo DNAse-free™ Kit	Thermo Scientific

2.1.3 Kits

Table 4. Kits.

Kit (trade name)	Manufacturer (City, Country)
Agilent RNA 6000 Kit	Agilent Technologies (Santa Clara, USA)
BigDye™ Terminator v3.1 Cycle Sequencing Kit	Thermo Scientific
DNeasy Blood & Tissue Kit	Qiagen
Phire Hot Start II DNA Polymerase	Thermo Scientific
RNeasy Plus Universal	Qiagen
SYBR™Select Master Mix for CFX, 5 ml	Applied Biosystems

2.1.4 Solutions

Table 5. Solutions.

Solution (trade name)	Manufacturer (City, Country)
DNA Ladder 100 bp 250 ng/µl	BioLabs New England
Gel Loading Dye 6 x Purple	BioLabs New England (Ipswich, USA)
SYBR Safe DNA gel stain	Invitrogen
Triethlyamine (TEA) > 99.5%	Sigma Aldrich (St. Louis, USA)

2.1.5 Gene information

Information like locus, base pairs (bp) and splice variants of all investigated genes was extracted from Nucleotide data bank (https://www.ncbi.nlm.nih.gov/gene/) of National Center for Biotechnology Information.

2.1.6 Oligonucleotides

2.1.6.1 Primers for MAPT genotyping

All primer pairs used derived from Sigma Aldrich. Amplicon sizes were determined with Primer-Blast (https://www.ncbi.nlm.nih.gov/tools/primer-blast/index.cgi).

Table 6. Primers for *MAPT* genotyping.

Primer	Primer pair sequence (5'-3') forward/reverse	Product size (bp)
*MAPT*_rs807072	Fwd TAATAGCAAGCCCCAGTTGTC	299
	Rev CAGTGATGAACCCAAGCTCCT	
*MAPT*_rs17650901	Fwd CGGCCAACTGTTAGAGAGGG	361
	Rev CTGGATGCAAACTGTTCCCG	
MAPT _rs1052553	Fwd CTTCCACCTGCCTAACCCAG	400
	Rev CCAGCCACTCTCACCTTCCC	
MAPT _rs9468	Fwd AACCCACAAGCTGACCTTCC	371
	Rev GCCAAAGCCGAGTGACAAAAG	
Fwd, forward; Rev, reverse, bp, base pairs. Derived from Tauber et al., 2022 [1].		

2.1.6.2 Primers for qPCR target genes

Table 7. Primers for qPCR target genes.

Gene	Description	Primer pair sequence (5'-3') Forward/Reverse	Product size (bp)

Total MAPT	Microtubule associated protein tau	Fwd GAGTCCAGTCGAAGATTGGGT	223
		Rev GGCGAGTCTACCATGTCGATG	
MAPT 3R	Microtubule-associated protein tau 3-repeat	Fwd AGGCGGGAAGGTGCAAATAG	104
		Rev CCTGGCCACCTCCTGGTTTATG	
MAPT 4R	Microtubule-associated Protein tau 4-repeat	Fwd GCCCATGCCAGACCTGAAGA	165
		Rev CCTCCCGGGACGTGTTTGAT	
MAPT 0N	Microtubule-associated protein tau 0 N-terminal inserts	Fwd GCTGGCCTGAAAGCTGAAG	120
		Rev ATCGCTTCCAGTCCCGTCT	
MAPT 1N	Microtubule-associated protein tau 1 N-terminal inserts	Fwd CAACAGCGGAAGCTGAAGAA	68
		Rev GTGACCAGCAGCTTCGTCTT	
MAPT 2N	Microtubule-associated protein tau 2 N-terminal inserts	Fwd ACTCCAACAGCGGAAGATGT	159
		Rev GTGACCAGCAGCTTCGTCTT	
MAPT-AS1	Microtubule-associated protein tau antisense RNA 1	Fwd AGATGCACCTGCAGCCC	121
		Rev CCCGTCCTTGTTCTGACTCC	
NSF	N-ethylmaleimide sensitive factor, vesicle fusing ATPase	Fwd GCTGGGCTTTCTATTGGGCAA	100
		Rev GCAGGAAATCAATCTCGATGGT	
NRF2	Nuclear Factor, Erythroid 2 Like 2	Fwd TCAGCGACGGAAAGAGTATGA	174
		Rev CCACTGGTTTCTGACTGGATGT	
PLEKHM1	Pleckstrin homology and run domaining containing M1	Fwd GGAGTCCCCCTGTAAGAAGC	132
		Rev GCTGGTAGTTTCCTCACCCA	
STH	Saitohin	Fwd ACAGAACCCTCAGCTTAGCAT	161
		Rev GCCTTCAATGGAAAGTTGTCTTC	
SNCA	Alpha-synuclein	Fwd AAGAGGGTGTTCTCTATGTAGGC	106
		Rev GCTCCTCCAACATTTGTCACTT	
SNCB	Beta-synuclein	Fwd GGGCTCAATCAGTGGTTCTT	91
		Rev CACAGGACTGGTGAAGAGGG	
SNCG	Gamma-synuclein	Fwd CACAGGACTGGTGAAGAGGG	148
		Rev GGAGAACATCGCGGTCAC	
KANSL1	KAT8 regulatory NSL complex subunit	Fwd CTGAAGCACACCATATCCGGT	85
		Rev CTGAAGCACACCATATCCGGT	
KANSL1- AS1	KAT8 regulatory NSL complex subunit antisense RNA	Fwd AGGGCACCTCCACCATTTG	109
		Rev GACACTAACACGCCGAAGTCA	

Fwd, forward; Rev, reverse; bp, base pairs. Adapted from Tauber et al., 2022 [1].

2.1.6.3   Primers for qPCR reference genes

Table 8. Primers for qPCR reference genes.

Gene	Description	Primer pair sequence (5'-3') Forward/Reverse	Product size (bp)

GAPDH	Glyeraldehyde-3-Phosphate Dehydrogenase	Fwd TCGGAGTCAACGGATTTGGT	195
		Rev CCTGGAAGATGGTGATGGGA	
ACTIN	Actin Beta	Fwd TCACCAACTGGGACGACATG	208
		Rev GAGGCGTACAGGGATAGCAC	
TBP	TATA-Box Binding Protein	Fwd AAAGAACGCTGTACTCAGTGTG	155
		Rev CCCCGGTTGAGGGCTTTTA	
LUC7L2	LUC7 Like 2, Pre-MRNA Splicing Factor	Fwd AGCAAAGGCAGAACGTGTTCA	225
		Rev GCAGAGCAGACTTCACAGACT	
GPBP1	GC-rich Promotor Binding Protein 1	Fwd ATCATTCGGTCTTCAACCTTCC	135
		Rev ATCCTCAGTTAAGGGAGCACA	
HMBS	Hydroxymethylbilane Synthase	Fwd ATTCGGGGAAACCTCAACACC	248
		Rev ATGCAGCGAAGCAGAGTCTC	
PPIA	Peptidylprolyl Isomerase A	Fwd CCCACCGTGTTCTTCGACATT	432
		Rev GGACCCGTATGCTTTAGGATGA	
MRPS18S1	Mitochondrial Ribosomal Protein S18	Fwd TAATTGAAGGCCGTATCACAGC	123
		Rev GCAGCAGAACATCGTCATAGTT	
UBQLN1	Ubiquilin 1	Fwd TGCAGGTCTGAGTAGCTTGG	159
		Rev AACTGTCTCATCAGGTCAGGAT	
CTBP1	C-Terminal Binding Protein 1	Fwd AAAGCCCTCCGCATCATCG	85
		Rev AGACGGCAATGCCTAAATCCC	
POLR2A	RNA Polymerase II Subunit A	Fwd GCGGAATGGAAGCACGTTAAT	113
		Rev CCCAGCACAAAACACTCCTC	
RPL22	Ribosomal Protein L22	fwd CACGAAGGAGGAGTGACTGG	116
		Rev TGTGGCACACCACTGACAT	
PSMC1	Proteasome 26S Subunit, ATPase 1	Fwd CACACTCAGTGCCGGTTAAAA	212
		Rev GTAGACACGATGGCATGATTGT	
TRIM27	Tripartite Motif Containing 27	Fwd AGCCCATGATGCTCGACTG	88
		Fwd TCGGAGTCAACGGATTTGGT	
PAPOLA	Poly(A) Polymerase Alpha	Fwd GGTGCTGATATTGATGCGTTGT	236
		Rev AGACTGTCATCTCGTAGATCCAA	
Fwd, forward; Rev, reverse; bp, base pairs. Adapted from Tauber et al., 2022 [1].			

2.1.7 Buffers

Table 9. Buffers for immunoblotting.

Buffer	Components
MES stock	213.2 g MES monohydrate, 121.14 g Tris base, 20 g SDS, 5.85 g EDTA
Milk	5% w/v nonfat dry milk, 1X TBS, 0.1% Tween-20
Running buffer MES	50 ml 20x MES stock, 1 L dd H2O
Stripping buffer	25 ml Stripping buffer stock, 200 µl ß-mercaptoethanol
Stripping Buffer stock	100 ml 20% SDS, 125 ml 0.5 M Tris-HCl pH 6.8, filled to 1 L with dd H2O

TBST	500 ml 10x TBS, 2.5 ml Tween20, filled to 5 L with dd H2O
Transfer buffer	100 ml 10x Transfer buffer, 100 ml methanol, filled to 1 L with dd H2O

2.1.8 Antibodies

Tabe 10. Antibodies used for immunoblotting.

Antibody	Incubation conditions	Characteristic (host)	Settings for imaging (Channel + min)	Manufacturer (City, Country) (Reference number)
Primary antibodies				
Dako total tau	1:3000 (24 h, 4 °C)	Polyclonal (rb)	600 - 1 min 700 - 1min Chemi - 15 min	Agilent Technologies (A0024)
3R Tau	1:1000 (48 h, 4 °C)	Monoclonal (ms)	700 - 5 min 680 - 10 min	Merck Millipore (Burlington, USA) (P10636)
4R Tau	1:1000 (48 h, 4 °C)	Monoclonal (rb)	700 - 5 min 800 -10 min	Cosmo Bio Co. (Tokyo, Japan) (TIP-4RT-P01)
aSyn	1:500 (48 h, 4 °C)	Polyclonal (rb)	600 - 1 min 700 - 1min Chemi - 20 min	Cell Signaling Technology (2642S)
GAPDH	1:3000 (24 h, 4 °C)	Monoclonal (rb)	600 - 1 min, 700 - 1min Chemi - 8 min	Merck Millipore (CB1001)
Secondary antibodies				
Peroxidase	1:5000 (2h, RT)	Anti-rb (goat)	-	Merck Millipore (PI1000)
Fluorescent 680	1: 15000 (2h, RT)	Anti-rb (goat)	-	IRDye, LI-COR (925-68071)
Fluorescent 800	1:15000 (2h, RT)	Anti-ms (goat)	-	IRDye, LI-COR (926-32210)
Chemi, chemiluminescence; Rb, rabbit; RT, room temperature. Adapted from Tauber et al., 2022 [1].				

2.1.9 Equipment

Table 11. General and protein biochemical equipment.

General equipment (trade name/version)	Manufacturer (City, Country)
310 Genetic Analyzer	Thermo Scientific
Agilent 2100 Bioanalyzer System (Version B.02.07.SI532)	Agilent Technologies
Analytical scale (DV215CD)	Ohaus (Parsipanny, USA)
Centrifuge (Fresco Pico 17)	Thermo Scientific
Centrifuge (Heraeus Pico 17)	Thermo Scientific
ChemiDoc™ XRST	Bio-Rad Laboratories
Fume Hood (Delta 30 System)	Wesemann (Syke, Germany)
Laminar Flow Biosafety Cabinet Class II	Nuaire (Plymouth, USA)
Mini PCR plate spinner (MPS 1000)	Labnet International (Edison, NJ)
Pipettes	Gilson (Middleton, USA)
PowerPac Basic	Bio-Rad Laboratories
Spectrophotometer (Nanodrop™2000c)	Thermo Scientific

StepOnePlus Real Time PCR System (Software Version 2.2.2, Serial Number 272004772)	Applied Biosystems
Thermocycler (Labcycler)	SensoQuest GmbH (Göttingen, Germany)
Thermomixer (Thermomixer comfort)	Eppendorf
Tissue grinder, Potter-Elvehjem	VWR (Radnor, USA)
Vortex (Vortex-Genie 2)	Scientific Industries (Pittsburgh, USA)

Equipment for protein biochemistry	Manufacturer (City, Country)
IKA Rocker 2D	IKA (Staufen im Breisgau, Germany)
Injection needle (Sterican)	Braun (Melsungen, Germany)
Low Fluorescene 0.2 μm PVDF (Amersham Hybond)	GE Healthcare (St Gilles, UK)
Microplate reader (CLARIOstar)	BMG Labtech (Ortenberg, Germany)
Microtest Plate 96 well	Sarstedt
Odyssey Imaging System	LI-COR Biosciences (Lincoln, USA)
Pipet filler (Pipetboy)	Integra LifeSciences (Princetion, USA)
Protran® nitrocellulose membrane	Whatman (Little Chalfont, UK)
PVDF Immun-Blot membrane	Bio-Rad Laboratories
Rocker	Edmund Bühler (Bodelshausen, Germany)
Semi-dry blotting chamber (Trans-Blot Turbo)	Bio-Rad Laboratories
Serological pipette (5-50 mL)	Sarstedt
Transfer System (Trans-Blot Turbo)	Bio-Rad Laboratories
Ultra-Clear Centrifuge Tubes	Beckman Coulter™, Brea, USA
XT Criterion Pre-Cast gels	Bio-Rad Laboratories

2.1.10 Chemicals

Table 12. Chemicals.

Chemical	Manufacturer (City, Country)
λ protein phosphatase	New England Biolabs (Ipswich, USA)
Acrylamide/bis solution (30%)	Bio-Rad Laboratories
Agarose NEEO Ultraqualität	Carl Roth (Karlsruhe, Germany)
Ammonium persulfate (APS)	Sigma Aldrich
Clarity™ Western ECL Substrate, peroxide and enhancer solution	Bio-Rad Laboratories
Guanidine hydrochloride	Sigma Aldrich
M-PER Mammalian Protein Extraction Reagent	Thermo Scientific
Methanol, > 99.9%	Carl Roth (Karlsruhe, Germany)
Pierce BCA Protein Assay, Reagent A and B	Thermo Scientific
Precision Plus Protein Standard Dual Color	Bio-Rad Laboratories
Protease Inhibitor (complete tablets, EDTA-free)	Roche (Rotkreuz, Switzerland)
QIAzol Lysis Reagent	Qiagen
RIPA buffer	Sigma Aldrich
Rotiblock 10 x	Carl Roth (Karlsruhe, Germany)
SDS Pellets, > 99.9%	Carl Roth (Karlsruhe, Germany)
Sodium Fluoride	Sigma Aldrich
ß-mercaptoethanol	Appli-Chemicals
Tau Protein Ladder, 6 isoforms, human	Sigma

Temed	Bio-Rad Laboratories
Total Protein Stain solution	LI-COR Biosciences
Tween 20	Sigma Aldrich
XT Reducing Agent 20 x	Bio-Rad Laboratories
XT Sampling Buffer 4 x	Bio-Rad Laboratories

2.1.11 Software

Table 13. Software.

Software (Version)	Manufacturer (City, Country)
Microsoft Excel (2016)	Windows (Redmond, USA)
ImageLabTM (5.2.1)	Bio-Rad Laboratories
qBase+ (3.2)	Biogazelle (Gent, Belgium)
Graphpad Prism (8.2)	GraphPad Software Inc. (San Diego, USA)

2.2 Human postmortem brain tissue

2.2.1 Tissue collection

The methodological description of the tissue collection is taken in parts from the submitted publication Tauber et al. 2022 [1]. Human postmortem brain tissue was obtained from the Neurobiobank of the Ludwig-Maximilians-University of Munich (n = 92) and the Parkinson's UK Brain Bank (n = 84). A multi-step selection process was used to identify the best cases for the study population (**Fig 13**). The specimen ultimately included derived from clinically well documented and neuropathologically confirmed cases of PD and healthy controls. Donors were collected in accordance with the requirements of the local Ethics committee. Either the donors had given their full consent to the use of their brains for research during lifetime or the relatives consented in accordance with the presumed patient wishes. The analyses have been approved by the Research Ethics committee of the Technical University Munich (Nr. 265/16 S) and Imperial College London (18/WA/0238). For exclusion of high tau burden AD Braak and Braak scores [130] was assessed by board-certified neuropathologists. Exclusion criteria for control and PD cases were either severe concomitant tau pathology (> AD Braak and Braak stage 3), clinical report of dementia or positive family history of PD, or a postmortem interval (PMI) from death to tissue fixation of more than 50 h. The postmortem interval is considered as tissue quality parameter and was taken from the neuropathologic records. Inclusion criteria for PD cases was Lewy Body Disease (LBD) Braak stage > 3 [25]. Additionally, all cases were assessed according to The Consortium to Establish a Registry for Alzheimer's Disease (CERAD) score [131] and PD cases according to the McKeith classification [132]. Aged individuals without history or neuropathological diagnosis, or infectious meningitis or prior head-injuries were chosen for the group of healthy controls. Reported history of seizures, depression or hallucinations led to no exclusion (**Table 14**).

Table 14. Inclusion criteria for postmortem brain tissue collection.

General criteria	
Postmortem interval < 50h, no history of infectious meningitis, no severe head-injuries, AD pathology: Braak stage ≤ 3, no ß-amyloid plaques present, no clinical report of dementia	
Parkinson's disease cases Neuropathological diagnosis of sporadic PD Clinical diagnosis of sporadic PD	**Control cases** No history or diagnosis of neurodegenerative diseases Matched for age and gender to PD cases

The CERAD score assesses the frequency of ß-amyloid neuritic plaques in the subjects´ brain. [131] The Mc Keith classification is embedded in the guidelines of Dementia with Lewy Bodies Consortium for clinical and pathologic diagnosis. By a semi-quantitative grading of Lewy-related pathology in five cortical regions, five LB pathology types are classified: Brainstem predominant, limbic, diffuse neocortical, amygdala predominant, olfactory bulb only. Overall this classification predicts the likelihood of the association between pathologic findings and clinical syndrome of dementia with Lewy bodies [132]. Presence of α-syn pathology was confirmed for PD donors by semi-quantitative evaluation in the target brain region ctx-fg through an experienced neuropathologist (**Fig 3**).
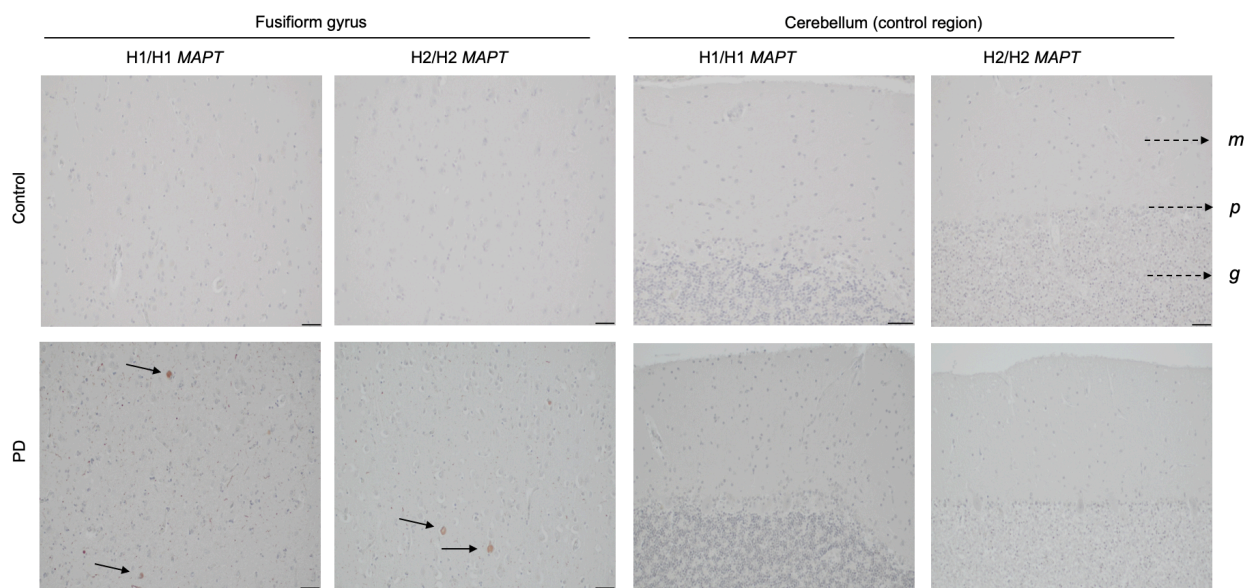
Figure 3. Semi-quantitative evaluation of α-syn pathology in human postmortem brain tissue. Black arrows indicate exemplary Lewy bodies (LB) in the samples of PD cases of both haplotypes (H1/H1 and H2/H2) in cortex of fusiform gyrus. As expected, no LB pathology was present in cortex of cerebellum of PD cases nor in both brain regions of control cases of both haplotypes. Besides Purkinje cells (p), the molecular layer (m) and granular layer (g) of cerebellar tissue architecture are displayed. Immunohistochemical staining was performed in lower cortical cell layers of fusiform gyrus and cortex

of cerebellum. Representative images derive from postmortem brain donors with H1/H1 (C2, PD9) and H2/H2 (C9, PD2). Scale bar: 50 µm. Derived from Tauber et al., 2022 [1].

Comprehensive neuropathological reports were available for all included cases, and clinical data from medical records were gathered, as far as available (**Table 15**). The causes of death were also reported (**Table 15**). Since sex-related differences in alterations of mRNA expression associated with PD have been described, sex matching was done for the final study population [133, 134].

Two types of tissue were included: cortex of gyrus fusiformis, as pathologic region typically affected by LB pathology from LBD Braak stage 3 on [25], and cortex of cerebellum, as control region. The gyrus fusiformis is located in the anteromedial temporal mesocortex. It plays a role in the sensory association cortex enabling categorization of visual input and leading in the case of malfunction to prosopagnosia, a cognitive disorder of face perception [22, 135]. The cerebellum is considered to be preserved from PD related pathology, and therefore not embedded in the Braak PD staging model [136]. Tissue blocks were dissected in grey and white matter, fresh frozen and stored at -80 °C. To focus on neuronal enrichment only grey matter was used for mRNA expression and protein level analysis. In summary, 115 donors with sufficient tissue available (PD n = 60, control n = 55) were available for the step-wise selection process. Samples were consecutively numbered and snap-frozen stored at - 80 °C.

Clinical diagnosis of sporadic PD was made according to the UK brain bank criteria and all diagnosis were well documented in clinical notes with the exception of one case. For one brain donor (PD 11) no clinical signs of PD or review by a clinical neurologist were found in the sparse notes, but neuropathological diagnosis of sporadic PD was assessed. This made a missed PD diagnosis at lifetime for this case likely and justified its analysis in the PD cohort.

Table 15. Demographic, clinical and neuropathologic characteristics of individual postmortem brain donors.

Brain donor	Sex	Brain bank	*MAPT* haplotype	Age at diagnosis (y)	Age at death (y)	Disease duration (y)	Cause of death	PMI (h)	LBD Braak stage	Lewy inclusion pathology in ctx-fg	LBD McKeith subtype	AD Braak and Braak stage	CERAD score
PD1	F	LMU	H1/H1	68	79	11	CRF	17	6	++	neo	II	0
PD2	F	LMU	H1/H1	58	72	14	Ovarial carcinoma	12	5	+	limb/neo	I	0
PD3	F	LMU	H1/H1	n.i.	76	n.i.	Pulmonary embolism	12	6	+++	limb	II	0
PD4	M	LMU	H1/H1	n.i.	74	n.i.	CRF	n.i.	>= 5	+	n.a.	I	0
PD5	M	LMU	H1/H1	69	72	3	Cancer bleeding	28	6	++	neo	I	0
PD6	M	LMU	H1/H1	73	74	2	Pneumonia	14	6	++	neo	III	0
PD7	F	IMP	H1/H1	55	79	24	Pneumonia	9	6	+	neo	II	B
PD8	M	IMP	H1/H1	66	72	6	Pneumonia	19	4	n.i.	bst	II	0
PD 9	M	IMP	H1/H1	61	70	7	n.a.	17	6	+	neo	I	0
PD10	F	LMU	H2/H2	67	82	15	GI bleeding	n.i.	6	+	neo	I	0
PD11	F	LMU	H2/H2	78	85	7	Lung cancer	29	6	+++	neo	I	0
PD12	M	IMP	H2/H2	68	78	10	Pneumonia	11	6	n.i.	neo	I	A
PD13	M	IMP	H2/H2	59	66	7	Metastatic CUP	14	6	+	bst	I	0
PD14	F	LMU	H2/H2	n.i.	77	n.i.	Aneurysm rupture	9	>= 5	+	neo	II	A
C1	F	LMU	H1/H1	n.a.	77	n.a.	CRF	8	*	0	*	II	0
C2	F	LMU	H1/H1	n.a.	73	n.a.	Sepsis	14	0	0	0	II	0
C3	F	LMU	H1/H1	n.a.	66	n.a.	Pneumonia	n.i.	0	0	0	II	0
C4	M	LMU	H1/H1	n.a.	74	n.a.	Cardiac arrest	28	0	0	0	I	0
C5	M	IMP	H1/H1	n.a.	65	n.a.	SCLC	12	0	0	0	I	0
C6	F	IMP	H1/H1	n.a.	84	n.a.	Pancreatic cancer	11	0	0	0	II	0
C7	M	IMP	H1/H1	n.a.	79	n.a.	Pneumonia	21	0	0	0	I	0
C8	F	LMU	H2/H2	n.a.	60	n.a.	Exacerbated COPD	15	0	0	0	I	0
C9	M	LMU	H2/H2	n.a.	70	n.a.	n.a.	40	0	0	0	I	0
C10	F	LMU	H2/H2	n.a.	89	n.a.	n.a.	22	0	0	0	I	0
C11	F	IMP	H2/H2	n.a.	95	n.a.	Pneumonia, CKD	28	0	0	0	III	0
C12	F	IMP	H2/H2	n.a.	91	n.a.	Pneumonia	22	0	0	0	I	0

The LBD Braak stage and AD Braak and Braak stage each consist of six stages. The CERAD score describes neuritic Amyloid-ß plaques in levels of 0, A, B, C. Lewy inclusion pathology assessed semi-quantitatively the burden of Lewy neurites and Lewy Bodies in the target brain region cortex of fusiform gyrus (+ few, ++ moderate, +++ many inclusions). * Since brain stem of this specimen was not available for neuropathological assessment, exclusion of LBD of stage 3 or lower was not possible. Abbreviations: AD, Alzheimer´s disease; bst, brain stem predominant; CERAD, The Consortium to Establish a Registry for Alzheimer´s Disease; C, Control; F, female; CRF, cardiac-respiratory failure; ctx-fg, cortex of fusiform gyrus; CUP, cancer of unknown primary; GI, gastrointestinal; IMP, Imperial College London Brain Bank, LBD, Lewy body disease; limb, limbical; LMU, Neurobiobank of the Ludwig-Maximilians-University of Munich; M, male; n.a. data not available; neo, neocortical; PD, Parkinson´s disease; PMI, postmortem interval; SCLC, small squamous cell lung cancer;.CKD, chronic kidney disease; COPD, chronic obstructive pulmonary disease; n.a., not applicable; n.i. no information. Derived from Tauber et al., 2022 [1].

2.2.2 Genotypying for *MAPT* Haplotype

2.2.2.1 DNA Extraction

In general, sterile, nuclease-free working conditions were required for all work in order to prevent degradation process during the experimental workflow. Therefore, all working surfaces were prepared with RNAse-Zap and UV-C-Light for 20min and styrofoam thermos boxes full of dry ice were used for transportation.

For *MAPT* genotyping DNA deriving from grey matter of ctx-fg of each brain donor was analyzed. For tissue preparation under a Laminar Flow Biosafety Cabinet Class II (Nuaire) the unfixed, snap-frozen samples of approximately 2 cm^3 size were placed on sterile petri dishes filled with dry ice preventing severe thawing. A small section was cut with sterile forceps and a disposable scalpel. Tissue samples were scaled with Analytical Scale (Ohaus) and as recommended only further processed with a maximum weight of 25 mg.

Deoxyribonucleic acid (DNA) extraction was performed using Blood & Tissue DNA Extraction kit (Qiagen, Venlo, The Netherlands) according to the recommended protocol. Hereby, the tissue is first lysed and afterwards the DNA bound to silica-membranes. Through repeated steps of washing kations, proteins and other interfering substances get removed [137]. After dissolving from the membrane with diethyl pyrocarbonate (DEPC) treated water (H$_2$O), concentration of DNA extracts were measured photometrically with Nanodrop™ (Thermo Scientific).

Protocol for DNA extraction

1. Adding of 180 µl ATL Buffer and 20 µl Proteinase K to the tissue block, vortexing, and shaking in Thermomixer at 56 °C until complete lysis.
2. Vortexing for 35 seconds (s).
3. Adding of 200 µl AL Buffer, vortexing for 35 s.
4. Adding of 200 µl 100% ethanol (Honeywell Chemicals) and vortexing for 35 s.
5. Transfer of the solution into a DNeasy Mini spin column placed in a collection tube.
6. Centrifuging for 1 minute (min) at 6000 gravity (g)), discarding flowthrough by exchanging collection tube.
7. Adding of 500 µl Buffer AW1, centrifuging for 1 min at 6000 g, exchanging collection tube.
8. Adding of 500 µl Buffer AW2, followed by centrifuging for 3 min at 20.000 g in order to dry out the membrane.
9. Elution with 50 µl AE Buffer directly onto the membrane in new column.
10. Incubation at room temperature for 1 min, afterwards centrifugation for 1 min at 6000 g
11. Second elution with 20 µl in another tube.
12. Measurement of concentration and purity with NanoDrop, calibration with 1 µl RNAse free water.

2.2.2.2 Genotyping for *MAPT* haplotype

The *MAPT* haplotype is defined through 21 SNPs which exist in a linkage desequilibirum [138]. Linkage

desequilibirum refers to the non-random association of alleles at two loci and the prediction about one adjacent allele on the basis of the other allele. This allows to detect only for a subset of haplotype tagging SNPs in order to genotype the *MAPT* haplotype [139]. The *MAPT* H1 and H2 allele are characterized by one certain nucleic acid at the specific gene loci, respectively.

Four haplotype-tagging single-nucleotide-polymorphisms (SNP) were determined (SNP rs17650901, rs1052553, rs9468, rs8070723) in cooperation with the Institute of Human Genetics, Friedrich-Alexander University of Erlangen-Nürnberg (Erlangen, Germany) (Table 16). The SNP rs8070723 is associated with an increased risk for PD and also for PSP independent of the *MAPT* H1/H2 status [53, 81].

Table 16. Analyzed single nucleotide polymorphisms defining the *MAPT* polymorphism.

Gene loci	SNP Name	MAPT H1 Allele	MAPT H2 Allele
chr17:44039691	rs17650901	A	G
chr17:44073889	rs1052553	A	G
chr17:44101563	rs9468	T	C
chr17:44081064	rs 8070723	A	G
Three SNPs were used for *MAPT* genotyping of the postmortem brains. In addition, the risk SNP rs8070723 was evaluated. The *MAPT* alleles H1 and H2 are each defined by one certain nucleic acid at the specifc gene locus. SNP, single nucleotide polypmorphism; A, Adenosine; G, Guanine; C, Cytosine; T, Thymine. GGCG			

The DNA extracts (300 ng DNA with a minimum concentration of 60 ng/µl) of 115 cases were anazlyed using Taq DNA polymerase followed by BigDye Terminator v.3.1 Cycle Sequencing Kit with 310 Genetic Analyzer (all from Thermo Scientific, Waltham, USA). Principal steps are amplification of the template DNA by polymerase chain reaction (PCR), PCR clean-up for digesting of unincorporated PCR primers, cycle sequencing, sample purification and finally electrophoresis. Reaction mixes for PCR and cycle sequencing are listed in Table 17.

Table 17. Reaction mix for genotyping.

PCR mix		Cycle sequencing mix	
Reagent	Volume (µl)	Reagent	Volume (µl)
Buffer	2	RNAse free water	5,5
Magnesium chloride	1	BigDye reagent	0,2
RNAse free water	6,9	Primer	0,3
Dimethyl sulfoxide	1	Product	2
Betain	4		
Polymerase	0,1		
Primer reverse (3.2 µM)	1		
Primer forward (3.2 µM)	1		

DNA (10 ng)	2		
Total	20	Total	10

2.2.3   Tissue dissection

Under the same RNAse-free conditions as described above, brain tissues of both regions were macroscopically dissected in white and grey matter. The tissue pieces of approximately 100 mg were separately given into 1.5 ml microtubes resulting in three tubes with grey matter, and three tubes with white matter of each sample respectively. To focus on neuronal enrichment only grey matter was used for gene expression and protein level analysis. Dissected samples and stock tissue were stored fresh frozen and stored at -80 °C.

2.2.4   Selection for final analysis

The premise for reliable experiments is high quality postmortem tissue. Due to that fact the most suitable tissue samples were selected of the postmortem brain tissue collection consisting of 95 PD and 81 healthy control donors (total n = 176).

In our study we concentrated on the difference in gene expression between *MAPT* haplotypes H1/H1 and H2/H2 with the focus of neuronal enrichment (grey matter). First, care was taken to match subject groups as closely as possible for age and gender. Second, RNA extraction was performed for 45 postmortem brain donors in triplicates of both brain regions. Five donors were excluded due to insufficient quality of RNA extracts. Of all RNA quality criteria RNA intregrity number (RIN) was evaluated of highest relevance for the success of down-stream applications like quantitative polymerase chain reaction (qPCR). RIN was measured for 40 brain donors (for thresholds of RNA quality marker and results see chapter 2.3.1). The stepwise selection procedure is illustrated in **Fig 13**.

2.3   RNA extraction and analysis

2.3.1   Evaluation of an optimal protocol for RNA extraction

Gene expression analysis in postmortem tissue is premised on high quality of ribonucleic acid (RNA) and due to its vulnerability RNA isolation can be challenging. Given the fact that many factors promoting RNA degradation, such as pre- and postmortem factors, are outside of control, finding an optimal RNA extraction method of postmortem brain tissue was an essential point. The key steps of total RNA isolation are the following:

- Lysis of brain tissue
- Homogenization

- Phase separation
- Removal of genomic DNA (gDNA)
- Binding of total RNA and washing
- Elution

In terms of performance of the protocols, criteria such as RNA quantity, purity and integrity were assessed. Four main questions were addressed in the preliminary experiments:

1) Which is the best lysis reagent and homogenization for postmortem human brain tissue?
2) How to remove genomic DNA from RNA extracts?
3) How to accomplish a clear phase separation?
4) Does an additional clean-up step of impure RNA extracts impair qPCR performance?

Therefore, different commercially available kits and established protocols for total RNA extraction were tested in prior to the main experiments (Table 18). Tested protocols were 1) protocol after Chomczynski with lysis in Trizol (QIAzol Lysis Reagent, Qiagen) and RNA precipitation as pellet [140]; 2) RNEasy+ Mini kit with lysis in RLT buffer and two forms of homogenization; 3) Hybrid protocol after Rodriguez-Lanetty with lysis in Trizol with subsequent RNA isolation using RNEasy+ Mini kit spin columns [141]; 4) RNEasy+ Mini Universal kit with lysis in Trizol.

Table 18. Evaluated methods for RNA extraction.

Step Tested Sample	1) Protocol after Chomczynski	2) RNEasy+ Mini Kit		3) Hybrid after Rodriguez-Lanetty	4) RNeasy+ Mini Universal Kit
Maximal tissue amount	70-100 mg	30 mg		30 mg	100 mg
Lysis reagent	Trizol + Chloroform	RLT		Trizol + Chloroform	Trizol + Chloroform
Homogenization	TissueRuptor	Tissue Ruptor	Liquid nitrogen, QiaShredder	TissueRuptor	TissueRuptor
Phase separation	Centrifugation	Spin column		MaXtract tube	MaXtract tube
gDNA elimination	TurboDNAse	Spin column		Spin column	Elimination solution
RNA binding and washing	Pellet (Isopropanol, linear acrylamide)	RNEasy spin column		RNEasy spin column	RNEasy spin column
Tested sample (*n*)	Luhmes (2) Mouse brain (3) Human brain (3)	Human brain (3)		Human brain (3)	Human brain (3)

All RNA extractions with commercially available kits were performed according to the manufacturers´ instructions. Protocol 1) and 3) are described in detail below, protocol 4) in chapter 2.3.2. Protocol 2) was performed according to the manufacturers´ instructions.

Protocol 1 after Chomczynski

1. Homogenizing tissue samples in 1 ml of Trizol reagent per 100 mg of tissue using a tissue grinder. Incubation at room temperature (RT) for 5 min. Centrifuging to remove cell debris at 12 min at 10.000 g.
2. Adding of 0.2 ml of chloroform per 1 ml of Trizol reagent. Vortexing for 15 s and incubation at RT for 3 min. Centrifuging at 12.000 g for 15 min at 4 °C. Transfering the upper aqueous phase carefully into a fresh tube.
3. Precipitation of the RNA by adding 10 µg of 5 µg/µl linear acrylamide and 0.5 ml isopropyl alcohol per 1 ml of Trizol reagent used for the initial homogenization. Incubation at RT for 10 min and centrifugation at 12.000 g for 10 min at 4 °C.
4. Removing the supernatant and washing the pellet in 75% ethanol, at least 1 ml of 75% ethanol per 1 ml of Trizol reagent. Vortexing and centrifugation at 7500 g for 5 min at 4 °C. Repeating washing once. Removing residual ethanol.
5. Air-drying the RNA pellet for 5-10 min. Resuspending the RNA in 30-50 µl of DEPC-treated water. Storage at -20 °C or below.

Protocol 3 Hybrid after Rodriguez-Lanetty

1. Homogenizing tissue samples in 1 ml of Trizol reagent per 100 mg of tissue using a tissue grinder. Maximum amount of 30 mg brain tissue was used. Incubation at RT for 5 min. Centrifuging to remove cell debris for 10 min at 12.000 g at 4 °C.
2. Adding of 0.2 ml of chloroform per 1 ml of Trizol reagent. Vortexing for 20 s and incubation at RT for 3 min. Centrifuging at 10.000 g for 18 min at 4 °C. Transfering the upper aqueous phase carefully into a fresh tube.
3. Slowly adding an equal volume of 100% ethanol.
4. Loading the sample (700 ml) into a RNeasy column (Qiagen kit) seated in a collection tube and spinning for 30 s at 8000 g. Discarding flow-through.
5. Transferring the column into a new collection tube, adding of 500 µl buffer RPE and spinning for 30 s at 8000 g. Discarding flow-through.
6. Adding 500 µl buffer RPE and spinning 2 min at 8000 g. Discarding flow-through.
7. Spinning the column for 1 min at 8000 g to get rid of remaining buffer. Transfering the column to a new 1.5 µl collection tube and pipetting 30-50 µl of DEPC-treated water directly onto the new column membrane.
8. RT for 2 min, spinning at 8000 g for 1 min to elute RNA. Storage at -20°C or below.

Protocol 1) was not suitable for RNA isolation

Initially protocol 1), well established in our laboratory, was tested. In order to evaluate the quality of extraction process samples a positive control was included. Lund human mesencephalic cells (Luhmes) and postmortem mouse (ms) brain were used as positive control. Both materials derived from other projects within our work group and were kindly placed at the disposal. RNA of Luhmes cells were extracted by standard procedure. Disadvantage of this protocol is the lack genomic DNA removal which makes an additional treatment necessary. Consequently, all samples extracted with protocol 1

were treated with the enzyme-based kit TurboDNAse (ThermoFisher). This will be explained in the section "Removal of genomic DNA". For this experiment isolated RNA of Luhmes cells ($n = 2$), postmortem human ($n = 3$) and mouse brain tissue ($n = 3$) were used. An aliquot treated with TurboDNAse was compared to untreated aliquot of the same RNA extraction.

Eventually, the protocol 1) after Chomczynski was considered to be not suitable for the RNA extraction in postmortem human brain tissue and therefore further protocols were tested. The experiment comparing method 2), 3) and 4) was performed with a setup of postmortem human brain tissue ($n = 3$).

Optimal lysis buffer and homogenization of brain tissue

Tested lysis buffers were the RLT buffer, included in the RNEasy+ Mini kit (protocol 3a, 3b) and Trizol, part of the RNEasy+ Mini Universal kit (protocol 1, 3, 4). Tested ways of homogenization of tissue samples were mechanical disruption by a TissueRuptor, a mortar-style pestle, (protocol 1, 2a, 3, 4) and grinding of liquid nitrogen frozen samples followed by the QIAShredder (Qiagen). The QIAShredder is a spin-column shredding system which homogenizes lysates further after complete initial disruption. As suggested by the RNeasy+ Mini protocol (protocol 2b) the tissue powder plus appropriate volume of RLT lysis buffer were centrifuged in a QIAShredder spin column for 2 min at full speed.

Removal of genomic DNA

The above-mentioned setup of brain samples was extracted similarly with the RNeasy Universal Kit. Three methods for gDNA elimination were tested (a, b, c).

a) Column-based removal

With the gDNA Elimination spin column (Qiagen) gDNA removal is incorporated into the protocol of RNEasy+ Mini kit. The reaction is performed by spinning the homogenized lysate for 30 s at 8000 g.

b) Solution-based removal

The gDNA elimination solution (Qiagen) provided with the RNEasy+ Mini Universal Kit removes genomic DNA contamination, making additional DNase treatment obsolete. After homogenization, 100 µl of solution were added to the lysate and shaken vigorously for 15 s at RT, followed by the rest of the standard protocol.

c) Enzyme treatment

Total RNA was treated with Turbo DNAse (ThermoFisher) according to the manufacturer´s instructions. The samples are incubated for a period of 20-30 min at 37°C which is required for inactivation of the DNase enzyme. In a second modified approach, 100 µl ethylendiamintetraacetat (EDTA) and 1 µl RNAse inhibitor (Sigma) were also added to the RNA extract of 3 samples (Luhmes $n = 1$, mouse $n =$

1, human n = 1) before the incubation period.

Phase separation

Apart from the RNEasy+ Mini Kit with specialized spin columns, the separation of cell components is achieved through centrifugation. Due to that the lysate is split up in three phases: on the upper side an aqueous colorless phase, a white interphase and a red organic phase on the bottom. RNA is located only within the aqueous phase, DNA, proteins and organic solvents (such as Trizol lysis reagent) are trapped within the other parts. This results in the difficulty of transferring the RNA purely from the other phases which contain DNA- and RNAses. In the case of the MaXtract High Density tube, the gel within the tubes migrates below the aqueous phase during centrifugation, building a solid barrier between the phase of interest and organic phases. This allows to simply decant the upper RNA containing phase in a new tube without potential contamination. This facilitated the handling when working with methods based on Trizol lysis reagent and improved purity of nucleid acids compared to the method after Chomczynski where the nucleic acid containing phase is transferred by pipetting from a standard tube.

Influence of clean-up of RNA extracts on qPCR performance

If RNA extracts are impure indicated by a low A_{260}/A_{230} ratio, a clean-up step can be performed. Contaminating substances detected with the A_{260}/A_{230} ratio are salts, free nucleotides or residual phenol. For purification, the chloroform extraction followed by ethanol precipitation is the preferred method. The used protocol derived from New England BioLabs (E2040). In a preliminary experiment the influence of the clean-up step on qPCR performance was evaluated using postmortem human brain tissue (n = 3, PD cases, grey matter). Complementary DNA (cDNA) of cleaned up RNA aliquots was used in comparison to untreated aliquots of the same sample. qPCR was performed for the reference genes *PPIA*, *huUBQLN1* and *TRIM* in two repeats according to the same qPCR protocol described below.

Protocol for purification of extracted RNA

1. Adjusting the reaction volume to 180 µl by adding 160 µl nuclease-free water. Adding of 20 µl of 3 M sodium acetate, pH 5.2 or 20 µl of 5 M ammonium acetate, mixing thoroughly.
2. Extraction with an equal volume of 1:1 phenol/chloroform mixture, followed by two extractions with chloroform. Collecting the aqueous phase and transfering to a new tube.
3. Precipitation of the RNA by adding 2 volumes of ethanol. Incubation at -20°C for at least 30 min and collection of the pellet by centrifugation.
4. Removing the supernatant and rinsing the pellet with 500 µl of cold 70 % ethanol.
5. Resuspending the RNA in 50 µl of 0.1 mM EDTA. Storage at -20°C or below.

2.3.2 RNA extraction

In conclusion to the results of the preliminary experiments for an optimal total RNA isolation method (see 3.1), the RNEasy+ Universal Mini Kit (Qiagen) was used (modified version of the recommended protocol, see below). All tissue samples were scaled and as recommended only further processed with a maximum weight of 100 mg. A minimum of three extractions with two elutions were performed for each tissue sample. The best RNA sample among each triplet was taken into account for the experiments.

Protocol 4 for RNA isolation with RNEasy+ Universal Mini Kit

1. Preparation: RNA Isolation performed under a fume hood (Wesemann). Scaling of tissue samples (maximum weight 100mg). Potter-Elvehjem-Tissue-Grinder placed in an inced bucket.
2. Homogenizing tissue samples (maximum weight 100mg) in 1 ml of Trizol reagent per 100 mg of tissue using a Potter-Elvehjem-Tissue-Grinder. To avoid loss of lysate, split amount of lysis reagent in three times. Giving the frozen sample and 333 ml Trizol into the mortar for mechanical disruption. Transfering the homogenized lysate into a cooled 2 ml tube. Washing of the mortar with another 333 ml Trizol for another two times. Isolation of only 6 samples at a time to avoid unnecessary thawing.
3. Washing of mortar and pestle after each homogenization with 70% ethanol and air-drying before next use.
4. Incubation at RT for 5 min. Adding of 100 µl gDNA Eliminator solution and vortexing for 30s. Adding of 180 µl of chloroform per 1 ml of Trizol reagent and vortexing for 1 min and incubation at RT for 3 min.
5. Preparing 2 ml MaXtract High Density Tubes (Qiagen) by centrifugation for 1 min at full speed (12000 g). Transfering samples and **centrifuging** at 12.000 g for 15 min at 4 °C.
6. Transfering the upper aqueous phase carefully into a fresh tube. Adding of one volume (approximately 600 µl) of 70% ethanol and mixing thoroughly.
7. Transfering 700 µl of the sample to a RNeasy Mini spin column (Qiagen) placed in a collection tube and centrifuging for 25 s at 8000 g at RT. Discarding flow-trough and repeating step 7 once.
8. Adding of 700 µl RWT Buffer and centrifuging for 25 s at 8000 g at RT. Transfering of the RNeasy spin column in a new collection tube and centrifuging at full speed for 1min to eliminate left-over buffers.
9. Washing of the membrane with 500 µl RPE Buffer and centrifuging for 2 min at 8000 g at RT.
10. Eluting RNA with 30 µl DEPC-H_2O. Repeating step 10 twice with 20 µl DEPC-H_2O. Storage at -20 °C or below.
11. This protocol was also used and described in the submitted publication Tauber et al, 2022 [1].

2.3.1 RNA quantification and quality

As stated in the Minimum Information for Publication of Quantitative Real-Time PCR Experiments (MIQE) it is imperative that a reliable protocol for analysis of sample quality and quantity is defined [142]. RNA quality is a factor of both the purity of the sample and the degradation status of the RNA molecules. Purity and concentration were determined through photometric quantification and

degradation through RNA integrity measurement.

2.3.1.1 Concentration and purity

Yield and purity values such as ratios A_{260}/A_{280} and A_{260}/A_{230} of each sample were photometrically quantified using NanoDrop. After calibration with 1 µl RNA free H_2O, 1µl of each RNA sample was pipetted onto the sensor. The A_{260}/A_{280} ratio consists of the absorbance of nucleic acid at wavelength 260 nm and protein at 280 nm. A ratio of 2.0 proves the absence of protein contamination. In addition with an equal A_{260}/A_{230} ratio, a high purity is estimated [143]. Contaminants such as guanidium thiocyanate, part of lysis reagent Trizol, are detected at 260 nm. To guarantee a sufficient quality of the starting material, a cut-off for purity was set. For A_{260}/A_{280} ratio, a threshold of > 1.8 was applied [144]. With no existing consensus in literature, a minimum threshold A_{260}/A_{230} ratio > 1.5 was applied. Only RNA extracts with higher purity were included to the experiments making a clean-up step as described above obsolete.

2.3.1.2 RNA Integrity

Besides to case screening and quantification of purity, we ascertained the tissue quality by determining total RNA Integrity Number. The RNA integrity number is a score between 0-10 which displays the grade of degradation of the RNA sample with 0 fully degraded and 10 fully intact. The integrity categories are automatically calculated by the distribution of sizes of RNA molecules within each sample. Using microfluid technology and electrophoretic separation an electropherogram is created which shows the number of ribosomal bands of specific size. Of special interest are the ribosomal RNA units 28S and 18S, as a ratio of 2.0 characterizes intact RNA. While RNA degradation presents with increased shorter fragments and at the same time a decreased signal for the 18S and 28S species [145] (**Fig 4**). These shorter fragments of RNA potentially interfere with downstream applications. Measurements were performed using the RNA 6000 Nano chip technology and Bioanalyzer 2100 (Agilent Technologies) together with the provided software (Version B.02.07.SI532).
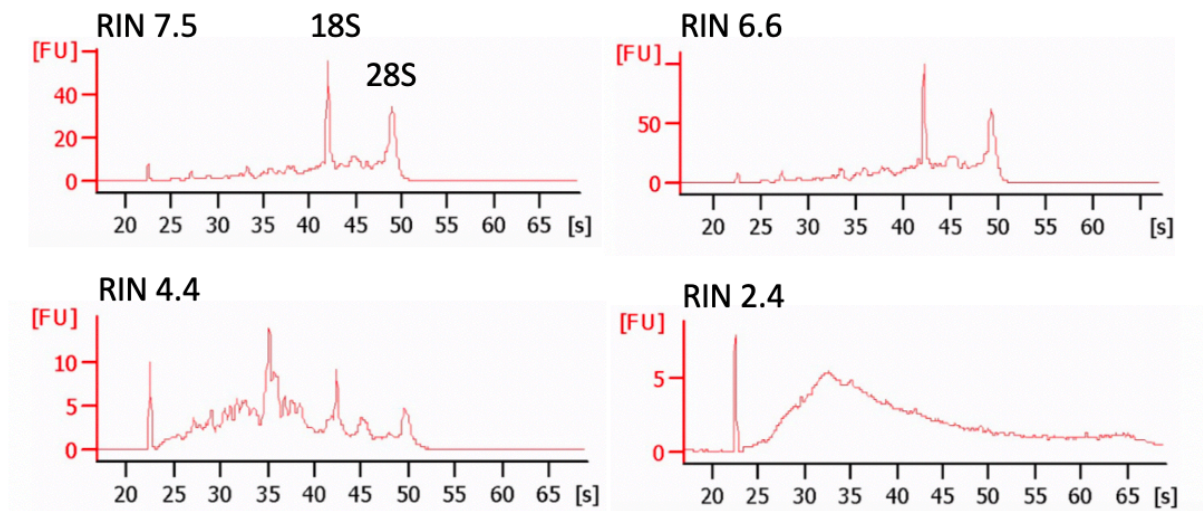
Figure 4. Examples of RNA integrity of postmortem brain samples. Electropherograms of extracted RNA of different postmortem brain samples are displayed. With degradation and lower RIN values shorter fragments become present, while the signal intensities for 18S and 28S units decrease. RIN, RNA integrity number, FU, Fluorescence unit; s, seconds

Protocol for determination of RNA integrity number

1. Preparing the Bioanalyzer by decontaminating electrodes with chPD, one filled with 350 µl RNAseZap followed by one with 350 µl DEPC-H2O.
2. Preparing the ladder by denaturating it for 2 min at 70 °C.
3. Preparing the gel by spinning RNA 6000 Nano gel matrix in a spin column at 1500 g for 10 min. Stored aliquots of 65 µl at 4 °C can be used within one month.
4. Preparing the Gel-Dye-Mix by giving 1µl RNA 6000 Nano dye in 65 µl aliquot of gel. Vortexing and centrifuging for 10 min at 13000 g.
5. Minimum concentration of RNA samples 200 ng/µl. Diluting of samples with higher concentration if necessary.
6. Transfering 3 µl of each sample into cooled tubes and heating it up with an Eppendorf cycler for 2 min at 70 °C. Cooling of samples at 4 °C until usage.
7. Setting up the chip priming station (**Fig. 5**). Insert the base plate in position C, adjust the syringe clip to the upper position and place the syringe on the 1ml position.
8. For loading the chip, pipetting 9 µl of gel into the black marked well "G". Closing the chip station and pulling down the plunger of the syringe until it is hold by the clip (gel is equally pressed into the capillaries of the chip). Release the clip after 30s and slowly pulling the syringe back to its top position.
9. Appling 9 µl gel to each of the other two wells marked with "G".
10. Pipetting 5 µl RNA 6000 Nano Marker into all left 13 wells. The fluorescent marker serves for the assignment of samples through the algorithm.
11. Pipetting 1 µl of ladder into the corresponding well which serves as running control.
12. 12 samples can be measured at the same time, 1 µl each.
13. Avoiding air bubbles, vortexing the chip with the included IKA mixer for 1 min at 2400 rpm. Placing the chip within 5 min into the Bioanalyzer.
14. Measuring RIN with the "Eukaryot Total RNA" assay.
15. This protocol was also used and described in the submitted publication Tauber et al, 2022 [1].
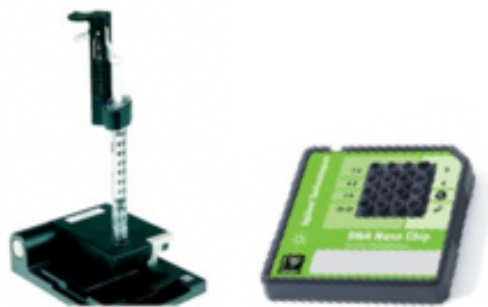
Figure 5: Illustration of the chip priming station. Attached syringe (left) and Agilent RNA Nano Chip (right) are displayed. Adapted from RNA 6000 Kit Handbook.

Measurement was performed according to the described protocol in 40 preselected tissue donors in grey matter of both brain regions. In each case a duplicate was obtained to establish mean RIN values. For postmortem brain tissue cut-off values of RIN ≥ 6 or even ≥ 3.95 are suggested in literature [146, 147]. In order to secure sufficient results in down-stream applications samples with the best RIN values were selected for the study population. This led to the exclusion of 14 donors (**Table 19**). RIN values included in the study population are listed in **Table 32, chapter 3.3.2**. The approach and selection of the RIN is taken from the publication Tauber et al., 2022 [1].

Table 19. RNA integrity values measured in exlcuded postmortem samples.

Brain region	Participant number	PD		Controls	
		H1/H1 (*n* = 6)	H2/H2 (*n* = 0)	H1/H1 (*n* = 8)	H2/H2 (*n* = 0)
Fusiform gyrus	1	-	-	2.5	-
	2	-	-	5.5	
	3	5.4	-	3.8	-
	4	2.7	-	1.9	-
	5	3.3	-	2.4	-
	6	2.2	-	2.4	-
	7	3.3	-	2.5	-
	8	2.2	-	2.4	-
Cerebellum	1	-	-	2.7	-
	2	-	-	5.0	
	2	6.1	-	4.4	-
	3	2.2	-	2.4	-
	4	2.5	-	2.5	-
	5	2.3	-	2.5	-
	6	2.3	-	3.3	-
	7	2.6	-	2.9	-
RIN values from brain samples of gyrus fusiformis and cerebellum from initially evaluated postmortem brain donors with *MAPT* haplotype H1/H1. Due to low RIN values these samples were excluded from further experiments in the context of quality control.					

2.3.2 Realtime-qPCR

Gene expression levels were quantified by quantitative real time Polymerase Chain Reaction (qPCR). PCR is a molecular biological tool to amplify enzymatically specific nucleic acid sequences. Standard PCR reaction takes place in three phases: Heating, annealing and amplification. DNA is denatured through heating and designed short sequences of nucleotides, termed primers, anneal to the one-strand target sequence. Next complementary DNA strands are synthesized by heat-stable Taq DNA Polymerases. This enzyme adds deoxyribonucleosides triphosphates (dNTPs) to the end of primers and extends the sequence. These steps are repeated in cycles leading to an exponential increase of DNA copies. Thereby, qPCR allows the determination of quantity of the sequence of interest within the sample.

2.3.2.1 cDNA synthesis

Template for qPCR is first strand complementary DNA (cDNA), which is synthesized from RNA with reverse transcriptase enzymes. cDNA was generated from total RNA of postmortem brain tissue using the iScriptTM cDNA Synthesis kit (Bio-Rad Laboratories, Inc., Hercules, USA). According to the manufacturers´ instructions the mastermix for the reverse transcription was prepared as the following: To the volume of exactly 1 µg of RNA, 4 µl iScript Reaction Mix, 1 µl iScript Reverse Transcriptase and DEPC water filling up to the total volume of 20 µl were added. The temperature protocol of the Thermocycler (Sensoquest) was the following: 5 min at 25 °C, 20 min at 46 °C, 1 min at 95 °C, 4 °C hold. cDNAs were stored afterwards at -20 °C until use. This protocol was also used and described in the submitted publication Tauber et al, 2022 [1].

2.3.2.2 Reaction assay for qPCR

The expression profile of one gene was determined within the study population in one qPCR run. All assays were performed using three technical replicates, an intercalibrated standard curve mix, and a non-template control as negative control. Each real-time qPCR was carried out with SYBR™ Select Master Mix for CFX (Applied Biosystems). This ready-made mix contained dye, AmpliTaq™ DNA Polymerase, dNTPs (2 mM), deoxyuridine triphosphate (dUTPs) (4 mM), heat-labile Uracil-DNA Glycosylase and buffer components. The reaction mix was thoroughly vortexed and filled in a 96-well plate with the final volume of 20 µl per well (**Table 21**). The plate was sealed with MicroAmp™ Optical Adhesive Film PCR (Applied Biosystems), centrifuged with Mini PCR plate spinner (Labnet International) at 500 g for 30 s, and processed with the StepOnePlus system (Applied Biosystems, Software Version 2.2.2). qPCR amplifications were performed with a standard cycling profile (**Table 20**). The sequences

of the human primers used for qPCR, listed from 5' to 3' end, are listed in **Table 7** and **8**. This protocol was also used and described in the submitted publication Tauber et al, 2022 [1].

Table 20. qPCR reaction mix and cycling profile for SYBR Green assay.

qPCR Mastermix per well (96 wells in total)	qPCR reaction volume per well for three technical repeats	qPCR cycling profile
10 µl SYBR Green Mastermix 6.8 µl DEPC water 1 µl Forward primer 1 µl Reverse primer + 20 % Error bonus	57 µl Mastermix 3.75 µl Template + 15 % Error bonus	95 ℃ – 10 min 95 ℃ – 15 sec (40 cycles) 60 ℃ – 1 min (40 cycles) 95 ℃ – 15 sec 60 ℃ – 1 min 4 ℃ - ∞

2.3.2.3   Primer specificity

Primer specificity was previously confirmed with 3% agarose gel electrophoresis (**Fig 6**). PCR reactions were performed in a 19 µl volume, containing 1 µl cDNA, 1 µL forward primer, 1 µL reverse primer, 10 µl Phire Hot Start II DNA Polymerase (Thermo Scientific), and 7 µl DEPC water. The cycling profile for amplification was the following: 98°C for 30 s, 40 cycles at 98°C for 10 s each, 72°C for 1 min, one cycle of 72°C for 2 min. Primers for *0N*, *1N* and *2N MAPT* were designed based on the publication of Spicakova et al. [148].

Protocol for 3% agarose gel electrophoresis

1. Mixing of 1.5 g agarose in 200 ml TEA Buffer (Sigma Aldrich, 20 ml TEA solution in 100 ml ddH20).
2. Boiling for dissolution in a microwave for 3 min.
3. Adding of 1 µl SYBR Safe DNA gel stain (Invitrogen).
4. Pouring the mix into a gel tray with the well comb in place.
5. Preparing samples by adding 2 µl Gel Loading Dye 6x Purple (BioLabs News England) to each PCR product.
6. Loading the gel with 2 µl of 100 bp DNA Ladder (250 ng/µl), and if necessary 5 µg of 1 kbp DNA Ladder (100 ng/µl) and 10 µl of each sample.
7. Running the gel at 110 V for 45 min with PowerPac Basic (Biorad).
8. Imaging with ChemiDocTM XRST and Ima.
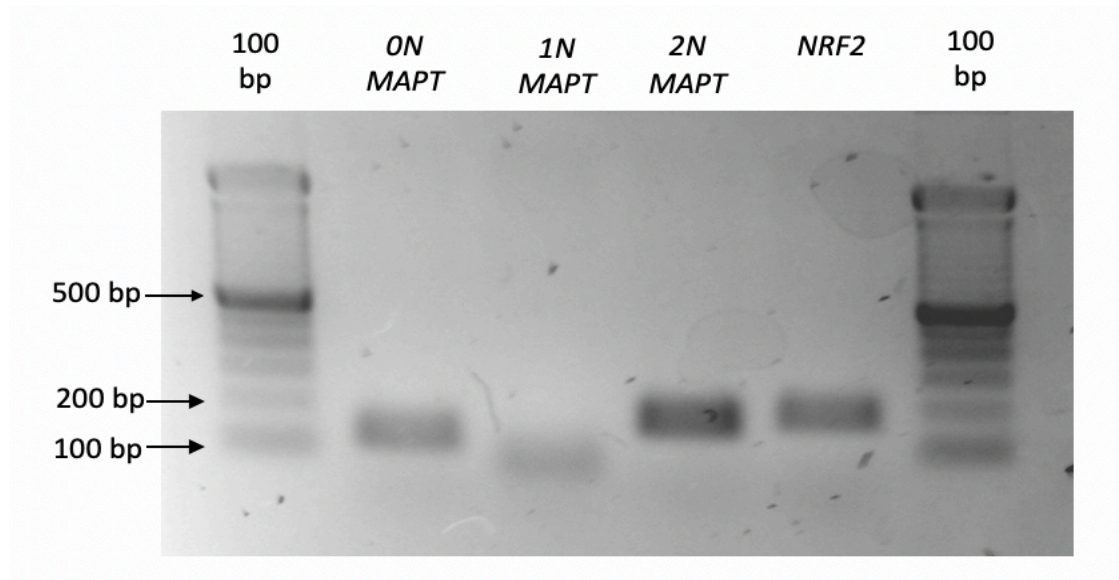
Figure 6. Example of gel electrophoresis for primer specificity. Primer specifity was confirmed previously by separation of PCR products by size and comparison to the DNA ladder. PCR products were consistent with the expected molecular size (0N *MAPT*, 120 bp; 1N *MAPT*, 68 bp; 2N *MAPT*, 159 bp; NRF2, 174 bp). Bp, base pairs.

2.4 Protein extraction and immunoblotting

2.4.1 Evaluation of an optimal protocol for protein extraction and immunoblotting

In order to establish a reliable protocol for protein extraction from postmortem brains, several preliminary experiments were conducted. At first, an attempt was made to reuse the lysates obtained during RNA extraction in Trizol. As described above, the organice phase contains proteins and organic solvents such as Trizol. This method would have had the advantage of obtaining RNA and protein from the exact same cell lysates for a direct comparison of the two. For this purpose, different protocols of protein extraction were tested aiming for high protein yield (> 1.5 µg/µl). Lysates obtained in Trizol from both brain regions and disease states were used. After establishing a suitable extraction protocol with the lysates in Trizol, preliminary tests for immunoblotting were carried out to find the best type of sample preparation, gel and blocking buffer, as well as selection and concentration of antibodies for tau. In summary, the proteins obtained from Trizol lysates were not optimally suited for a reliable semi-quantitative evaluation. Due to this, the method of sequential protein extraction from native brain tissue was used for the protein analysis of the main experiment. This protocol was adapted from the publication of Strauß et al. [149] and was also used and described in the submitted publication Tauber et al, 2022 [1]. Its main advantages were a constant quality of bands in Western blotting and the examination of different solubility forms of proteins.

Transfer of Trizol lysate out of Maxtract Tube

First, the transfer of lysate was carried out by pipetting through the wax layer of the Maxtraxt Tube, as suggested by some protocols. This turned out to be not ideal as wax was partly visible in the subsequent steps and impeded the elution of the protein pellet. Instead the maxtract tube was punctured with a needle at the bottom and the content was drawn out with a syringe resulting in a clear trizol phase.

Protein extraction from Trizol lysed brains

The residual solution of RNA extraction is Trizol lysed brain tissue and was starting material for the following protein extraction. Thus, mRNA and protein extraction were performed from the very same tissue sample. The protein extraction was modified from the publication by Hummon et al. [150] and initially proved to be a a suitable method.

Protocol for protein extraction from Trizol lysed brains

1. Transferring 300 µl Trizol reagent of thawed samples (residual of RNA extraction) to a new tube by punching a hole with a syringe into the Maxtract tube.
2. Adding of 90 µl 100% ethanol and mixing, incubation at RT for 3 min.
3. Centrifugation at 2000 g for 5 min.
4. Transfering of supernatant to a fresh 2 ml tube
5. Adding of 450 µl isopropanol and mix, incubation at RT for 10 min.
6. Centrifugation at 12000 g for 10 min at 4°C.
7. Discarding the supernatant, resuspending the protein pellet in 1ml wash buffer (0.3 M Guanidine hydrochloride (Sigma) in 95% ethanol) with mortar pestle tissue disruptor initially. Incubation at RT for 20 min.
8. Centrifugation at 7500 g for 5 min at 4°C.
9. Repeating step 7 twice.
10. Vortexing of the protein pellet in 2 ml of ethanol and incubation at RT for 20 min.
11. Centrifugation at 7500 g for 5 min at 4°C.
12. Removing the supernatant, air-drying the pellet for no more than 10 min. Pipetting the pellet up and down for resuspension in an appropriate volume (ca. 40 µl) of 1% SDS with 4x proteinase inhibitor (Roche). Incubation at RT for 5-10 min for complete dissolution.
13. Centrifugation at 17000 g for 10 min at 4°C prior to aliquoting and storage at -20°C.

Resuspension of protein pellet with RIPA Buffer and SDS

An important step of this protocol is the resuspension of the pellet after treatment with guanidine hydochloride (see protocol step 12). Two detergents were tested for this step. The protein extraction was performed with Radioimmunoprecipitation Assay (RIPA) . RIPA buffer is a commonly used cell lysis buffer which solubilizes proteins and contains amongst others 0.1% Sodium dodecyl sulfate (SDS) [151]. SDS is an anionic detergent which disrupts non-covalent bonds in proteins and denatures protein kinases and phosphatases [152, 153]. After three times washing with 0.3 M guanidine hydrochloride,

the pellet was eluted in RIPA Buffer with Protease inhibitor 1:1 (Roche). In a second run, sonification was tested as possible way of facilitating pellet elution. For this, pellets in elution buffer were sonificated for 6 x 30 s at 50% and shortly put in ice in between to avoid overheating. For resuspension with SDS a protocol with a higher concentration of SDS was tested. After three times washing with guanidine hydrochloride, another washing with ethanol and elution with 1% SDS in ddH$_2$O were carried out. To reach complete dissolution of the protein pellet, samples were homogenized with a mortar pestle tissue disruptor and incubated for 5-10 min at 50 °C.

Phosphatase Treatment with aPP and λPP

Two phosphatase enzymes were tested in advance. Phosphatase treatment with alkaline phosphatase (aPP) was evaluated on test samples. The protocol is based on the methods described in the study of Iovino et al. [154] with some modified steps. 20 µg protein was resuspended with four times amount of proteinase inhibitors and filled up to a volume of 30 µl. Followed by adding of 3 times aPP solution (0.3 U/µl) and a tenth volume of MgCl$_2$. Tubes were sealed with parafilm and phosphatase treatment was carried out overnight at 65°C. Lambda phosphatase (λPP) was tested on the very same protein samples. Main difference of this protocol is the gentle incubation period of 3h at 30°C. λPP revealed to be the best approach and all protein samples were dephosphorylated with λPP protocol.

Testing of Bis-Tris Gels

SDS-Polyacrylamide-Gel electrophoresis was applied for the separation of proteins according to molecular weight and charges [155]. Initially self-made gels were produced with the indicated components below (Table 21). The mixture for the resolving gel was applied to a gel caster system and isopropanol was added in order to smoothen the surface. After 30 min of hardening, isopropanol was discarded, the prepared 4% stacking gel was added, and a comb was inserted for 1 mm gel pockets. Ready gels were either immediately used for gel electrophoresis or stored in paper soaked with MPS Buffer at 4 °C for a period of maximum 2 weeks. Bis-Tris gels with 10% and 12% resolving gel were tested preliminary with an equal running time described below.

Table 21. Components of self-casted 12% Bis-Tris gel

Component	Resolving gel (12%)	Stacking gel (4%)
ddH$_2$O	2.67 ml	5.33 ml
1 M Bis-Tris pH 6.5	3.33 ml	3.33 ml
30% Acrylamide/bis solution	4.0 ml	1.33 ml
10% APS	50 µl	50 µl
Temed	5µl	10 µl

Testing of fluoresencet 3R and 4R tau antibodies

Testing Western blots were performed to ascertain the optimal concentration of antibodies, incubation and imaging parameters. In order to be able to analyse the individual tau forms separately, the idea was to use 3R and 4R tau antibodies with fluorescent secondary antibodies in addition to Dako total tau, which covers all 6 isoforms. For detection of 4R tau two antibodies were compared: 4R tau ms (Millipore, species type mouse) and 4R tau rb (Cosmobio, rabbit). In several blots with varying parameters (concentration of primary antibody 1:2000 or 1:333, increased incubation period, blocking buffer milk or rotiblock) 4R tau ms did not perform as sufficient as 4R tau rb antibody. In comparison to milk, best blocking conditions for both were reached with an incubation with 3x Rotiblock (Sigma) overnight. Despite many preliminary tests, the fluorescent antibodies did not work sufficiently consistently across all samples. Due to high background signal and high detection threshold of band signal the fluorescent antibodies were ultimately not used for data analysis (**Fig 12, chapter 3.2.4**).

Validation of housekeeping protein

Preliminary test blots were run to evaluate if the commonly used GAPDH is a suitable housekeeping protein in postmortem brain tissue. It proved to be equally stable detected among all kinds of protein extracts in all conditions and was therefore chosen as ideal reference for quantification.

2.4.2   Immunoblotting from Trizol lysed brains

Measurement of protein concentration

Protein concentration was determined by Bicinchoninic acid assay (BCA), in which the resulting protein-copper-complexes are photometrically measured and hereby the amount of protein can be quantified [156]. To establish a standard curve a MPER dilution series from 0-2000 µg/ml and a blank row of SDS were made. 5 µl of the respective diluted protein sample (1:5 with SDS) were loaded in triplicates on a 96-well cell culture plate. 100 µl of BCA assay were added to each well. The BCA assay dye stock solution (ThermoScientific) was mixed with one-part A reagent (Sodium carbonate, sodium bicarbonate, bicinchoninic acid and sodium tartrate in 0.1M sodium hydroxide) and 50-parts B reagent (4% cupric sulphate). After an incubation at 37°C for 30 min, the absorption was measured in a microplate reader at 562 nm. Concentration was analyzed by linear regression fit of the blank and standard curve. Measurement was performed in triplicates and the average of each triplicate was used.

Sample preparation and electrophoresis

Protein extracts were dephosphorylated using λ protein phosphatase (BioLabs) as pretreatment. Equal amounts of protein in SDS were incubated with 3 µl PMA Buffer (BioLabs), 3 µl MnCl2 and 2 µl λ protein

phosphatase (0,3 U/µl) for 3 h at 30°C. For sample preparation, 20 µg of protein samples together with 4 x XT loading buffer (BioRad) with 1:20 20x XT Reducing Agent (BioRad) were heated at 75°C and 400 rpm on a thermo shaker for 10 min for denaturation. For preparation of Tau Ladder, 3 µl tau ladder (Sigma) was mixed with 27 µl 1% SDS and 10 µl Tx. On each gel, all four subgroups (PD H1/H1, H2/H2; control H1/H1, H2/H2) were represented. Besides the protein extracts (40 µl), each gel contained the recombinant tau protein ladder (40 µl), protein standard ladder (5 µl) and a pool of all samples for intermembrane calibration. All western blots were run in a triplette. The gel was run on ice with cold MES Buffer at 75 V for 10 min, followed by 160 V for 125 min until the 25 kDA ladder reached the bottom of the gel.

Protocol for immunoblotting with Western Blot

1. Transferring of proteins from the SDS gel to membrane by the semi-dry blotting technique. Blotting paper (Wardman) and PVDF (BioRad) or fluorescence membrane (GE Healthcare) were cut and soaked in transfer buffer. Activation of membranes in methanol (Carl Roth) for 10 min. Transferring of SDS gel on membrane placed in a semi-dry blotting transfer chamber (BioRad). Placing of second blotting paper on top. Avoiding potential air bubbles. Electroblotting 1 A and 25 V for 40 min pulls negatively charged proteins from the gel onto the membrane.
2. Blocking of membranes 3 x Rotiblock (300 ml 10 x Rotiblock Stock in 1L dd H_2O) in order to prevent unspecific antibody binding. Incubation at RT for 1h under agitation.
3. Diluting of primary antibodies in 1x Rotiblock (100 ml 10 x Rotiblock Stock in 1L dd H_2O) and 20µl 10% NaN_3 in dd H_2O.
4. Incubation of membranes with primary antibodies at 4°C for 48h on a rocker (Edmund Bühler).
5. Washing of membranes three times in TBST (500ml 10x TBST stock solution with 2.5 ml TWEET in 4.5 L dd H_2O) to eliminate unbound antibody residuals.
6. Incubation of membranes with corresponding species-specific secondary antibody diluted in 1x Rotiblock for 2h at RT on a rocker (IKA). Secondary antibodies were either fluorescent marker (3R tau, 4R tau) or linked to the reporter enzyme peroxidase (DAKO total tau, GAPDH).
7. Washing of membranes three times in TBST.
8. For peroxidase-linked antibodies, covering of membranes in ECL solution (BioRad Clarity™ Western ECL Substrate 5 ml of each peroxide and luminol solution) and incubation for 10 min at RT.
9. Imaging of membranes with Odyssey Imaging System (LI-COR).
10. Stripping: Incubation of membranes in stripping buffer for 20 min at 50 °C. Washing intensively with TBST.
11. All concentrations, incubations of primary and secondary antibodies and imaging settings are listed under **Table 10, chapter 2.1.8**.

2.4.3   Sequential extraction and immunoblotting of the soluble and insoluble protein fraction

In conclusion to the preliminary experiments the sequential protein extraction was tested and chosen

to be the most suitable and informative extraction method. It was performed from the very same snap-frozen tissue blocks used for mRNA expression. Two different protein fractions (soluble, high salt-buffer soluble; insoluble, sarkosyl soluble) were obtained. The protocol for sequential protein extraction and immunoblotting was adapted from the publication of Strauß et al. [149] and was also used and described in the submitted publication Tauber et al, 2022 [1].

Protocol for sequential protein extraction from postmortem brain tissue

1. Preparation: Protein extraction performed under a fume hood (Wesemann). Scaling of tissue samples (maximum weight 100 mg). Potter-Elvehjem-Tissue-Grinder placed in an inced bucket.
2. Homogenizing of tissue samples in 4 volumes of high salt-buffer (50 mM Tris-HCl pH 7.4, 750 mM Sodium Chloride, 10 mM Sodium Fluoride, 5 mM EDTA, Sigma-Aldrich) supplemented with protease inhibitors (cOmplete, Roche Basel, Switzerland) and phosphatase inhibitors (PhoSTOP™, Roche). Incubation on ice for 20 min.
3. Ultracentrifugation at 100,000 g for 30 min at 4 °C in Ultra-Clear Centrifuge Tubes (Beckman Coulter™, Brea, USA). Reserving the supernatant as the high salt buffer soluble protein fraction.
4. Washing of the remaining pellet with 400 µl high salt-buffer and centrifugation at 100,000 g for 30 min at 4 °C.
5. Incubation of pellets overnight in 2 volumes of sarkosyl-buffer (High Salt Buffer supplemented with 1% sarkosyl (Sigma-Aldrich) in an end-over-end rotator.
6. Ultracentrifugation at 100,000 g for 30 min at 4 °C in Ultra-Clear Centrifuge Tubes. Collection of the supernatant as insoluble protein fraction (sarkosyl soluble fraction).
7. Protein concentrations were measured by Pierce™ Bicinchoninic Acid Assay Kit (Thermo Scientific) assay.

Sample preparation

As preliminary tested, the protein samples were stable after treatment with λPP (**Fig 13**). "For analysis of tau, equal amounts of protein were dephosphorylated using λ protein phosphatase (New England Biolabs, Ipswich, USA) at a final concentration of 0.3 U/µL for 3 h at 30 °C. 20 µg of protein were denatured with XT-Buffer (75 °C for 10 min) and loaded on (α-syn: 10%; tau: 12%) pre-made Bis-Tris Criterion polyacrylamide gels (Bio-Rad) and electrophoresis was run with MES running buffer (α-syn: 140 V for 70 min; tau: 160 V for 125 min)" [1].

Immunoblotting

"Proteins were blotted on a 0.2 µm PVDF membrane for 40 min at 1 A and 25 V with transfer buffer containing 20% methanol. Following the transfer, the membrane was fixed in 0.4% paraformaldehyde in PBS for 20 min. After washing 3x with PBS, the membrane was blocked with 5% skimmed milk (Sigma-Aldrich) in TBS supplemented with 0.05% Tween-20 (TBS-T, Sigma-Aldrich) for α-syn immunoblotting, and with 3x ROTI®Block (Carl Roth, Karlsruhe, Germany) for tau immunoblotting, for at least 1 h and then incubated overnight at 4° C with the primary antibodies. After washing, the membrane was

incubated with secondary peroxidase-linked antibodies for 2 h at room temperature. The blots were developed with Clarity Western ECL Substrate (Bio-Rad Laboratories) and the signal was detected with Odyssey Fc imaging system (LI-COR Biotechnology, Lincols, Netherlands). After imaging, the blots were analyzed with the Empiria StudioTM Software from LI-COR. Applied antibodies were diluted in 1x ROTI®Block in TBS-T (Carl Roth) (**Table 10**, **chapter 2.1.8**). For stripping, the membrane was rinsed with TBS-T after imaging and then incubated in stripping buffer for 20 min at 50°C. Thereafter, the membrane was washed thoroughly first with deionized water and then with TBS-T before blocking again with milk and 3x ROTI®Block respectively. The incubation with primary and secondary antibodies as well as the imaging was performed as described above. For each protein fraction a protein standard was generated by pooling some µl of all high salt buffer soluble or sarkosyl soluble samples. On every SDS gel, 20 µg of protein standard was loaded together with the samples of interest. All blots were run in triplets" [1].

2.5 Data analysis

2.5.1 Normalization strategy and data analysis of gene expression

For obtaining reliable results, a suitable normalization strategy in data analysis of qPCR is pivotal. This was guaranteed by two steps, an interrun-calibration and the determination of optimal reference genes.

Interrun-calibration

Data was referred to an inter-run calibrator represented on every qPCR plate which allows to compare data deriving from different qPCR plates. This calibrates for potential technical variances between different runs (i.e. variable efficiency of reagents). It consisted of a pool of all used cDNA samples (grey matter from cerebellum and gyrus fusiformis of all 26 donors) which was diluted to obtain a standard curve (dilution in steps of 5: Pool 50 ng, 10 ng, 2 ng, 0,4 ng, 0,08 ng).

Determination of optimal reference genes

To normalize the variability in expression levels, reference genes (RG) are used as internal control. RG are required to be stably expressed across all tested samples in any condition. For accurate normalization at least three control genes are generally suggested. Expression stability and optimal number of reference genes required for normalization of the respective setup were estimated using the geNorm algorithm (Biogazelle). The tested genes are ranked to their gene stability measure (M) which represents the mean pairwise variation of a gene with all the other reference genes tested within the samples [157]. The second indicator is the coefficient of variation (CV) of normalized reference gene relative quantities. A low M value and CV value is characterizing a stably expressed gene making it a

suitable RG. Proposed threshold values for appropriate gene stability in a heterogeneous setup, such as clinical biopsies or postmortem tissue, are means of the gene stability measure (M) < 1 and the coefficient of variation (CV) < 0.5 [158]. 17 candidate reference genes were evaluated previously in postmortem brain tissue (PD *n* = 6, control *n* = 6, Gf and Cbl). In this test 6 out of 15 genes passed *(PPIA, MRPS18S1, huUBQLN1, CTBP1, POLR2A, RPL22)*. However, these 6 genes did not prove to be stable expressed in the study population. In a second evaluation, genes which slightly missed the threshold value in first instance *(TBP, LUC7L2, GPBP1, HMBS)* and *ACTIN* and *GAPDH* were tested in the study population. The most stable reference genes were *TBP, ACTIN, GAPDH)* characterized by M = 1.037 and CV = 0.427 in both brain regions (**Table 22**) [1].

Table 22. Reference target stability assessed by geNorm analysis.

Brain region	Average gene stability measure	Average coefficient of variation
Cerebellum	0.782	0.331
Gyrus fusiformis	1.173	0.478
Both areas	1.037	0.427
Average gene stability measure and coefficient of variation for genes *ACTIN, GAPDH and TBP* in both brain regions were below the proposed thresholds for heterogeneous samples such as postmortem brain tissue.		

Analysis of gene expression

The RT-qPCR data were analyzed using the qBase+ 3.2 (Biogazelle). Cycle threshold values different > 0.5 among triplicates were removed from the analysis. Gene expression of target genes was normalized to the three most reliable reference genes (*ACTIN, GAPDH, TBP*) assessed by geNorm.

2.5.2 Normalization strategy and data analysis of protein expression

"Signals from every western blot were normalized, to the signal of the protein standard and to the signal from the reference protein of the same sample (soluble protein: GAPDH; insoluble protein: Revert™ 700 Total Protein Stain). Total tau was determined as the sum of the individual isoforms. Specific tau isoforms were identified by comparison to the recombinant tau ladder. Full length Western

Blots used for representative figures are displayed in **Fig 7 and 8**" [1].
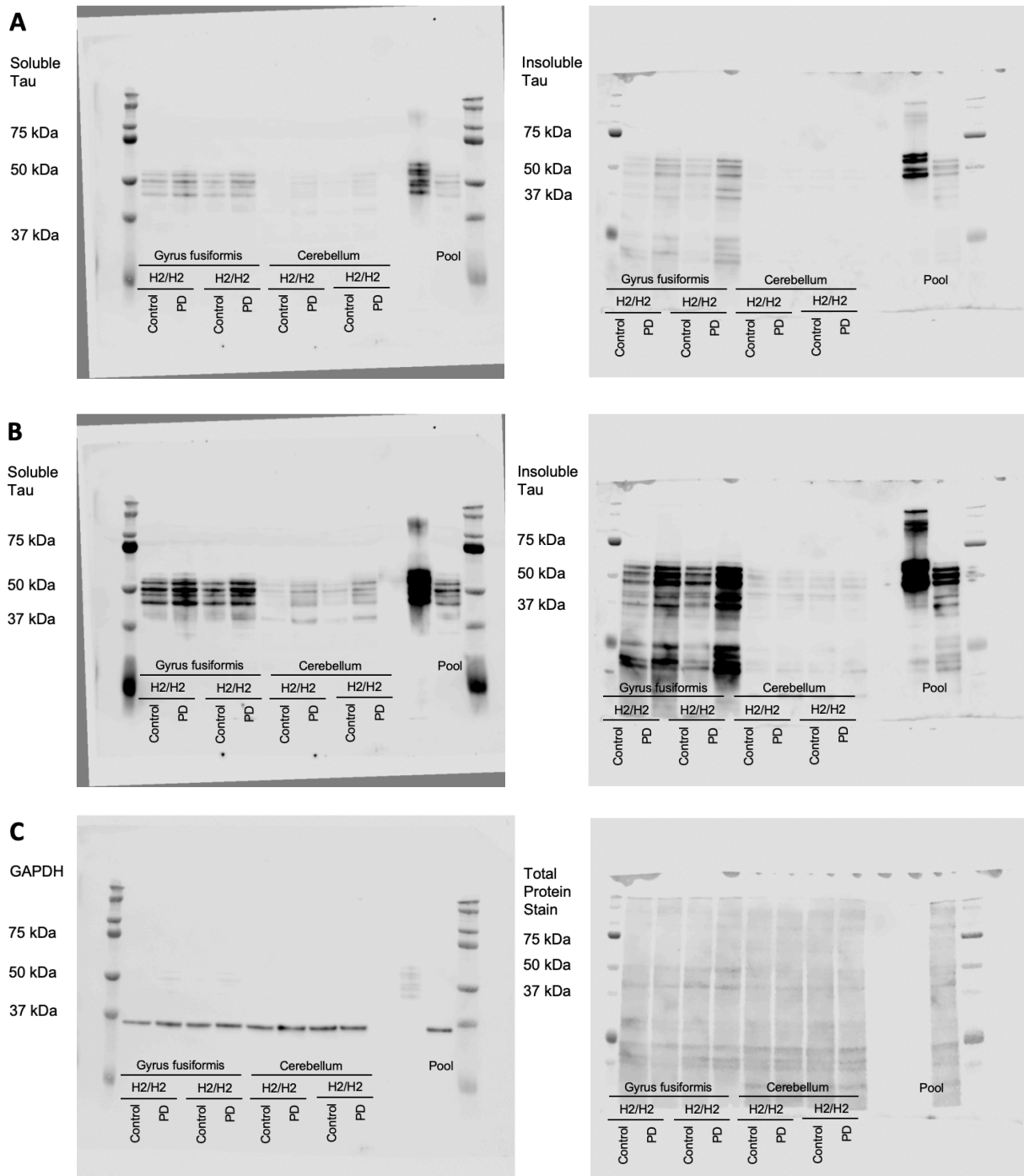
Figure 7. Full length Western blot from Figure 16 and 18. Western Blots probed with soluble tau protein fraction is displayed on the left side (Fig 16), insoluble tau on the right side (Fig 18). A) Lower exposed image of the Western Blots after staining with an antibody against tau (A0024, DAKO). (B) Higher exposed image of the Western blot after staining with an antibody against tau. (C) Image of the Western blot after staining with GAPDH (CB1001, Millipore) and Total Protein Stain (Revert™ 700, LI-COR) respectively. Representative images derive from postmortem brain donors with MAPT H1/H1 (C1, PD5) and H2/H2 (C9, PD14). Derived from Tauber et al., 2022 [1].
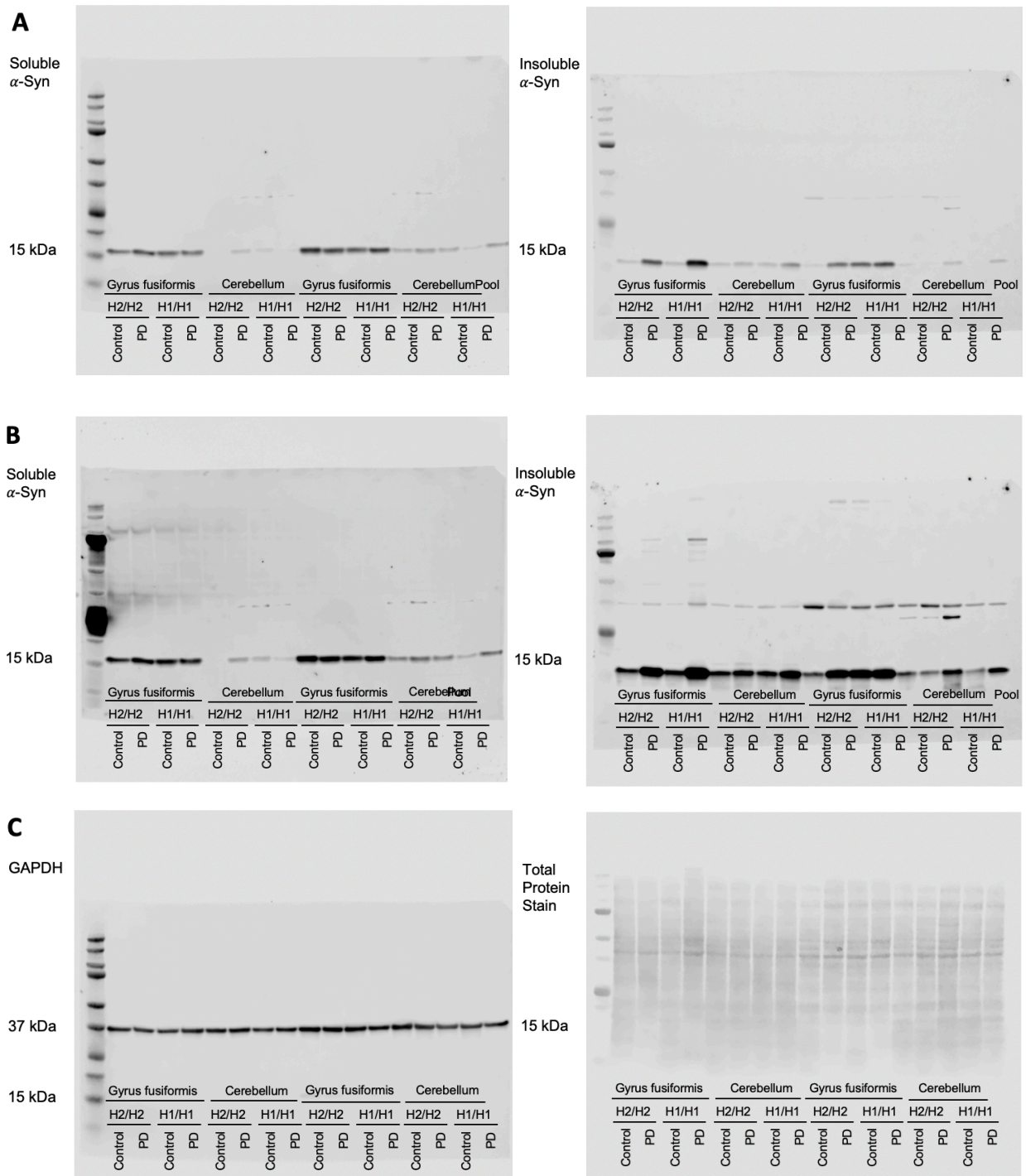
Figure 8. Full length Western blot from Figure 17. Western Blots probed with soluble α-Syn protein fraction is displayed on the left side, insoluble α-Syn on the right side. (A) Lower exposed image of the Western Blot probed with soluble protein fraction after staining with an antibody against α-Syn (2642S, Cell Signaling Technology). (B) Higher exposed image of the Western blot after staining with an antibody against α-Syn. ((C) Image of the Western blot after staining with GAPDH (CB1001, Millipore) and Total Protein Stain (Revert™ 700, LI-COR) respectively. Representative images derive from postmortem brain donors with *MAPT* H1/H1 (C1, PD5) and H2/H2 (C9, PD14) on the left side and *MAPT* H1/H1 (C6, PD4) and H2/H2 (C12, PD10) on the right side. Derived from Tauber et al., 2022 [1].

2.5.3 Statistics

"Statistical analysis was performed using Graphpad Prism 9.2.0 for Mac (GraphPad Software Inc., San Diego, CA, USA). For characterization of the study cohort, one-way ANOVA for quality markers such as age at death, mean RIN and mean postmortem interval was performed. For the prevalence of *MAPT* haplotypes within the study cohort a chi-squared test was conducted. For mRNA expression and protein level data, two-way ANOVA was conducted investigating the effect of disease (PD vs. control), of the *MAPT* haplotype (H1/H1 vs. H2/H2), and their interaction on the dependent variables. Correction for multiple testing was performed with Tukey´s *post hoc* test. Normality was assessed using Shapiro-Wilk test and homogeneity of variances was evaluated with Levene's test. Data was analyzed separately in gyrus fusiformis and cerebellum, as ratio of gyrus fusiformis to cerebellum, and ratio of *MAPT isoform/total MAPT*, tau isoform/total tau respectively. All pairwise comparisons were run with reported 95% confidence intervals and *P*-values were Bonferroni-adjusted. For all statistical tests the significance level was set to $P < 0.05$. Specifications are given in each figure and table legend. Data are presented as mean ± standard error, unless indicated otherwise" [1].

3 Results

3.1 Preliminary experiments regarding RNA

3.1.1 RNA degradation in postmortem human brain tissue due to treatment with TurboDNAse

The enzymatic elimination of genomic DNA using TurboDNAse was evaluated in RNA extracts of Luhmes cells, postmortem brain tissue of human donors and mice. Treatment of RNA extracts with TurboDNAse led to a 91.4% decrease of concentration (unpaired students' t-test, $P = 0.001$) in Luhmes cells compared to untreated RNA aliquots (**Fig 7, Table 23**). The same effect was observed in postmortem brain tissue of mice and human, but did not reach significane. Treatment with TurbDNAse did not influence purity ($A_{260/230}$) significantly in all samples.

Regarding RNA integrity, treated RNA samples of postmortem human brain tissue showed a significant decrease compared to untreated RNA extracts (unpaired students' t-test $P = 0.039$). This reflects a higher degradation of RNA in the treated extracts. However, no significant difference between treated and untreated RNA aliquots in RIN values was observed in Luhmes cells or postmortem brain of mice (**Fig 7, Table 23**).
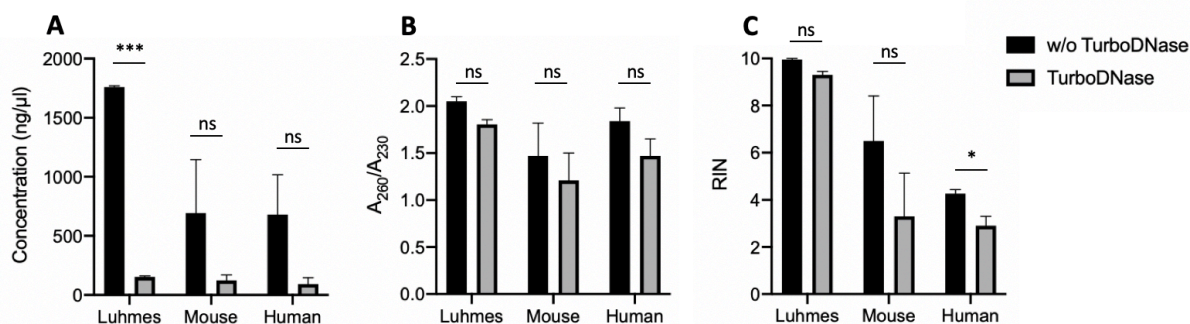
Figure 9. Influence of gDNA elimination with TurboDNase on RNA transcripts of Luhmes cells and postmortem brain tissue of mice and humans. The quality parameter concentration (A), purity A_{260}/A_{230} ratio (B) and RIN (C) were assessed. All RNA extractions were performed with the method after Chomczynski. Luhmes cells were used as positive control. Data are shown as mean ± SEM of Luhmes ($n = 2$), mouse ($n = 3$), human specimen ($n = 3$). *P-value*s were calculated using unpaired students' t-test. Abbreviation: RIN, RNA Integrity Number; w/o, without TurboDNAse; ***$P < 0.001$, *$P < 0.05$.

Table 23. Influence of gDNA elimination with TurboDNAse on RNA quality parameter.

Parameter	Sample	w/o TurboDNAse Mean ± SEM	with TurboDNAse Mean ± SEM	*P*-Value w/o vs with TurboDNAse
Concentration µg/µl	Luhmes ($n = 2$)	1760.3 ± 10.7	152.1 ± 8.3	**<0.0001**
	Mouse ($n = 3$)	693.8 ± 452.8	124.1 ± 44.7	0.278

	Human (n = 3)	681.2 ± 336.5	92.5 ± 55.3	0.159
A 260/230	Luhmes (n = 2)	2.05 ± 0.05	1.80 ± 0.05	0.074
	Mouse (n = 3)	1.47 ± 0.35	1.21 ± 0.29	0.597
	Human (n = 3)	1.84 ± 0.14	1.47 ± 0.18	0.180
RIN	Luhmes (n = 2)	9.95 ± 0.05	9.3 ± 0.20	0.054
	Mouse (n = 3)	6.50 ± 1.91	3.3 ± 1.80	0.294
	Human (n = 3)	4.26 ± 0.18	2.9 ± 0.40	**0.036**
P-values were calculated using unpaired students' t-test. Abbreviation: w/o, without TurboDNAse.				

In a second approach, EDTA and RNAse inhibitor were added to prevent any residual RNAse activity prior to the treatment with Turbo DNAse with no relevant improvement (**Table 24**).

Table 24. Influence on RNA integrity by additional EDTA and RNAse inhibitor in Turbo DNAse treated RNA extracts.

Tissue samples	RNA integrity	
	Treatment with Turbo DNAse w/o EDTA and RNAi	Treatment with Turbo DNAse with EDTA and RNAi
Luhmes cells [n = 1]	9.5	10.0
Mouse postmortem brain [n =1]	2.3	2.1
Human postmortem brain [n = 1]	2.4	2.2
RNA integrity values are displayed for RNA extracts in groups without (w/o) and with additional treatment with EDTA and RNAi before the incubation period of TurboDNAse enzyme. Abbreviation: RNAi, RNAse inhibitor. w/o, without; RNAi, RNAse inhibitor.		

3.1.2 Higher RNA yield with Trizol compared to RLT Lysis Buffer

Three methods of RNA extraction were compared in terms of RNA concentration, purity and integrity to evaluate the the most suitable one for postmortem brain tissue, Regarding RNA concentration, method 3) produced the highest RNA yield, followed by method 2) and method 1), but without a significant difference. Regarding RNA purity, all methods led to an equal sufficient A_{260}/A_{280} ratio demonstrating absence of protein in the lysates. However, the A_{260}/A_{230} was significantly decreased in method 2) compared to the other methods (one-way ANOVA, P = 0.025) showing contaminated RNA lysates. RIN did not differ between RNA extracted with different protocols (**Table 25**). The different ways of gDNA elimination spin column [method 1) and 2)] or solution [method 3)] did not influence the parameters of interest for RNA quality (**Table 25**).

Table 25. Influence of different RNA extraction methods on RNA quality and integrity.

Method	Postmortem human brain sample (n = 3)	RNA concentration [ng/µl]	A_{260}/A_{280}	A_{260}/A_{230}	RIN

1)	1	206.2	2.1	1.1	8.4
RNEasy+ Mini Kit	2	60.8	2.0	1.5	7.3
	3	142.5	2.0	1.6	6.8
	Mean ± SEM	136.5 ± 42.1	2.0 ± 0.03	1.4 ± 0.2	7.5 ± 0.5
2)	1	270.9	2.0	0.8	8.5
Method after Rodriguez-Lanetty	2	120.9	2.1	0.9	7.7
	3	137.6	2.1	0.7	6.8
	Mean ± SEM	176.5 ± 47.5	2.1 ± 0.03	0.8 ± 0.6	7.7 ± 0.5
3)	1	274.0	2.0	1.9	8.3
RNeasy+ Mini Universal Kit	2	160.5	2.0	1.2	7.6
	3	195.7	2.0	1.9	6.9
	Mean ± SEM	210.1 ± 33.5	2 ± 0.0	1.7 ± 0.2	7.6 ± 0.4
Groupwise comparison P-values		0.495	0.296	0.025	0.967
Parameters of interest were RNA intregrity and concentration, purity ratios A_{260}/A_{280} and A_{260}/A_{230} for RNA quality which were assessed in RNA extracted from postmortem human brain samples (n =3) with three different RNA extraction methods. For groupwise comparison between methods one-way ANOVA was used. A A_{260}/A_{280} ratio of > 2.0 proves the absence of protein contamination. A high A_{260}/A_{230} ratio reflects the purity of substances like Trizol. P-values were not significant for all parameters ($P > 0.05$).					

3.1.3 Investigation of the effect of the clean-up step of RNA extracts

Decontaminated RNA extracts with insufficient A_{260}/A_{230} ratio can be treated with an additional clean-up after extraction. Next, it was investigated wether the clean-up impairs RNA quality or qPCR performance. With the clean-up, RNA extracts showed less RNA yield (mean 39%), ean qual A_{260}/A_{280} ratio and signfiicantly improved A_{260}/A_{230} ratio (mean 1,13%, $P = 0.005$). There was no difference in qPCR performance of three reference genes between human brain RNA extracts with and without a clean-up step after RNA extraction (**Table 26**).

Table 26. Comparison of qPCR performance between RNA extracts with and without clean-up step in human postmortem brain samples.

Parameter	Treatment w/o clean-up	Treatment with clean-up	Groupwise comparison P – Value
Concentration [ng/μl]	694.5 ± 204	463.4 ± 303	0.438
A_{260}/A_{230}	2.0 ± 0.03	2.0 ± 0.03	0.778
A_{260}/A_{280}	1.0 ± 0.3	2.1 ± 0.03	**0.005**
PPIA [ct-value]	23.7 ± 0.66	22.9 ± 0.67	0.444
Human UBQLN1 [ct-value]	26.4 ± 0.53	26.1 ± 0.65	0.753
TRIM [ct-value]	31.6 ± 0.76	31.6 ± 0.77	0.980

Quality parameters are displayed of RNA extracts treatetd without and with clean-up step after RNA extraction of three tissue samples (n = 3). Parameters were measured using NanoDrop. Below Cycle threshold values are displayed for qPCR runs of the very same RNA extracts treated without (w/o) and with clean-up step. The gene expression of reference genes *PPIA, human UBQLN1* and *TRIM* were evaluated in triplets. *P*-values were calculated using unpaired student's-test. Data are presented as mean ± SEM. Abbreviation: Ct-value, cycle threshold value; w/o, without.

3.2 Preliminary experiments regarding protein

3.2.1 Comparison of detergents for resuspension of protein pellet after Trizol lysis

Following protein extraction with Trizol two detergents, SDS and RIPA buffer, were tested for resuspension of the protein pellet (human ctx-fg, *MAPT* H1/H1, n = 3). With RIPA, the pellet was hardly resuspendable and in a crumbly consistence despite intensive up and down pipetting. Protein concentration within a triplet measurement was not consistent and protein yield was often too low for immunoblotting. Additional sonification did not improvement protein concentration consistently (n = 2) (Table 27).

Table 27. Protein concentration after extraction with RIPA.

Sample (ctx-fg)	Without sonification (µg/µl)				With sonification (µg/µl)			
	Repeat measurement concentration			Mean ± SEM	Repeat measurement concentration			Mean ± SEM
PD1	2.08	0.97	0.90	1.32 ± 0.38	0.63	0.66	0.67	0.65 ± 0.01
PD2	0.45	0.45	0.94	0.61 ± 0.34	0.26	0.26	0.24	0.25 ± 0.13
PD3	2.45	1.41	0.41	1.42 ± 0.46	-	-	-	-
Control 1	0.50	0.54	0.49	0.51 ± 0.10	0.44	0.29	0.37	0.37 ± 0.05
Control 2	0.20	0.21	0.19	0.20 ± 0.10	0.19	0.27	0.22	0.23 ± 0.05
Control 3	0.38	0.38	0.33	0.36 ± 0.05	-	-	-	-

RNA extraction using RIPA Buffer with and without following sonification was compared in postmortem human brain samples. Concentration measurement was performed three times. Abbreviations: PD, Parkinson´s disease; RIPA, Radioimmunoprecipitation Assay.

In comparison to RIPA Buffer, SDS led to no differences in resuspending of the pellet, but a significantly higher yield of protein concentration (one-way ANOVA RIPA buffer without sonification vs. SDS Buffer, 0.7 ± 0.2 vs. 2.4 ± 0.2, P = 0.0004). SDS buffer was chosen for protein extraction from Trizol lysed brains because of the sufficient protein yield (Table 28).

Table 28. Protein concentration after extraction with SDS Buffer.

Sample (ctx-fg)	Repeat measurement concentration (µg/µl)			Mean ± SEM
PD1	2.22	2.14	1.92	2.15 ± 0.98
PD2	3.73	3.22	3.26	3.42 ± 0.17
PD3	2.47	3.01	2.68	2.72 ± 0.16
Control 1	1.98	1.82	1.85	1.88 ± 0.28
Control 2	1.82	1.79	1.89	1.83 ± 0.04

Control 3	2.02	2.19	2.74	2.32 ± 0.21

RNA extraction using SDS Buffer was performed in the very same postmortem human brain samples used for the RIPA test. Concentration measurement was performed three times. Abbreviations: PD, Parkinson´s disease; SDS, Sodiumdodecyl sulfate.

3.2.2 Comparison of different phosphatase treatments

Two different phosphatase treatments of Trizol protein lysates were tested (human ctx-fg, *MAPT* H1/H1, n = 4). Repeated Western Blots of aPP treated samples revealed multiple bands with lower molecular weights or smears which indicated degraded protein samples not suitable for quantification. Samples treated with λPP performed better with clearly separated protein bands compared to aPP. This was confirmed later on for lysates of the sequential protein extraction (human ctx-fg, *MAPT* H1/H1, n = 6). Basing on these findings, all protein samples were dephosphorylated with λPP protocol (**Fig 10**).
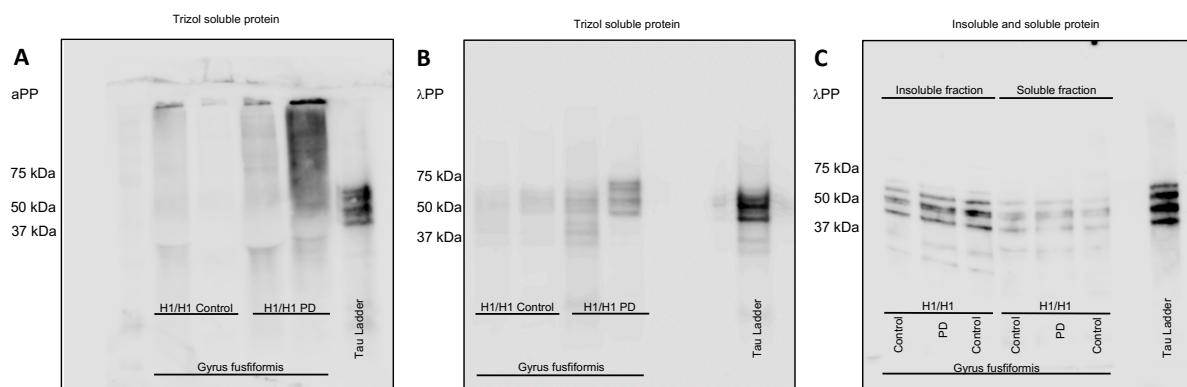
Figure 10. Exemplary total tau immunoblotting of postmortem brain samples treated with different protein phosphatases. Trizol lysed proteins were treated with (A) aPP and (B) λPP prior to immunoblotting with an antibody against total tau. (C) LPP was also tested on extracts from insoluble (sarkosyl soluble) and soluble (high salt buffer soluble) protein fraction for total tau blots. The very same trizol lysed proteins of postmortem brain samples (ctx-fg, *MAPT* H1/H1) were used for blots (A) and (B). For (C), samples from the same postmortem brain donors were sequentially extracted once again. aPP, alkaline phosphastase; λPP, lambda phosphatase; PD, Parkinson´s disease; kDa, kilo Dalton.

3.2.3 Comparison of different self-casted Bis-Tris gels

Two different concentrations of Bis-Tris in self-casted gelese were tested with regard to the question of how good the separation of the individual tau isoforms is. Gels containing 12% Bis-Tris showed a clearer separation for individual tau isoforms compared to 10% Bis-Tris gels, with no difference for the housekeeping protein GAPDH (**Fig 11**). Therefore, 12% Bis-Tris Gels were used for total tau protein levels.
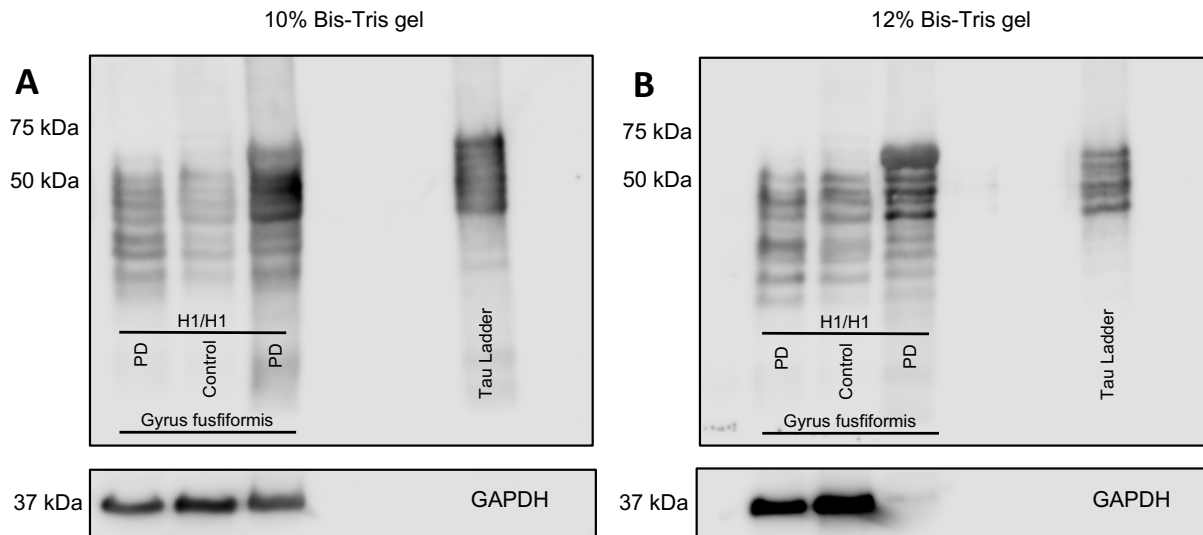
Figure 11. Comparison of 10% and 12% Bis-Tris gels probed with postmortem brain samples and total tau. Immunoblotting with an antibody against total tau in Trizol lysed proteins was tested with (A) 10% and (B) 12% Bis-Tris self-cast gels. The very same trizol lysed proteins of postmortem brain samples (human ctx-fg, *MAPT* H1/H1, n = 3) were used for blots (A) and (B). PD, Parkinson´s disease; kDa, kilo Dalton.

3.2.4   Poor performance of Trizol lysed proteins in tau immunoblotting

Tau immunoblotting with the Trizol extracted proteins showed poor performance (**Fig 12**). Firstly, the bands were smeared and made the identification of the tau isoforms by comparison with the recombinant tau ladder much more difficult. Secondly, bands of the housekeeping protein were visibly inhomogeneous between samples, which made normalisation of the protein values difficult. Third, fluorescent antibodies for 3R and 4R tau did not work sufficiently. Due to the inferior quality of the immunoblotting, the Trizol-based protein extraction protocol and simultaneous fluorescent antibodies were discarded. Instead sequential protein extraction was used for the main experiments.
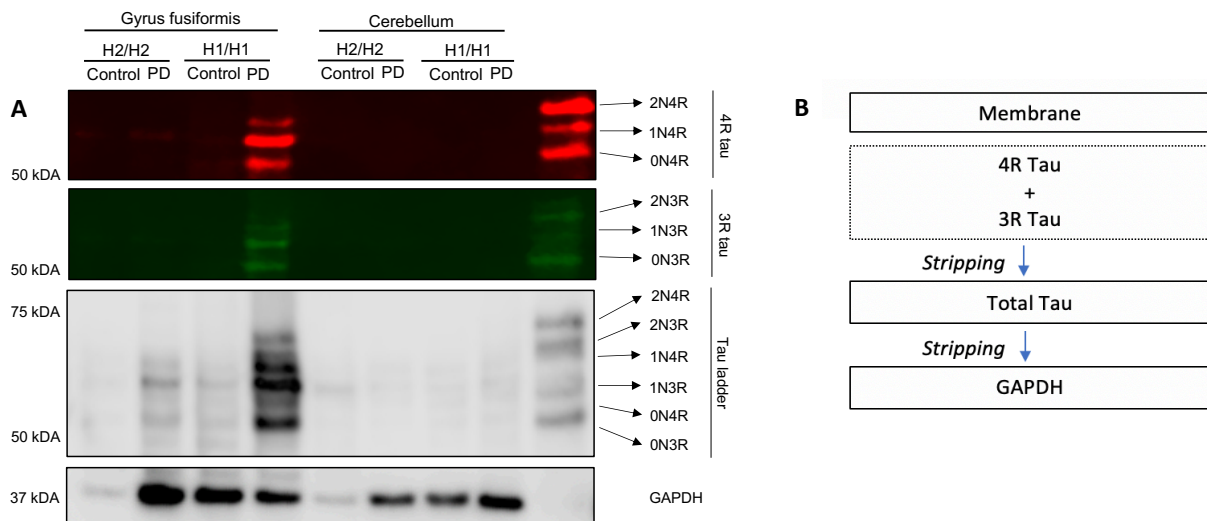
Figure 12. Exemplary Western Blot of Trizol soluble protein from postmortem brain of PD and controls. (A) Proteins extracted from gyrus fusiformis and cerebellum of donors representing subgroups according to *MAPT* haplotype (H1/H1 and H2/H2) and disease (PD, control) are represented. Fluorescent antibodies did not perform sufficiently with high background signal and weak signal from the individual tau isoforms. (B) Schematic overview of immunoblotting. After simultaneous detection of 4R and 3R tau isoforms with fluorescent secondary antibodies, Dako total tau was was applied followed by GAPDH as reference protein. For the latter, peroxidase-linked secondary antibodies were used. Fluorescent antibodies did not perform sufficiently and were not used for data analysis. Abbreviation: PD, Parkinson´s disease; kDa, kilo Dalton.

3.3 Selection of postmortem brain tissue and characteristics of study population

3.3.1 Selection of postmortem brain tissue and genotyping for *MAPT* haplotype

"A stepwise identification process of suitable donors and tissue samples was performed (**Fig 13**). A sample of postmortem brains, including 95 PD cases and 81 controls without neurodegenerative diseases, has been genotyped for the *MAPT* haplotype. The H1/H1 haplotype constellation was most frequent (70%), followed by H1/H2 (24%), and the rare H2/H2 haplotype (6%) (**Table 29**). In our sample, the PD disease status and the *MAPT* haplotype were not significantly associated. After exclusion of donors without sufficient brain tissue 115 donors were available. Next, brains with *MAPT* H1/H1 genotypes were matched for age and sex to the H2/H2 brains and RNA quality criteria were applied (RNA purity, concentration and integrity number). At the end of selection process 15% of the samples were included into the study" [1].
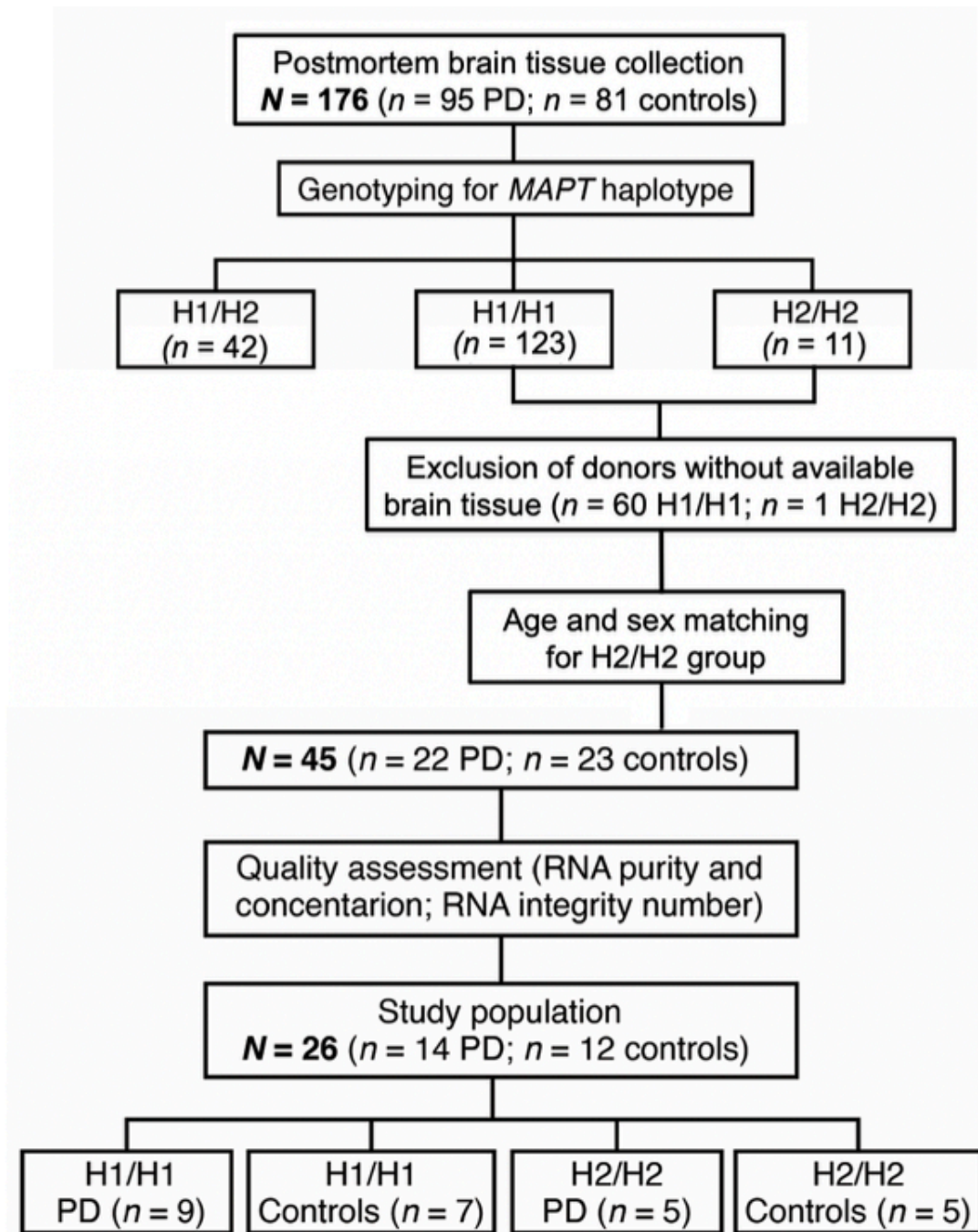
Figure 13. Schematic overview of processing and selection of human postmortem brain samples. Postmortem brain tissue of two brain regions were obtained from sporadic PD patients and healthy controls. After genotyping for *MAPT* haplotype and matching of donors, a tissue quality assessment was performed to select the most suitable tissue for the study population. Derived from Tauber et al., 2022 [1].

Table 29. Frequency of *MAPT* haplotypes determined in postmortem brain donors.

MAPT haplotype	Controls (*n* = 81)		PD (*n* = 95)		PD vs. Controls *P* – Value
H1/H1 [*n* (%)]	55	(67.9)	68	(71.6)	0.596
H1/H2 [*n* (%)]	21	(25.9)	21	(22.1)	0.553
H2/H2 [*n* (%)]	5	(6.2)	6	(6.3)	0.968
P-values were calculated using Chi-squared test. Derived from Tauber et al., 2022 [1].					

3.3.2   Characteristics of study population

The study population comprised 14 PD donors [*n* = 9 (64%) with *MAPT* H1/H1, *n* = 5 (36%) with H2/H2] and 12 controls (Con) [*n* = 7 (58%) with *MAPT* H1/H1, *n* = 5 (42%) with H2/H2) (**Fig 14**).

In terms of RNA quality, the RNA extracts of the study population showed a high purity (mean $A_{260/280}$ 1.98; mean $A_{260/230}$ 1.93) and sufficient concentration (mean 1.02 µg/µl). Regarding RNA integrity (RIN), values ranged from 2.8 – 8.1 in the study population. With respect to the limited sample size, especially within the *MAPT* H2/H2 cohort, four samples with slightly lower RIN values (PD 11 ctx-fg 3.1; PD 13 ctx-cbl 2.8; C8 ctx-cbl 3.2; C10 ctx-fg 2.8) were taken into account. Apart from that, all samples passed the RIN threshold proposed for brain tissue of 3.95 [147]. Subgroups did not differ in RIN values neither in fusiform gyrus (*P* = 0.704) nor in cerebellum (*P* = 0.107) with nearly equal RIN values (**Table 30**). Brain samples with insufficient high RIN values were excluded (**Table 19, chapter 2.3.1.2**).

Table 30. RNA integrity values measured in the study population.

Brain region	Participant number	PD		Controls		Groupwise comparison *P*–Value
		H1/H1 (*n* = 9)	H2/H2 (*n* = 5)	H1/H1 (*n* = 7)	H2/H2 (*n* = 5)	
Cortex of fusiform gyrus	1	5.1	5.8	8.8	6.1	
	2	6.4	3.1	6.4	6.5	
	3	5.5	4.8	5.7	2.8	
	4	5.0	6.7	5.5	5.6	
	5	6.1	6.4	5.9	6.5	
	6	4.5	-	4.4	-	
	7	8.5	-	6.2	-	
	8	6.6	-	-	-	
	9	6.5	-	-	-	
	Mean ± SEM	6.0 ± 0.4	5.4 ± 0.7	6.1 ± 0.5	5.5 ± 0.7	0.704
Cortex of cerebellum	1	7.0	5.6	8.3	3.2	
	2	7.0	2.8	7.4	7.0	
	3	7.0	5.1	5.5	4.6	
	4	6.5	2.8	5.0	4.6	
	5	3.3	6.1	4.9	5.5	
	6	5.4	-	4.4	-	
	7	8.1	-	6.8	-	
	8	6.3	-	-	-	
	9	6.2	-	-	-	

	Mean ± SEM	6.3 ± 0.4	4.5 ± 0.7	6.1 ± 0.6	5.0 ± 0.6	0.107

For groupwise comparison of the four subgroups according to *MAPT* haplotype and disease *P*-values were calculated using one-way ANOVA. Derived from Tauber et al., 2022 [1].

"The sex distribution was 15:11 female to male in the total study population and did not differ between the PD and control subgroups. There were no significant differences in demographic, clinical or neuropathologic characteristics between groups (**Table 31**). The severity of α-syn pathology in the PD cases was overall high with a median LBD Braak stage of 6 (of max. 6) in both H1/H1 and H2/H2 PD brains, with no difference between both groups. Presence of α-syn pathology was confirmed in the target brain region, i.e. ctx-fg, of most PD donors (86%) by semi-quantitative evaluation of Lewy inclusion pathology (Lewy neurites and LB) with no difference between H1/H1 and H2/H2 PD cases (**Table 31, Fig 3**). The pattern of LB pathology according to the McKeith classification [46] were distributed among PD cases as neocortical (n = 9), brain stem predominant (n = 2), limbical (n = 1) and limbical / neocortical (n = 1). Controls had neither clinical Parkinsonism during lifetime, nor any LB pathology. The burden of tau pathology was equally low with only two cases of AD Braak score III (H1/H1 PD n = 1; H2/H2 Con n = 1). Neither did subgroups of PD and controls differ significantly regarding concomitant AD pathology in terms of ß-amyloid neuritic plaques (CERAD score, **Table 31**). The cause of death was different with cluster of cardiovascular, pulmonary to cancer diseases (**Table 15, chapter 2.2.1**)" [1].

Table 31. Demographic, clinical and neuropathologic characteristics of postmortem brain donors.

		Controls		PD		Groupwise comparison *P*–value
		H1/H1 (*n* = 7)	H2/H2 (*n* = 5)	H1/H1 (*n* = 9)	H2/H2 (*n* = 5)	
Sex (female)	[*n* (%)]	4 (57.1)	4 (80.0)	4 (44.4)	3 (60.0)	0.380†
Age at death (y)	[*mean* (SD)]	74.0 (6.8)	81.0 (15.2)	74.2 (3.2)	77.6 (7.2)	0.433#
PMI (h)	[*mean* (SD)]	15.7 (7.5)	25.3 (9.2)	15.9 (5.9)	15.7 (9.1)	0.145#
Age at diagnosis (y)	[*mean* (SD)]	-	-	64.3 (6.5)	68.0 (7.8)	0.415‡
Disease duration (y)	[*mean* (SD)]	-	-	9.0 (7.4)	10.25 (3.4)	0.760‡
Lewy inclusion pathology in ctx-fg						0.536*
None	[*n* (%)]	-	-	1 (11.1)	1 (20.0)	
Few	[*n* (%)]	-	-	4 (44.4)	3 (60.0)	
Moderate	[*n* (%)]	-	-	3 (33.3)	-	
Many	[*n* (%)]	-	-	1 (11.1)	1 (20.0)	
LBD Braak stage						0.504*
1	[*n* (%)]	-	-	-	-	
2	[*n* (%)]	-	-	-	-	
3	[*n* (%)]	-	-	-	-	
4	[*n* (%)]	-	-	1 (11.1)	1 (16.7)	
5	[*n* (%)]	-	-	2 (22.2)	-	

6	[*n* (%)]	-		-		6	(66.7)	4	(83.3)	
LBD McKeith stage										0.472*
Neocortical	[*n* (%)]	-		-		5	(55.6)	4	(80.0)	
Limbical	[*n* (%)]	-		-		2	(22.2)	-		
Brain stem predominant	[*n* (%)]	-		-		1	(11.1)	1	(20.0)	
AD Braak and Braak stage										0.363*
I	[*n* (%)]	3	(42.9)	3	(75.0)	4	(44.4)	4	(80.0)	
II	[*n* (%)]	4	(57.1)	-		4	(44.4)	1	(20.0)	
III	[*n* (%)]	-		1	(25.0)	1	(11.1)	-		
IV	[*n* (%)]	-		-		-		-		
V	[*n* (%)]	-		-		-		-		
VI	[*n* (%)]	-		-		-		-		
CERAD score										0.280*
0	[*n* (%)]	7	(100.0)	5	(100.0)	8	(88.9)	3	(60.0)	
A	[*n* (%)]	-		-		-		2	(40.0)	
B	[*n* (%)]	-		-		1	(11.1)	-		
C	[*n* (%)]	-		-		-		-		

The LBD Braak stage and AD Braak and Braak stage each consist of six stages. The CERAD score describes neuritic Amyloid-ß plaques in levels of 0, A, B, C. Lewy inclusion pathology assessed semi-quantitatively the burden of Lewy neurites and Lewy Bodies in the target brain region cortex of fusiform gyrus. For groupwise comparison of the indicated subgroups according to *MAPT* haplotype and disease *P*-values were calculated by: *, Chi-squared test; #, one-way ANOVA; ‡, unpaired Student's *t*-test; †, Fisher's exact test. Abbreviation: AD, Alzheimer's disease; CERAD, The Consortium to Establish a Registry for Alzheimer's Disease; ctx-fg, cortex of fusiform gyrus; LBD, Lewy body disease; PD, Parkinson's disease; PMI, postmortem interval. Derived from Tauber et al., 2022 [1].

3.4 Analysis of the influence of the PD disease status and *MAPT* haplotype on mRNA expression

3.4.1 mRNA expression analysis of genes encoded in the *MAPT* locus

The influence of *MAPT* haplotype or disease on mRNA expression was investigated in a groupwise comparison according to haplotype and disease status in the study sample. Expression levels of 18 genes encoded in the *MAPT* inversion region were investigated (*total MAPT, MAPT transcripts, MAPT-AS1, KANSL1, KANSL1-AS1, NSF, PLEKHM1, STH*). Additionally, genes were looked at which are of interest in PD such as the synuclein genes *SNCA, SNCB, SNCG* and *NRF2*.

"As shown by qPCR, the PD disease status had no effect on the expression of *total MAPT, MAPT* splice variant transcripts *0N, 1N, 2N, 3R* and *4R MAPT, MAPT-AS1* and the synuclein genes *SNCA, SNCB* and *SNCG*, neither in ctx-fg nor in ctx-cbl (**Fig 14, Table 32**).

However, the *MAPT* haplotype did influence mRNA expression of *total MAPT*, with significantly higher expression in H1/H1 (~2-fold) compared to H2/H2 in ctx-fg (F (1.22) = 4.41, *P* = 0.047), but not in ctx-cbl (**Fig 14, Table 32**). For the *MAPT* splice variant transcripts, no significant differences were found between both haplotypes in both brain regions (**Table 32**).

The *MAPT* haplotype affected mRNA expression of several genes within the *MAPT* locus with no

observed influence of the PD disease. The transcription profile of *MAPT-antisense 1* (*MAPT-AS1*) was significantly lowered in H1/H1 (-2.6 fold) compared to H2/H2 (F (1.22) = 14.21, *P* = 0.001) in ctx-cbl, but not in ctx-fg (**Fig 14, Table 32**)" [1].

The mRNA expression of *KANSL1* was significantly altered by *MAPT* haplotypes with lower levels in in H1/H1 compared to H2/H2 carriers in both brain regions (ctx-fg: -2.29-fold, F (1.22) = 7.46, *P* = 0.012; ctx-cbl: -2.71-fold, F (1.22) = 17.88, *P* = 0.0003; **Fig 15, Table 32**). Likewise, a significant effect of haplotype on the corresponding antisense *KANSL1-AS1* was found with lower expression levels in H1/H1 compared to H2/H2 carriers (ctx-fg: -2.97-fold, F (1.22) = 7.94, *P* = 0.010; ctx-cbl: -3.61-fold, F (1.22) = 20.19, *P* = 0.0003). Expression of *KANSL1* and *KANSL1-AS1* were not found to be affected by disease or interaction haplotype × disease (**Fig 15, Table 32**).

The mRNA expression of *PLEKHM1*, *NSF* and *STH* within the *MAPT* inversion region were not statistically significant different neither between H1/H1 and H2/H2 carriers nor between control and PD cases in both brain regions (**Table 32**). The expression levels of all examined transcripts were not affected by an interaction haplotype × disease (two-way ANOVA, **Table 32**).

Figure 14 ... **expressi**... controls) ... brain sam... haplotype ...

status. Data are fold change (log2, mean ± SEM) relative to H2/H2 controls (H2/H2 C). Two-way ANOVA (haplotype × disease status), followed by Tukey´s post-hoc test: *$P < 0.05$; **$P < 0.01$. Derived from Tauber et al., 2022 [1].
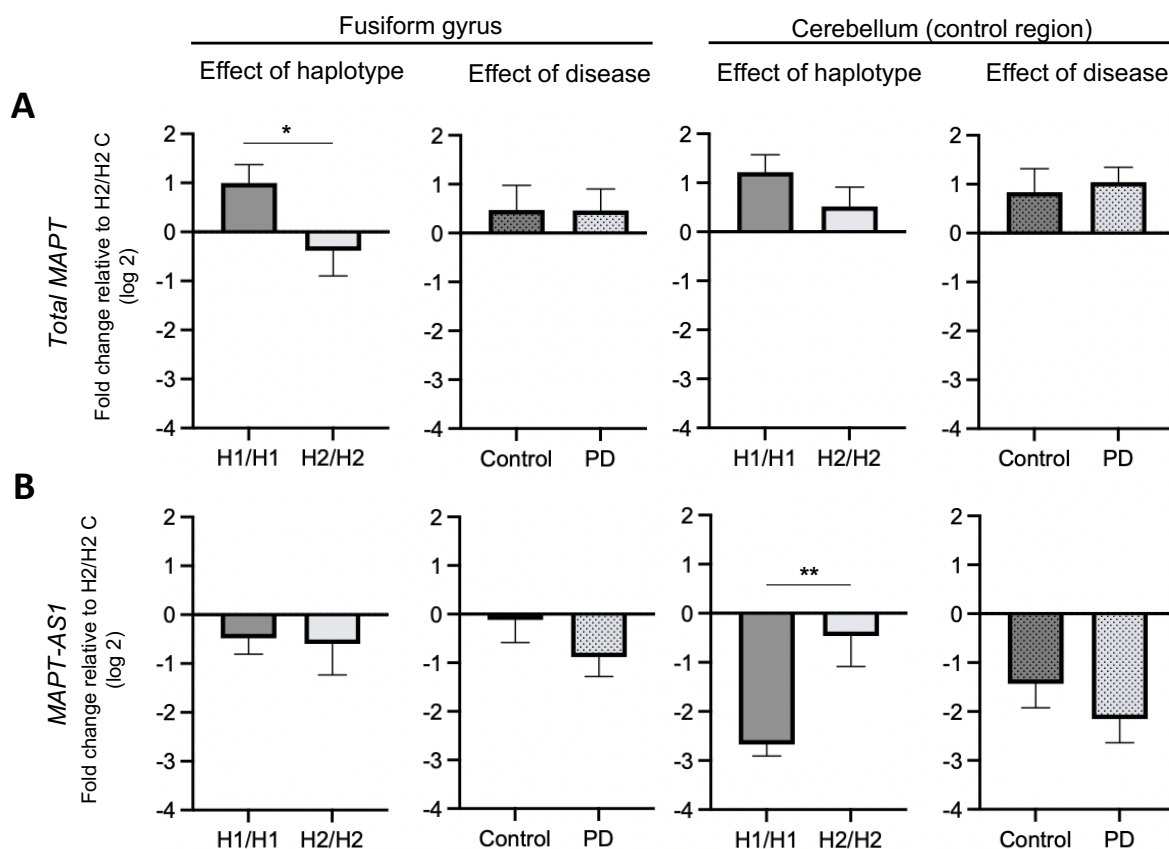
Figure 15. Influence of *MAPT* haplotype and disease status on *KANSL1 and KANSL1-AS1* mRNA expression. Bar graphs showing the effect of *MAPT* haplotype (H1/H1, H2/H2) and diseases status (PD, controls) on the mRNA expression of *KANSL1* (**A**) and *KANSL1-AS1* (**B**) measured by qPCR in human brain samples of the cortex of fusiform gyrus and the cortex of cerebellum. For analysis of the *MAPT* haplotype effects, PD cases and controls were combined, and vice versa for analysis of the disease status. Data are fold change (log2, mean ± SEM) relative to H2/H2 controls (H2/H2 C). Two-way ANOVA (haplotype × disease status), followed by Tukey´s post-hoc test: *$P < 0.05$; **$P < 0.01$. Derived from Tauber et al., 2022 [1].

3.4.2   mRNA expression analysis of *NRF2* and synuclein genes

Expectedly, the *MAPT* haplotype did not affect synuclein (*SNCA, SNCB, SNCG*) mRNA expression in both brain regions (**Table 32**). Also no difference was observed for mRNA expression of *NRF2* in both brain regions separately (**Table 32**). The expression levels of all examined transcripts were not affected by an interaction haplotype × disease (two-way ANOVA, **Table 32**).

Table 32. Effects of *MAPT* haplotype and disease status on expression of candidate mRNAs in human samples of fusiform gyrus and cerebellum.

mRNA	Brain region	Two-way ANOVA *P*-Value	Main effect of haplotype *P*-Value	Main effect of disease *P*-Value	Haplotype × disease *P*-Value	Direction of significant effect
Total MAPT	ctx-fg	0.182	**0.047**	0.741	0.404	H1/H1 > H2/H2
	ctx-cbl	0.365	0.147	0.698	0.725	-
0N MAPT	ctx-fg	0.367	0.546	0.331	0.123	-
	ctx-cbl	0.614	0.228	0.672	0.710	-
1N MAPT	ctx-fg	0.162	0.229	0.538	0.062	-
	ctx-cbl	0.534	0.151	0.988	0.910	-
2N MAPT	ctx-fg	0.540	0.781	0.651	0.671	-
	ctx-cbl	0.155	0.703	0.196	0.130	-
3R MAPT	ctx-fg	0.290	0.752	0.541	0.300	-
	ctx-cbl	0.614	0.938	0.244	0.743	-
4R MAPT	ctx-fg	0.338	0.896	0.809	0.369	-
	ctx-cbl	0.652	0.796	0.149	0.316	-
MAPT-AS1	ctx-fg	0.617	0.822	0.201	0.600	-
	ctx-cbl	**0.007**	**0.011**	0.272	0.647	H2/H2 > H1/H1
KANSL1	ctx-fg	0.058	**0.012**	0.793	0.250	H2/H2 > H1/H1
	ctx-cbl	**0.002**	**< 0.001**	0.380	0.224	H2/H2 > H1/H1
KANSL-AS1	ctx-fg	**0.040**	**0.010**	0.304	0.298	H2/H2 > H1/H1
	ctx-cbl	**0.003**	**< 0.001**	0.586	0.797	H2/H2 > H1/H1
STH	ctx-fg	0.594	0.728	0.813	0.568	-
	ctx-cbl	0.458	0.170	0.646	0.432	-
NSF	ctx-fg	0.745	0.285	0.615	0.953	-
	ctx-cbl	0.822	0.442	0.618	0.915	-
PLEKHM1	ctx-fg	0.487	0.544	0.162	0.535	-
	ctx-cbl	0.497	0.467	0.519	0.101	-
NRF2	ctx-fg	0.325	0.734	0.297	0.1033	-
	ctx-cbl	0.577	0.754	0.428	0.212	-
SNCA	ctx-fg	0.640	0.777	0.214	0.661	-
	ctx-cbl	0.730	0.533	0.679	0.438	-
SNCB	ctx-fg	0.325	0.242	0.159	0.874	-
	ctx-cbl	0.388	0.488	0.915	0.143	-
SNCG	ctx-fg	0.839	0.768	0.407	0.753	-
	ctx-cbl	0.916	0.556	0.923	0.626	-

Main effect of haplotype was analyzed by comparison of H1/H1 (Controls + PD) vs. H2/H2 (Controls + PD). Main effect of disease was analyzed by comparison of PD (H1/H1+H2/H2) vs Controls (H1/H1+H2/H2). The interaction haplotype × disease examined the relationship between the independent variables (haplotype + disease) on the dependent variable of mRNA expression. *P*-values were calculated using two-way ANOVA followed by Tukey´s multiple comparisons test. Abbreviation: ctx-fg, cortex of fusiform gyrus; ctx-cbl, cerebellum. Derived from Tauber et al., 2022 [1].

3.4.3 Proportion of N- and R-terminal variants of *MAPT* transcripts relative to total *MAPT*

Next, we aimed to explore whether *MAPT* haplotype or disease influence the expression of *MAPT* splice variant transcripts relative to *total MAPT*. In this analysis, only trends in the proportions of *MAPT* transcripts were apparent between groups in both analyzed brain regions, which did not reach significance in all comparisons (Table 33) [1].

Table 33. Proportion of *MAPT* splice variant mRNA transcripts relative to total *MAPT* in conditions defined by *MAPT* haplotype and disease status.

MAPT transcript	Controls		PD		Two-way ANOVA		
	H1/H1	H2/H2	H1/H1	H2/H2	Main effect of haplotype *P*-Value	Main effect of disease *P*-Value	Haplotype × disease *P*-Value
ctx-fg							
0N / total MAPT (%)	35 ± 18	42 ± 18	35 ± 17	50 ± 42	0.664	0.865	0.865
1N / total MAPT (%)	32 ± 20	24 ± 14	40 ± 17	4 ± 3	0.230	0.743	0.427
2N / total MAPT (%)	33 ± 32	34 ± 33	25 ± 22	46 ± 43	0.721	0.954	0.754
ctx-cbl							
0N / total MAPT (%)	31 ± 7	29 ± 8	34 ± 2	29 ± 5	0.592	0.794	0.729
1N / total MAPT (%)	28 ± 4	29 ± 8	36 ± 2	28 ± 7	0.536	0.538	0.447
2N / total MAPT (%)	41 ± 10	42 ± 11	30 ± 3	43 ± 4	0.426	0.553	0.453
ctx-fg							
3R / total MAPT (%)	35 ± 31	42 ± 19	34 ± 29	34 ± 31	0.910	0.902	0.921
4R / total MAPT (%)	65 ± 50	58 ± 20	66 ± 18	66 ± 31	0.907	0.898	0.919
ctx-cbl							
3R / total MAPT (%)	45 ± 18	90 ± 34	54 ± 14	47 ± 22	0.823	0.870	0.829
4R / total MAPT (%)	55 ± 47	10 ± 9	46 ± 12	53 ± 28	0.610	0.496	0.473

For groupwise comparison results were combined according to *MAPT* haplotype and disease status. *P*-values were calculated using two-way ANOVA followed by Tukey´s multiple comparisons test. Main effect of haplotype was analyzed by comparison of H1/H1 (Controls + PD) vs. H2/H2 (Controls + PD). Main effect of disease was analyzed by comparison of PD (H1/H1+H2/H2) vs Controls (H1/H1+H2/H2). The interaction haplotype × disease examined the relationship between the independent variables (haplotype + disease) on the dependent variable of proportions of *MAPT* transcripts. Data are mean ± SEM. Statistic analysis were not significant for all parameters (*P* > 0.05). Derived from Tauber et al., 2022 [1].

3.4.4 Comparison of gene expression between brain regions

Further, the regional gene expression was evaluated by relating expression levels in ctx-fg to ctx-fg in each specimen. Altogether, no significant differences were observed in all comparisons (Table 34) [1].

Table 34. Expression of candidate mRNAs in human samples of fusiformis gyrus compared to cerebellum.

Transcript	mRNA levels ctx-fg vs. ctx-cbl Mean ± SEM				Two-way ANOVA		
	Controls		PD				
	H1/H1	H2/H2	H1/H1	H2/H2	Main effect of haplotype *P*-Value	Main effect of disease *P*-Value	Haplotype × disease *P*-Value

Total MAPT	-0.04 ± 0.16	0.15 ± 0.32	0.17 ± 0.14	-0.40 ± 0.18	0.342	0.415	0.067
0N MAPT	-0.33 ± 0.35	0.48 ± 0.25	-0.02 ± 0.11	0.01 ± 0.09	0.296	0.748	0.112
1N MAPT	-0.14 ± 0.22	0.25 ± 0.32	0.06 ± 0.13	-0.15 ± 0.20	0.667	0.643	0.172
2N MAPT	-0.62 ± 0.52	0.42 ± 0.53	0.44 ± 0.20	0.34 ± 0.18	0.245	0.220	0.162
3R MAPT	-0.09 ± 0.44	0.21 ± 0.25	0.36 ± 0.09	0.13 ± 0.11	0.895	0.512	0.349
4R MAPT	0.14 ± 0.41	0.43 ± 0.37	0.43 ± 0.37	0.24 ± 0.28	0.823	0.593	0.264
MAPT-AS1	0.29 ± 0.35	-0.39 ± 0.30	0.25 ± 0.12	-0.47 ± 0.21	0.182	0.876	0.953
KANSL1	0.12 ± 0.19	-0.05 ± 0.22	0.03 ± 0.15	-0.18 ± 0.24	0.346	0.592	0.907
KANSL1-AS1	0.09 ± 0.22	-0.06 ± 0.36	0.16 ± 0.09	-0.36 ± 0.25	0.128	0.597	0.340
STH	0.13 ± 0.15	0.01 ± 0.32	-0.02 ± 0.11	-0.15 ± 0.23	0.438	0.513	0.978
PLEKHM1	0.27 ± 0.21	-0.08 ± 0.27	-0.06 ± 0.17	-0.19 ± 0.22	0.285	0.336	0.616
NSF	0.07 ± 0.18	-0.05 ± 0.21	0.06 ± 0.13	-0.15 ± 0.2	0.343	0.763	0.789
NRF2	0.02 ± 0.17	-0.01 ± 0.24	0.06 ± 0.12	-0.13 ± 0.21	0.522	0.798	0.655
SNCA	0.15 ± 0.16	0..06 ± 0.21	-0.06 ± 0.10	-0.16 ± 0.23	0.589	0.208	0.998
SNCB	0.24 ± 0.31	0.41 ± 0.35	-0.56 ± 0.38	0.27 ± 0.10	0.177	0.204	0.372
SNCG	0.03 ± 0.18	0.18 ± 0.36	-0.14 ± 0.20	0.03 ± 0.30	0.541	0.530	0.946

For the comparison of gene expression between the brain regions, the difference in mRNA levels between gyrus fusiformis and cerebellum were calculated. For groupwise comparison of these differences results were combined according to *MAPT* haplotype and disease status. *P*-values were calculated using two-way ANOVA followed by Tukey´s multiple comparisons test and were not significant for all parameters (*P* > 0.05). Abbreviation: ctx-fg, cortex of fusiform gyrus; ctx-cbl, cortex of cerebellum. Derived from Tauber et al., 2022 [1].

3.5 Analysis of the influence of the PD disease status and MAPT haplotype on soluble and insoluble protein levels of tau and α-syn

### 3.5.1 Soluble protein levels of tau and α-syn in postmortem brain

Having investigated the mRNA expression, we were interested on how different *MAPT* haplotypes and disease influence the protein level of tau, tau isoforms and α-syn in the very same tissue samples (**Table 35**). Protein levels of total tau, its isoforms, or α-syn in the sarkosyl-soluble protein fraction did not differ when analyzed in terms of disease, *MAPT* haplotypes or interaction in both analyzed brain regions (**Fig 16, Fig 17 A, Table 35**) [1].

Table 35. Effects of *MAPT* haplotype and disease status on levels of tau isoforms and α-syn in the soluble protein *fraction* in human samples of fusiform gyrus and cerebellum.

Protein fraction	Brain region	Two-way ANOVA *P*-Value	Main effect of haplotype *P*-Value	Main effect of disease *P*-Value	Haplotype × disease *P*-Value	Direction of significant effect
α-syn	ctx-fg	0.830	0.595	0.511	0.899	-
	ctx-cbl	0.926	0.563	0.946	0.790	-
Total tau	ctx-fg	0.737	0.279	0.877	0.908	-
	ctx-cbl	0.285	0.415	0.875	0.077	-
0N3R tau	ctx-fg	0.312	0.101	0.406	0.734	-
	ctx-cbl	0.207	0.207	0.150	0.205	-
0N4R tau	ctx-fg	0.341	0.103	0.479	0.724	-
	ctx-cbl	0.301	0.176	0.332	0.251	-

1N3R tau	ctx-fg	0.308	0.093	0.455	0.721	-
	ctx-cbl	0.412	0.223	0.519	0.263	-
1N4R tau	ctx-fg	0.446	0.145	0.552	0.700	-
	ctx-cbl	0.480	0.898	0.919	0.132	-
2N3R tau	ctx-fg	0.538	0.653	0.184	0.551	-
	ctx-cbl	0.581	0.251	0.574	0.610	-
2N4R tau	ctx-fg	0.709	0.316	0.607	0.749	-
	ctx-cbl	0.072	0.569	0.482	0.052	-

Main effect of haplotype was analyzed by comparison of H1/H1 (Controls + PD) vs. H2/H2 (Controls + PD). Main effect of disease was analyzed by comparison of PD (H1/H1+H2/H2) vs Controls (H1/H1+H2/H2). The interaction haplotype × disease examined the relationship between the independent variables (haplotype + disease) on the dependent variable of protein levels. *P*-values were calculated using two-way ANOVA followed by Tukey´s multiple comparisons test. Abbreviation: ctx-fg, cortex of fusiform gyrus; ctx-cbl, cerebellum. Derived from Tauber et al., 2022 [1].
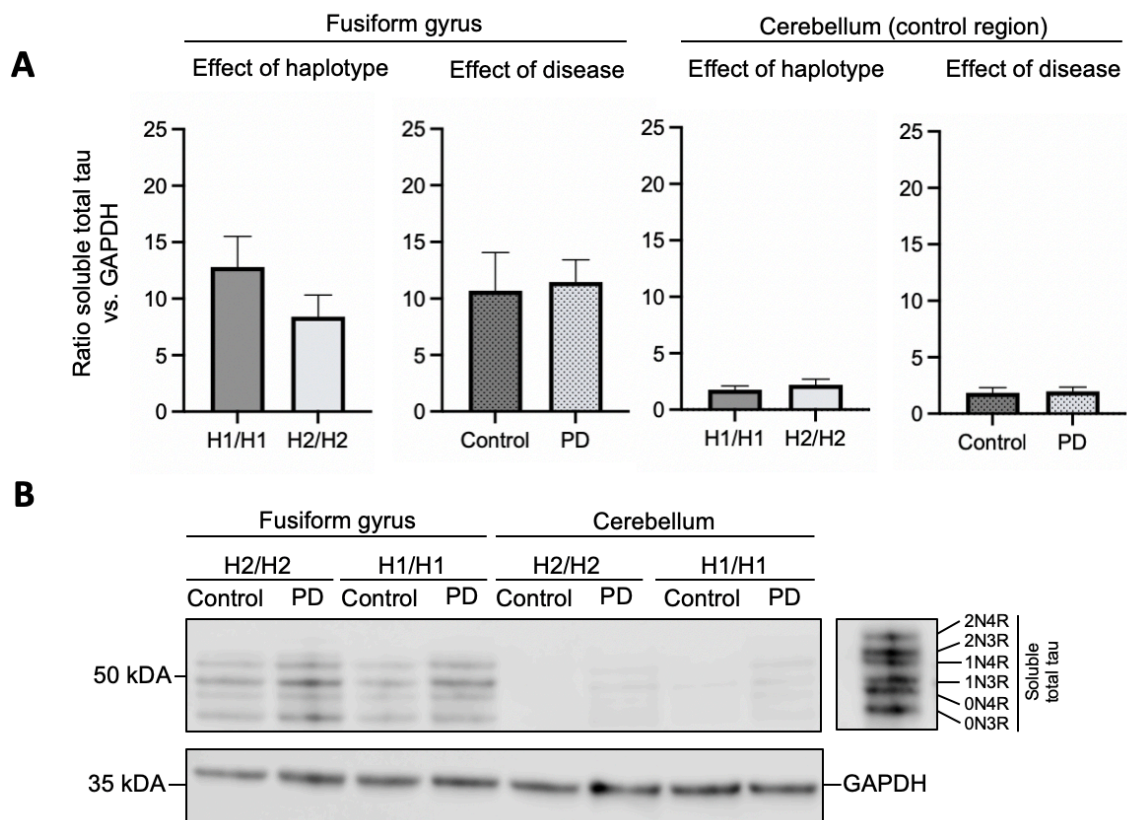
Figure 16. Effect of *MAPT* haplotype and disease status on soluble tau protein levels. (**A**) Bar graphs showing the effect of *MAPT* haplotypes (H1/H1, H2/H2) and diseases status (PD, control) on soluble total tau protein levels in human brain samples of cortex of fusiform gyrus and the cortex of cerebellum. For analysis of the *MAPT* haplotype effects, PD cases and controls were combined, and vice versa for analysis of the disease status. Data are protein quantity (mean ± SEM) relative to GAPDH and normalized to an inter-run calibration consisting of pooled protein samples. Two-way ANOVA (haplotype × disease status) showed no significant group differences. (**B**) Representative Western blots for soluble total tau with GAPDH as reference protein. The six tau isoforms were identified by

comparison to a recombinant tau ladder. Full length Western blots are shown in **Fig 7**. Derived from Tauber et al., 2022 [1].
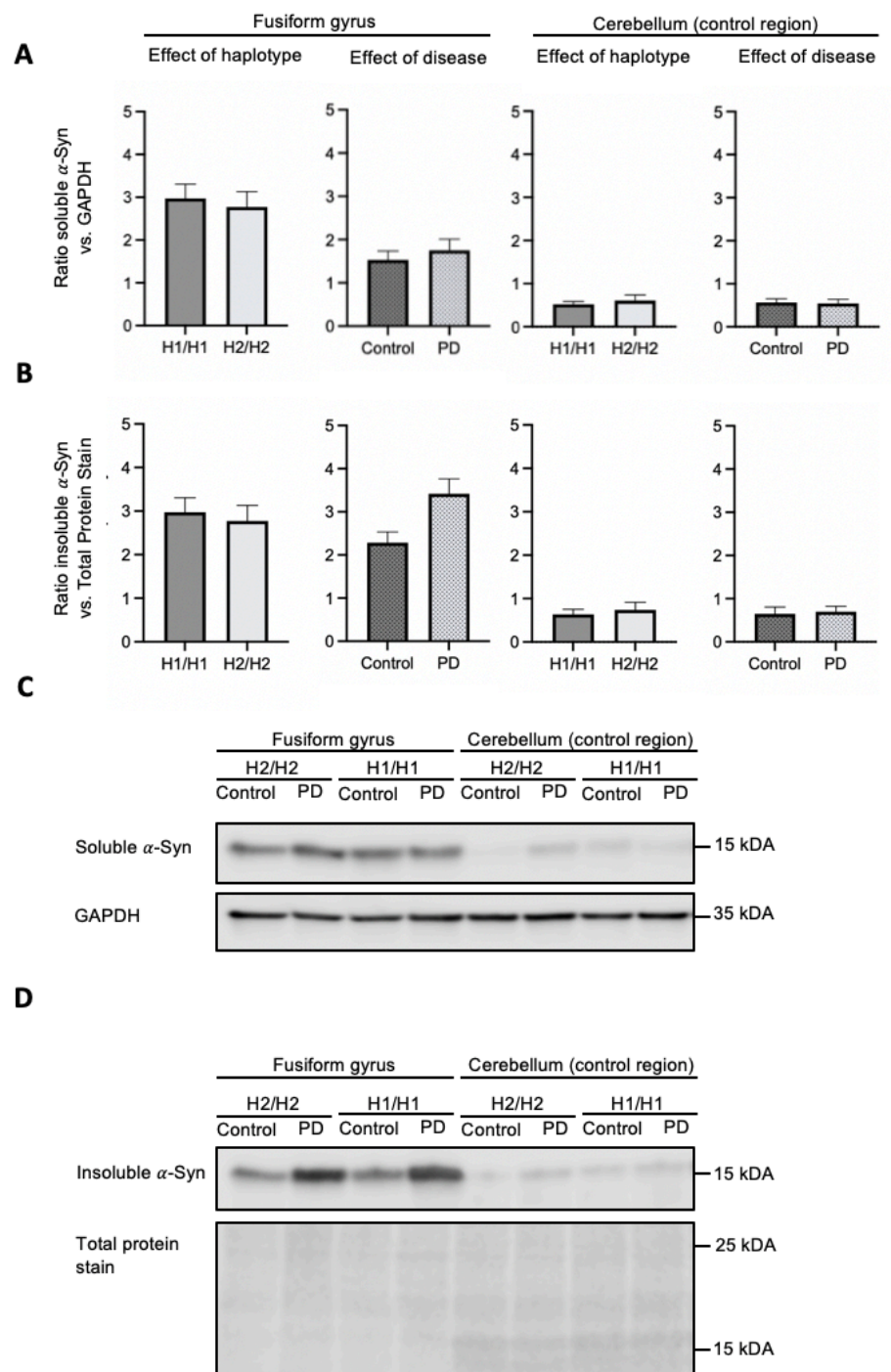
Figure 17. Influence of *MAPT* haplotype and disease status on soluble and insoluble α-synuclein protein levels. Bar graphs showing the effect of *MAPT* haplotypes (H1/H1, H2/H2) and diseases status (PD, control) on protein levels of soluble (**A**) and insoluble (**B**) α-synuclein (α-Syn) in human brain samples of the cortex of fusiform gyrus and the cortex of cerebellum. For analysis of the *MAPT* haplotype effects, PD cases and controls were combined, and vice versa for analysis of the disease status. Data are protein quantity (mean ± SEM) relative to GAPDH and normalized to an inter-run calibration consisting of pooled protein samples. Two-way ANOVA (haplotype × disease status), followed by Tukey´s post-hoc test: *$P < 0.05$. (**C, D**) Representative Western blot for soluble (**C**) and insoluble (**D**)

α-Syn with GAPDH (**C**) and Total Protein Stain (**D**) as reference. Full length Western blots are shown in **Fig 8**. Derived from Tauber et al., 2022 [1].

3.5.2 Insoluble protein levels of tau and α-syn in postmortem brain

"In the insoluble protein levels of α-syn were significantly elevated in PD compared to controls in ctx-fg (PD vs. Con 3.4 ± 0.3 vs. 2.3 ± 0.2, F (1.22) = 5.69, P = 0.026, **Fig 17B, Table 36**). This effect was independent of the *MAPT* haplotype and not present in the reference region cerebellum.

The PD also significantly increased insoluble levels of 0N3R and 1N4R tau isoforms compared to controls in ctx-fg (0N3R tau: 4.2 ± 0.4 vs. 2.6 ± 0.5, F (1.22) = 4.99, P = 0.036; 1N4R tau: 3.6 ± 0.9 vs 2.3 ± 0.3, F (1.22) = 4.60, P = 0.043), but not in the ctx-cbl (**Fig 18, Table 36**). Other tau isoforms (0N4R, 1N3R, 2N3R, 2N4R) did not differ significantly PD and controls in both brain regions (**Table 36**). There was a trend towards increased total tau levels in PD in the ctx-fg, without reaching the statistical significance. There was no effect of the *MAPT* haplotype or haplotype × disease interaction on insoluble levels of total tau, tau isoforms, or α-syn (**Table 36**)" [1].

Table 36. Effects of *MAPT* haplotype and disease status on levels of tau isoforms and α-syn in the insoluble protein fraction in human samples of fusiform gyrus and cerebellum.

Protein fraction	Brain region	Two-way ANOVA *P*-Value	Main effect of haplotype *P*-Value	Main effect of disease *P*-Value	Haplotype × disease *P*-Value	Direction of significant effect
α-syn	ctx-fg	0.134	0.781	**0.026**	0.995	PD > Control
	ctx-cbl	0.953	0.628	0.767	0.875	-
Total tau	ctx-fg	0.150	0.243	0.099	0.587	-
	ctx-cbl	0.576	0.580	0.590	0.229	-
0N3R tau	ctx-fg	0.108	0.252	**0.036**	0.881	PD > Control
	ctx-cbl	0.226	0.301	0.080	0.669	-
0N4R tau	ctx-fg	0.215	0.453	0.098	0.554	-
	ctx-cbl	0.371	0.380	0.145	0.469	-
1N3R tau	ctx-fg	0.362	0.491	0.130	0.889	-
	ctx-cbl	0.385	0.226	0.298	0.375	-
1N4R tau	ctx-fg	0.031	0.062	**0.043**	0.289	PD > Control
	ctx-fg	0.616	0.779	0.199	0.643	-
2N3R tau	ctx-cbl	0.596	0.790	0.303	0.535	-
	ctx-fg	0.966	0.626	0.939	0.992	-
2N4R tau	ctx-cbl	0.564	0.395	0.605	0.287	-
	ctx-fg	0.299	0.079	0.803	0.651	-

Main effect of haplotype was analyzed by comparison of H1/H1 (Controls + PD) vs. H2/H2 (Controls + PD). Main effect of disease was analyzed by comparison of PD (H1/H1+H2/H2) vs Controls (H1/H1+H2/H2). The interaction haplotype × disease examined the relationship between the independent variables (haplotype + disease) on the dependent variable of protein levels. *P*-values were calculated using two-way ANOVA followed by Tukey´s multiple comparisons test. Abbreviation: ctx-fg, cortex of fusiform gyrus; ctx-cbl, cerebellum. Derived from Tauber et al., 2022 [1].
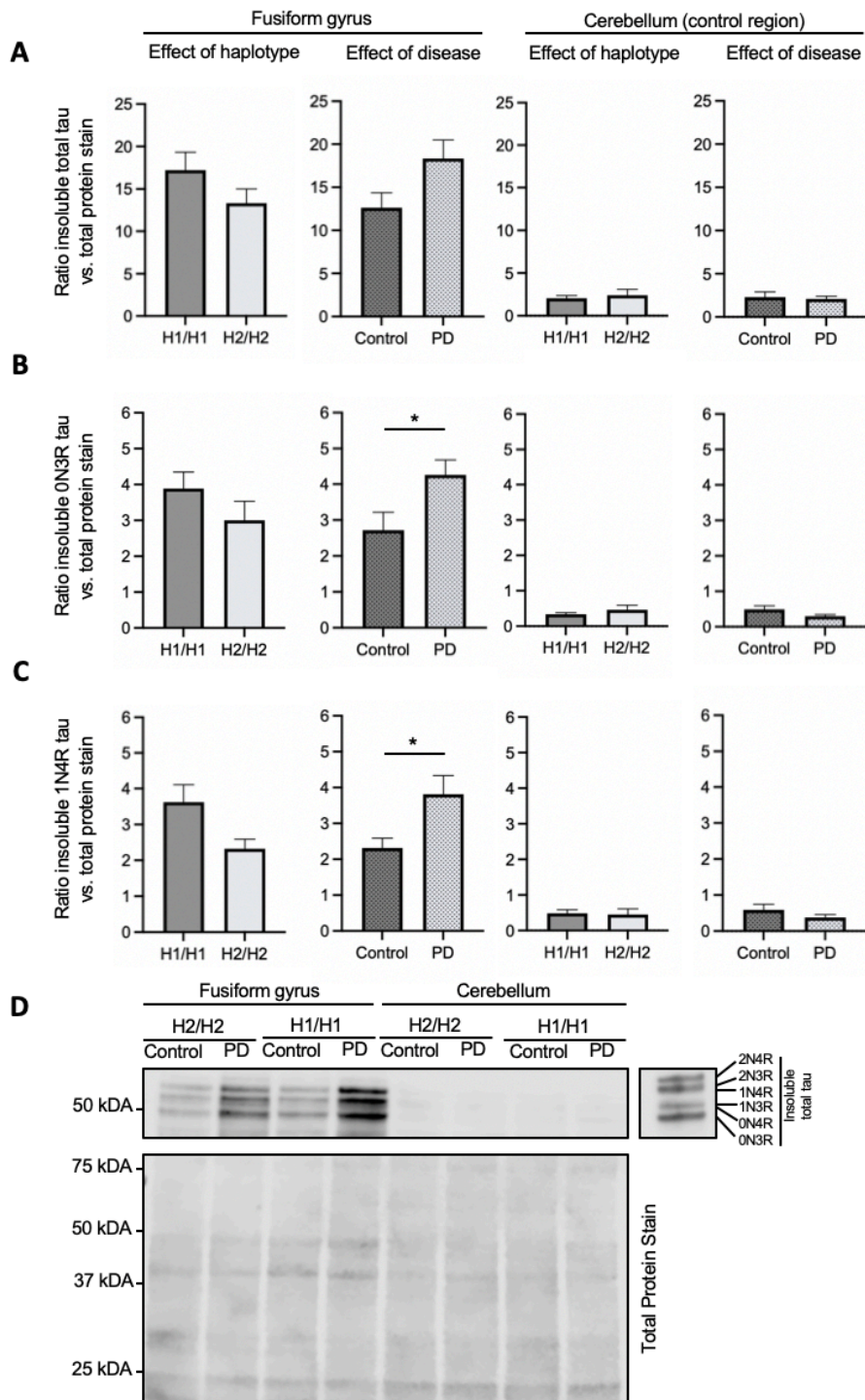
Figure 18. Influence of *MAPT* haplotype and disease status on insoluble tau protein levels. Bar graphs showing the effect of *MAPT* haplotypes (H1/H1, H2/H2) and disease status (PD, control) on insoluble protein levels of total tau (**A**), 0N3R tau (**B**) and 1N4R tau (**C**) in human brain samples of the cortex of fusiform gyrus and the cortex of cerebellum. For analysis of the *MAPT* haplotype effects, PD cases and controls were combined, and vice versa for analysis of the disease status. Data are protein quantity (mean ± SEM) relative to Total Protein Stain and normalized to an inter-run calibration consisting of pooled protein samples. Two-way ANOVA (haplotype × disease status), followed by Tukey´s post-hoc test: *$P < 0.05$. (**D**) Representative Western blot for soluble total tau with Total Protein Stain as reference. The six tau isoforms were identified by comparison to a recombinant tau ladder. Full length Western blots are shown in **Fig 7**. Derived from Tauber et al., 2022 [1].

3.5.3 Proportion of N- and R-terminal variants of tau protein isoforms relative to total tau

The proportion of N- and R-terminal variants of tau protein isoforms relative to total tau were not affected by *MAPT* haplotype nor disease status (**Table 37**) [1].

Table 37. N-and R-terminal variants of tau protein isoforms relative to total tau in conditions defined by *MAPT* haplotype and disease status.

Tau isoform	Controls		PD		Two-way ANOVA		
	H1/H1	H2/H2	H1/H1	H2/H2	Main effect of haplotype *P*-Value	Main effect of disease *P*-Value	Haplotype × disease *P*-Value
Soluble tau							
ctx-fg							
0N / total tau (%)	33 ± 12	23 ± 6	37 ± 8	35 ± 4	0.553	0.413	0.653
1N / total tau (%)	34 ± 14	22 ± 9	37 ± 7	35 ± 7	0.519	0.487	0.641
2N/ total tau (%)	33 ± 15	55 ± 26	26 ± 8	30 ± 5	0.375	0.293	0.522
ctx-cbl							
0N/ total tau (%)	43 ± 8	32 ± 8	25 ± 3	32 ± 8	0.977	0.291	0.127
1N/ total tau (%)	42 ± 8	33 ± 9	36 ± 11	34 ± 7	0.599	0.800	0.779
2N/ total tau (%)	15 ± 13	35 ± 18	39 ± 11	34 ± 16	0.556	0.419	0.383
ctx-fg							
3R/ total Tau (%)	48 ± 19	64 ± 19	45 ± 11	45 ± 4	0.669	0.556	0.686
4R/ total Tau (%)	52 ± 22	36 ± 12	55 ± 12	55 ± 10	0.626	0.502	0.645
ctx-cbl							
3R/ total Tau (%)	64 ± 13	48 ± 13	41 ± 9	31 ± 22	0.368	0.158	0.847
4R/ total Tau (%)	36 ± 12	52 ± 11	59 ± 16	75 ± 12	0.286	0.137	0.957
Insoluble tau							
ctx-fg							
0N / total tau (%)	40 ± 9	38 ±7	42 ± 4	45 ± 11	0.951	0.647	0.766
1N / total tau (%)	42 ± 8	38 ± 7	42 ± 5	40 ± 10	0.893	0.692	0.841
2N/ total tau (%)	18 ± 4	24 ± 5	16 ± 3	15 ± 4	0.563	0.198	0.393
ctx-cbl							
0N/ total tau (%)	34 ± 5	39 ± 16	28 ± 5	36 ± 11	0.423	0.589	0.860
1N/ total tau (%)	39 ± 9	45 ± 16	38 ± 9	39 ± 10	0.745	0.707	0.846
2N/ total tau (%)	27 ± 4	16 ± 5	34 ± 7	25 ± 9	0.169	0.295	0.830
ctx-fg							
3R/ total Tau (%)	52 ± 10	51 ± 9	50 ± 7	58 ± 11	0.713	0.763	0.671
4R/ total Tau (%)	48 ± 9	49 ± 10	50 ± 8	42 ± 7	0.694	0.748	0.650
ctx-cbl							
3R/ total Tau (%)	48 ± 6	55 ± 16	48 ± 10	59 ± 13	0.445	0.864	0.845
4R/ total Tau (%)	52 ± 11	45 ± 14	52 ± 10	41 ± 13	0.518	0.885	0.869

For groupwise comparison results were combined according to *MAPT* haplotype and disesase status. Statistic analysis for groupwise differences with two-way ANOVA were not significant (*P* > 0.05) for all parameters. Abbreviation: ctx-fg, cortex of fusiform gyrus; ctx-cbl, cortex of cerebellum. Derived from Tauber et al., 2022 [1].

3.5.4 Differences in protein levels between brain regions

"Despite comparable mRNA expression levels, there was a differential protein ratio with higher insoluble α-syn protein levels in ctx-fg relative to ctx-cbl of PD brains compared to controls (PD vs. Control 2.7 ± 0.3 vs. 1.6 ± 0.2, F (1.22) = 5.72, P = 0.025; **Fig. 16-18**). The same trend for increased insoluble protein ratios was also observed for insoluble total tau but did not reach statistical significance for the effect of disease (P = 0.067). However, the ratios of insoluble tau isoform 0N3R (PD vs. Control 3.9 ± 0.4 vs. 2.2 ± 0.5, F (1.22) = 6.58, P = 0.018) was significantly higher in PD, independent of the *MAPT* haplotype. For insoluble 1N4R tau protein, a significant increase in H1/H1 PD brains was also found with significant effect of both MAPT haplotype (H1/H1 vs. H2/H2 3.2 ± 0.9 vs. 1.9 ± 0.5, F (1,22) = 4.54, P = 0.045) and disease (PD vs. Control 3.2 ± 0.8 vs 1.8 ± 0.4, F (1.22) = 5.12, P = 0.034) (**Table 38**)" [1].

Table 38. Regional distribution of different protein levels in human samples of fusiform gyrus related to cerebellum.

| Protein | Protein levels ctx-fg vs ctx-cbl Mean ± SEM | | | | Two-way ANOVA | | |
| | Controls | | PD | | | | |
	H1/H1	H2/H2	H1/H1	H2/H2	Main effect of haplotype *P*-Value	Main effect of disease *P*-Value	Haplotype × disease *P*-Value
Soluble α-syn	0.92 ± 0.29	1.02 ± 0.18	1.29 ± 0.34	1.28 ± 0.30	0.894	0.350	0.861
Insoluble α-syn	1.72 ± 0.38	1.52 ± 0.20	2.82 ± 0.48	2.54 ± 0.40	0.601	**0.025**	0.936
Soluble tau							
Total tau	11.7 ± 5.12	5.08 ± 4.17	10.6 ± 3.08	7.93 ± 1.51	0.255	0.827	0.613
0N3R tau	1.98 ± 0.79	0.59 ± 0.30	2.29 ± 0.54	1.47 ± 0.22	0.082	0.334	0.646
0N4R tau	1.68 ± 0.78	0.33 ± 0.29	1.88± 0.48	1.10 ± 0.16	0.076	0.410	0.620
1N3R tau	1.61 ± 0.70	0.35 ± 0.29	1.78 ± 0.43	1.06 ± 0.16	0.068	0.407	0.608
1N4R tau	2.21 ± 1.04	0.46 ± 0.41	2.15 ± 0.69	1.35 ± 0.31	0.122	0.607	0.557
2N3R tau	1.90 ± 0.87	2.73 ± 2.51	0.77 ± 0.80	0.54 ± 0.86	0.812	0.194	0.673
2N4R tau	2.34 ± 0.97	0.59 ± 0.70	1.79 ± 0.50	1.7 ± 0.75	0.239	0.714	0.287
Insoluble tau							
Total tau	11.6 ± 2.72	8.54 ± 2.86	17.8 ± 2.76	13.2 ± 1.95	0.190	0.067	0.791
0N3R tau	2.67 ± 0.76	1.61 ± 0.57	4.23 ± 0.50	3.47 ± 0.75	0.186	**0.018**	0.824
0N4R tau	1.96 ± 0.42	1.64 ± 0.78	3.66 ± 0.66	2.70 ± 0.79	0.362	0.057	0.644
1N3R tau	2.37 ± 0.59	1.57 ± 0.72	3.68 ± 0.61	3.00 ± 1.01	0.322	0.075	0.935
1N4R tau	2.27 ± 0.48	1.39 ± 0.54	4.04 ± 0.66	2.34 ± 0.32	**0.045**	**0.034**	0.500
2N3R tau	0.73 ± 0.19	1.07 ± 0.17	1.27 ± 0.33	1.20 ± 0.47	0.693	0.310	0.536
2N4R tau	1.02 ± 0.34	1.26 ± 0.35	1.20 ± 0.49	0.56 ± 0.39	0.661	0.572	0.341

For the comparison of protein levels between the brain regions, the differences in protein levels between gyrus fusiformis and cerebellum were calculated. For groupwise comparison of these differences results were combined according to *MAPT* haplotype and disease status. *P*-values were calculated using two-way ANOVA followed by Tukey´s multiple comparisons test. Abbreviation: ctx-fg, cortex of fusiform gyrus; ctx-cbl, cortex of cerebellum. Derived from Tauber et al., 2022 [1].

3.5.5 No differences between insoluble and soluble protein levels

The differences between the insoluble to the soluble protein fraction of tau and α-syn was not affected by neither disease status, the *MAPT* haplotype, nor their interaction for haplotype x disease (Table 39). [1].

Table 39. Investigation of differences between insoluble and soluble protein levels in human samples of fusiform gyrus and cerebellum.

| Protein (Brain region) | Insolube vs. soluble protein levels Mean ± SEM | | | | Two-way ANOVA | | |
| | Controls | | PD | | | | |
	H1/H1	H2/H2	H1/H1	H2/H2	Main effect of haplotype *P*-Value	Main effect of disease *P*-Value	Haplotype × disease *P*-Value
α-syn (ctx-fg)	-0.87 ± 0.44	0.59 ± 0.46	1.67 ± 0.46	1.44 ± 0.51	0.610	0.112	0.970
α-syn (ctx-cbl)	0.07 ± 0.18	0.10 ± 0.42	0.15 ± 0.17	0.17 ± 0.35	0.932	0.787	0.990
Total tau (ctx-fg)	0.72 ± 5.54	3.68 ± 2.77	7.29 ± 4.21	6.13 ± 2.56	0.846	0.337	0.658
Total tau (ctx-cbl)	0.82 ± 0.63	0.22 ± 1.03	0.06 ± 0.64	0.79 ± 0.70	0.935	0.900	0.309
0N3R tau (ctx-fg)	0.84 ± 1.11	1.17 ± 0.52	1.95 ± 0.80	2.08 ± 0.85	0.808	0.293	0.912
0N3R tau (ctx-cbl)	0.15 ± 0.04	0.16 ± 0.20	0.01 ± 0.04	0.08 ± 0.07	0.698	0.244	0.722
0N4R tau (ctx-fg)	0.39 ± 0.81	1.44 ± 0.66	1.79 ± 0.79	1.61 ± 0.87	0.610	0.365	0.474
0N4R tau (ctx-cbl)	0.11 ± 0.06	0.13 ± 0.18	0.00 ± 0.07	0.01 ± 0.11	0.905	0.270	0.937
1N3R tau (ctx-fg)	0.87 ± 0.71	1.53 ± 0.54	1.94 ± 0.68	2.04 ± 1.15	0.641	0.333	0.728
1N3R tau (ctx-cbl)	0.11 ± 0.05	0.31 ± 0.29	0.05 ± 0.11	0.10 ± 0.14	0.418	0.372	0.634
1N4R tau (ctx-fg)	0.36 ± 1.13	1.05 ± 0.40	1.82 ± 1.02	0.89 ± 0.42	0.906	0.526	0.427
1N4R tau (ctx-cbl)	0.31 ± 0.14	0.12 ± 0.31	-0.07 ± 0.25	-0.11 ± 0.19	0.647	0.219	0.749
2N3R tau (ctx-fg)	-0.90 ± 0.95	-1.83 ± 2.35	0.53 ± 0.76	0.59 ± 0.79	0.724	0.130	0.691
2N3R tau (ctx-cbl)	0.27 ± 0.10	-0.16 ± 0.31	0.03 ± 0.17	-0.07 ± 0.32	0.237	0.724	0.459
2N4R tau (ctx-fg)	-0.84 ± 1.08	0.30 ± 0.58	-0.74 ± 0.74	-1.08 ± 0.74	0.649	0.478	0.413
2N4R (ctx-cbl)	0.48 ± 0.11	-0.37 ± 0.25	-0.15 ± 0.14	0.07 ± 0.21	0.089	0.557	0.946

For the comparison of protein levels between the protein fractions, the differences in protein levels between the insoluble and soluble protein fraction were calculated. *P*-values were calculated using two-way ANOVA followed by Tukey´s multiple comparisons test. Statistic analysis were not significant for all parameters (*P* > 0.05). Abbreviation: ctx-fg, cortex of fusiform gyrus; ctx-cbl, cortex of cerebellum. Derived from Tauber et al., 2022 [1].

4 Discussion

4.1 Methodical preliminary experiments

This study aimed to create the best possible conditions for the quality and reproducibility of the analysis by evaluating different technical methods of RNA and protein extraction for down-stream applications. As quantification results rely on optimal PCR efficiency conditions, removal of gDNA is strongly required. Otherwise compromising side effects occur, such as false high RNA concentrations or co-amplification of genomic DNA during RT-qPCR. If this takes place, PCR efficiency of the target sequence is reduced [159, 160]. Therefore, three different gDNA elimination methods were tested. While the column-based and solution-based gDNA elimination were part of established RNA protocols, the protocol after Chomczynski without gDNA elimination step required a subsequent enzymatic treatment with TurboDNAse. A strong decrease in RNA yield was evident in all samples treated with TurboDNAse, however significancy was only met in cells. Even more, a significantly higher RNA degradation in treated RNA from postmortem human brain compared to untreated RNA extracts occurred. RNA Purity was not affected by treatment with TurboDNAse in all samples. The increased RNA degradation with TurboDNase might be explained by residual endogenous RNAse activity. The severe decrease in RNA yield might be due to the obligatory high temperature at incubation. However, the treatment with EDTA and RNAse inhibitors prior to TurboDNAse achieved no consistent improvement.

Based on these two major disadvantages, the enzymatic gDNA elimination and hence the protocol after Chomczynski were considered unsuitable for postmortem brain tissue. In contrast, the column-based (RNEasy+ Mini Kit, method after Rodriguez-Lanetty) and solution-based removal (RNEasy+ Mini Kit and method after Rodriguez-Lanetty) have the advantage that no leftovers of gDNA or DNase enzyme activity remain, and no high-temperature incubation is necessary. Both performed similar in RNA quality parameters.

In reaction to resported differences of commercially available RNA kits, three protocols for RNA extraction were tested in terms of RNA concentration, purity and integrity in human brain samples [161]. The method after Rodriguez-Lanetty delivered the second-highest RNA yield, but at the same time the significantly lowest purity which was considered not acceptable for down-stream applications. The RNEasy+ Mini Kit using RLT buffer instead of Trizol led to the lowest RNA yield in all samples with sufficient purity. There was no significant influence on RIN by all protocols. Of note, a recent study described no impact on yield and RIN by preanalytical procedures in brain samples [162]. Altogether, the RNEasy+ Mini Universal kit showed the best performance regarding RNA quantity, purity and integrity. In addition to the excellent RNA quality, this method offered more advantages. A greater amount of starting tissue of 100 mg can be used compared to the RNEasy+ Mini Kit and method after

Rodriguez-Lanetty which allow only 30 mg tissue. The handling of the TissueRuptor for homogenization was easier and facilitated quick tissue processing without unnecessary thawing compared to the grinding with liquid nitrogen and subsequent QIAShredder. The gDNA elimination solution provided an easy and gentle treatment of RNA without a high-temperature incubation compared to the TurboDNAse treatment. Regarding phase separation, the use of MaXtract High Density tube facilitated the handling of Trizol as lysis reagent without compromising the RNA purity.

In general, phenol-based RNA extraction using Trizol bears the risk of phenol-based contamination and less pure RNA extracts. There are diverse views on the minimum level of purity which is acceptable for down-stream applications. In a work conducted by the manufacturer Qiagen, no compromising effect of RNA extracts with low A_{260}/A_{230} ratios down to 0.5 on qPCR performance was observed [163]. A clean-up step can purify contaminated RNA samples which was observed in the preliminary experiment with a significantly increased A_{260}/A_{230} ratio. Yet, the loss of RNA yield needs to be taken into account especially in study objects with limited availability such as postmortem brain tissue. A possible influence of the clean-up step on qPCR performance was not observed. In the context of quality control, only RNA extracts with sufficient purity were ulitmately included in the experiments making a clean-up step obsolete.

A common protocol of protein extraction was tested reusing the organic phase containing protein of the Trizol lysates obtained during RNA extraction [150]. Simultaneous extraction of DNA, RNA and protein from the exact same cell lysates is crucial for accurate correlations between genetic changes and their potential effects on the transcriptome and proteome [164, 165]. Although Trizol is not common for protein extraction, several studies demonstrated that efficient extraction from different tissue types including brain tissue and evaluation by immunoblotting of a wide range of proteins is feasible [166-169].

For the important step of resuspension of the pellet, high concenctrated SDS also failed to completely dissolve the pellet, but was significantly superior to RIPA buffer with low SDS concentration in terms of the achieved protein concentration. This result is consistent with results from a study conducted in brain tissue [169]. Phosphorylation of proteins can lead to retardation in gel mobility and shifts of protein bands in SDS-page [170], like in the case of pathogenic hyperphosphorylated tau [171]. For a correct identification of the isoform composition of tau an efficient dephosphorylation reaction is required because otherwise electrophoresis of untreated tau does not separate the individual tau isoforms [172]. Samples treated with λPP specifically targeting phosphate groups from threonine, serine, and tyrosine amino acids for dephosphorylation [173] performed better with clearly separated protein bands compared to aPP indicating a more efficient dephosphorylation [172]. This is in agreement with a previous study that suggests that the frequently described aPP has the problem of incomplete

dephosphorylation of tau and low yield, possibly due to the lacking coverage of thyrosine sites [173] and incubation at elevated temperature [172]. For identification of individual tau isoforms 12% Bis-Tris gels outperformed 10% Bis-Tris gels following the finer separation range [174].

Multiple tests were carried out to find the best type of sample preparation, gel and blocking buffer, as well as selection and concentration of tau antibodies. Despite this, did the preliminary tau immunoblotting with Trizol lysates fail to deliver adequate quality for a reliable semi-quantitative evaluation with regard to signal and background quality and homogenous signal from the housekeeping protein. Difficulties in immunoblotting from Trizol lysates have been described before [175]. Also worth considering is that there is no reference in the literature to rank the solubility of Trizol soluble proteins compared to other lysis buffers. Due to this, the method of sequential protein extraction from native brain tissue was used for the protein analysis of the main experiment. Its main advantages were a constant quality of bands in Western blotting and the examination of different solubility forms of proteins.

In conclusion, preliminary experiments were indispensable because there is no uniform methodology for postmortem brain tissue [176, 177]. Due to its particular susceptibility to preanalytical factors special caution is necessary to make maximum use of the brain tissue. In part, considerable differences in methods were found that could have prevented the main analyses from being carried out (too low RNA or protein yield) or could have had a negative impact on performance (RNA contamination or degradation, selection of incorrect reference genes, incomplete dephosphorylation, inhomogenous housekeeping protein). One major limitation in the preliminary experiments is the small sample size (n = 3-6) which was purposely restriced with regard to the limited brain tissue.

4.2   Expression of mRNA and protein under the paradigm of *MAPT* haplotype and disease status

"Several prior studies have tried to understand the mechanisms underlying the association of the *MAPT* haplotype H1/H1 as a major risk factor for several neurodegenerative diseases, including sporadic PD. So far, studies evaluating the *MAPT* expression in the human brain focused on either healthy controls with regard to *MAPT* haplotypes [34-37] or investigated Parkinson's disease and control cases without consideration of haplotypes [14]. To our knowledge, the present study is the first investigation of *MAPT* regional involvement on gene and protein expression in sporadic PD under the paradigm of different homozygous *MAPT* haplotypes in the human brain. Since sporadic PD is classified as synucleinopathy according to its main pathology, we investigated the mRNA and protein levels of the synucleins in the same context. The region ctx-fg as pathological region and ctx-cbl as reference from control brains and PD was used. Due to the strict selection process, the studie group size was rather small, but the included brains were well qualified by their tissue integrity, the severity of PD pathology, and absence

of significant concomitant AD pathology" [1]. H1 homozygosity was associated with increased *total MAPT* mRNA expression in ctx-fg in both PD and controls. H2 homozygosity was associated with increased expression of *MAPT-AS1* in the ctx-cbl, as well as incresesd *KANSL1* and *KANSL1-AS1* mRNA in both brain regions. PD patients had higher levels of insoluble 0N3R and 1N4R tau isoforms and also of insoluble α-syn in the ctx-fg, regardless of the *MAPT* genotype.

"In line with literature, we found a statistically significant increase of mRNA expression of total *MAPT* in donors with the H1/H1 haplotype [64]. Albeit the trend towards higher *MAPT* expression in the cerebellum of H1/H1 *MAPT* haplotype, statistically significant elevated total *MAPT* mRNA levels were detected in the ctx-fg only, a brain region affected by α-syn pathology. Our results are in accordance with previous studies describing the same association between homozygous *MAPT* haplotypes in frontal cortex and cerebellum of healthy donors [34]. This result was also described in prefrontal cortex of PD cases [65] not stratified for *MAPT* haplotype. However, there are studies which could not detect differences in haplotype-specific total *MAPT* expression in healthy human brains. These controverse findings could result from analysis of heterozygous *MAPT* haplotype [35] or from different brain regions being examined since *MAPT* was found to be differently expressed across brain regions [37].

Some studies suggest that the influence of the *MAPT* haplotype is more on differential splicing and thus *MAPT* transcript expression rather than overall elevated gene expression [35, 37]. Evidence for this has been provided by postmortem studies of healthy individuals with elevated levels of 4R *MAPT* [36], but lower levels of 2N *MAPT* transcripts for H1/H1 compared to H2/H2 [37]. We, however, did not observe a haplotype- or disease-specific influence on the expression of *MAPT* transcripts [35, 66, 67]. The absence of a clear relationship between *MAPT* mRNA and tau isoforms has already been observed in healthy controls by the large-scale work of Trabzuni et al. but remains difficult to interpret at first glance [37] given that only few studies exist regarding tau protein stability and half-life in postmortem brain. A possible explanation could be the lower stability of RNA than protein in postmortem tissue [68]" [1].

Interestingly, a potential epigenetic regulator of *MAPT* expression exists in the *MAPT* inversion locus. "In contrast to increased *total MAPT* expression in H1/H1 haplotype, we found *MAPT-AS1* mRNA to be markedly decreased in H1/H1 in the ctx-cbl. This effect was not observed in ctx-fg. The expression of *MAPT-AS1* has also been studied in postmortem brain tissue with similar sample size, but only in a comparison of PD versus control. In these studies, a PD-specific decrease in *MAPT-AS1* was found across brain regions with different levels of PD pathology, including SN and cerebellum [106, 113]. Overexpression of the promotor-associated long non-coding RNA *MAPT-AS1* was shown to inhibit *MAPT* promotor activity and *MAPT* expression in human striatal progenitor cells [106]. These findings suggest that haplotype-specific regulation of *MAPT* may not be restricted to a specific brain region

and could be independent of disease status" [1]. It is hypothesized that the H1/H1 haplotype associated decrease of *MAPT-AS1* might contribute to the likewise increase of *MAPT* in PD. Yet, no influence of disease on *MAPT-AS1* mRNA levels and no inverse relationship between the expression of *MAPT-AS1* and *MAPT* was evident, which is consistent with previous studies [113]. Further studies are required to to clarify the role of *MAPT-AS1* in PD.

Most importantly, this study further confirms that the *MAPT* haplotype regulates genes encoded in the inversion region besides *MAPT*. *KANSL1* and *KANSL1-AS1* expression was found to be *MAPT*-haplotype specific with a similar strong decrease in H1/H1 donors compared to H2/H2 in ctx-fg and ctx-cbl. These findings are in agreement with studies conducted in prenatal human brain [112] and in temporal cortex [111]. The correlation between *KANSL1* and *KANSL1-AS1* is currently unclear as the long non-coding RNA *KANSL1-AS1* can act either activating or repressing on gene expression [178]. The similar haplotype association might indicate an activating regulation. *KANSL1* encodes a nuclear protein product affecting gene expression [107]. In terms of PD, a GWAS identified *KANSL1* as a risk gene [109] and certain variants were identified to be strongly linked with the risk haplotypte H1/H1 [179]. *KANSL1* expression was also found upregulated in the SN in PD compared to controls [110]. Still, its functional role remains unclear. Our findings provide further evidence for the *MAPT* haplotype-specific expression of *KANSL1* and *KANSL1-AS1*. However, whether these differences in mRNA expression play a crucial role in pathologic changes mediated by the *MAPT* haplotypes might be addressed in future experiments.

"Unfortunately, the impact of *MAPT* haplotype on the *MAPT* inversion locus remains enigmatic. For the other investigated genes neither an effect of the *MAPT* haplotype nor disease was detectable. This is in contrast to previous studies, in which expression of *PLEKHM1* was found increased in the cerebellum of healthy H1/H1 compared to H2/H2 carriers [93] and increased expression of *STH* was observed in cerebellum of PD patients compared to controls [63]" [1]. There is no previous data about expression levels of *NSF* in the context of PD or *MAPT* haplotype. "However, the remaining genes of interest might be addressed in future experiments since differences in mRNA expression play a crucial role in pathologic changes mediated by the *MAPT* haplotypes.

Besides mRNA expression and protein levels itself, the proportion of *MAPT* transcripts to *total MAPT*, respectively tau isoforms to total tau, might also be of relevance. For mRNA, this has already been studied in a few cases in adult frontal cortex only (AD *n* = 3, Con *n* = 3). There the ratio of 3R to 4R *MAPT* was about one, while 1N, 0N, and 2N *MAPT* accounted for 54%, 37% and 9% of *total MAPT* [66, 180]. Despite the lack of significant differences, these data contribute to the understanding of *MAPT* splicing, and the distribution of tau isoforms respectively, in the human postmortem brain. Studies with

a larger sample size could further investigate and verify the trends observed here "[1].

"The presented findings support the concept that α-syn pathology in PD does not show up at the transcriptional level or in the soluble protein compartment but is discernible primarily in the insoluble protein compartment. Similar to the study of Quinn et al. [181] differences on the protein level despite unchanged α-syn mRNA levels were demonstrated. Levels of insoluble α-syn were increased in PD compared to controls independent of the *MAPT* haplotype. This result was observed only in the ctx-fg, but not in ctx-cbl which supports the value of the former as a relevant region of interest for PD. Our findings confirm results of prior postmortem brain studies in which higher levels of insoluble α-syn protein fractions were found in PD compared to controls, while soluble levels of α-syn did not differ, as observed in the amygadala and anterior cingulate gyrus [127], putamen and frontal cortex [128] and in striatum and inferior frontal gyrus [100]. It is worth noting that some prior studies reported a decrease of soluble α-syn levels in PD in cerebellum and occipital cortex [126, 129], yet, no prior data exist on the α-syn protein level in the same protein fractions and brain regions as studied here, making a direct comparison difficult" [1].

"Similarly to α-syn, tau pathology in PD was also not detectable at the transcriptional level or in the soluble proteome. In the insoluble protein compartment, 0N3R and 1N4R tau isoforms were significantly increased in the fusiform gyrus of PD cases. These isoform-specific findings need to be independently reproduced and understood pathophysiologically. The N-terminal region of tau has been shown to be involved in solubility and folding by inhibiting tau polymerization [71], and stabilizing tau in a folded state [72]. Yet, despite various functions, interactions and the potentially crucial role in tau pathology, little is known about the effect of each single exon within the N-terminal domain [71, 72, 182]. While for the number of repeats in the C-terminal domain, it is known that compared to 3R tau, 4R tau regulates microtubule dynamics more efficiently, binds with greater affinity to microtubule [73] and is more prone to aggregation [66]

For insoluble total tau, a tendeny towards higher levels in PD and H1/H1 was apparent, which did not reach statistical significance due to the small group size. In contrast to the study of Lei et al., which reported a 44% decrease of soluble levels of tau (phosphate-buffered-saline-soluble) in the substantia nigra in PD compared to controls [97], we did not find significant differences for soluble tau protein. This difference in result is probably owing to the fact that the SN in PD is strongly degenerated in contrast to the cortex of fusiform gyrus. Very few studies exist regarding tau quantity in postmortem human PD brain, however, differences in methodology might explain variable results. In our study design which allowed a simultanous mRNA and protein extraction from the very same tissue sample, haplotype-specific differences observed at *MAPT* mRNA level were not reflected in total tau protein

expression. Only 1N4R tau isoform of insoluble tau showed a trend towards increased expression in the H1/H1 haplotype, but this did not reach the level of statistical significance" [1].

"As expected, the *MAPT* haplotype, located on chromosome 17, did not influence mRNA expression of *SNCA*, encoded on chromosome 4. The predisposition to PD by the *MAPT* haplotype did not seem to manifest itself at the transcriptional level of the synuclein genes. The absent influence of disease on expression levels of synuclein genes *SNCA*, *SNCB* and *SNCG* is in good agreement with other postmortem studies. *SNCA* mRNA levels were increased only in substantia nigra in PD, [113, 183, 184] but did not differ in cerebellum or temporal cortex [113, 181] in comparison to controls. The expression of *SNCB* and *SNCG* in postmortem tissue had so far not been examined in the context of PD" [1]. Furthermore, mRNA expression of *NRF2* presented no significant differences.

"Taken together, these results show that the *MAPT* haplotype influences overall *MAPT* expression and disease leads to increased insoluble tau protein in parallel with insoluble α-syn aggregates. This may predispose as a risk factor for PD at the biochemical level according to the principle of mutual catalysis of aggregation of tau and α-syn, demonstrated *in-vitro* [101, 102] and *in-vivo* [185]. In all performed analysis, there was no interaction between disease status and *MAPT* haplotype on *MAPT* and *SNCA* gene expression and protein level. All the above observations were detected only in the vulnerable brain region ctx-fg, but not in the control region ctx-cbl, which supports the preferential vulnerability of certain brain regions in PD" [1].

"In addition, further data on the regional distribution of tau and α-syn protein across the human brain was provided. In comparison, tau protein levels of both protein fractions were visibly overall higher in ctx-fg compared to ctx-cbl, which has also been demonstrated by other studies [96]. In line with the main analysis, this regional difference was significantly altered in PD cases for insoluble tau isoforms 0N3R and 1N4R tau. Above that, the H1/H1 haplotype was associated with increased insoluble 1N4R tau in ctx-fg. This finding might be linked to the association of *MAPT* haplotype H1/H1 with increased risk of sporadic PD which primarily affects regions besides cerebellum. Still, it is difficult to explain these differences to its full extent, since other insoluble and soluble tau isoforms also showed differences between brain regions but without reaching level of significance. A disease-specific increase was also found for insoluble α-syn levels highlighting the relevance of ctx-fg as a target of study in PD" [1].

4.3   Limitations and strengths of this study

"The present study is subject to several limitations related to the use of postmortem tissue. First, the limited availability of high-quality brain tissue prevented us from working with larger sample sizes. In

addition, it turned out to be challenging to find a sufficient number of donors with H2/H2 *MAPT* haplotype which is less frequent in Europe (5 – 37.5%) [76, 89]. Secondly, ante- (agony phase, cause of death) and postmortem factors (PMI, tissue handling) are suspected to influence postmortem brain tissue quality. For this reason, donors with the shortest PMI and tissue samples with the highest RIN were selected. However, studies showed that the potential detrimental influence of PMI on mRNA is estimated low [186] and that mRNA of the central nervous system is most stable compared to mRNA of other tissues [187] " [1]. For protein, a Western blot study reported that proteins like phosphorylated tau and GAPDH remain intact in samples with a PMI up until 48h [188]. The PMI of the analyzed study population was well below this value.

Despite the need for appropriate evaluation of RNA integrity, no standardized recommendation of quality threshold is to be found in literature. Principally accepted as good RNA quality is RIN ≥ 5, while RIN ≥ 8 is estimated as optimal [189]. For postmortem brain tissue cut-off values of RIN ≥ 6 or ≥ 3.95 are suggested. [146, 147]. The presented RIN results were consistent to former studies in which brain tissue showed the lowest RIN values with a huge variation compared to other tissue types [177, 190]. With respect to the limited sample size, especially within the *MAPT* H2/H2 cohort, four samples with slightly lower RIN values (PD 11 ctx-fg 3.1; PD 13 ctx-cbl 2.8; C8 ctx-cbl 3.2; C10 ctx-fg 2.8) were taken into account. Apart from that, all samples passed the RIN threshold proposed for brain tissue of 3.95 [147].

Yet, the value of RIN as tissue quality marker is very controversial [144, 146, 159, 177, 189, 191]. It is hypothesized that RIN represents more the decrease in full-length mRNA quantity than integrity itself, since high-quality output was generated from postmortem samples with both high and low RIN values [146, 189]. At this stage of understanding, the impact of low RIN on RNA quality is not fully known which justified to some extent the inclusion of tissue samples with lower RIN in this study. Following the recommendation of previous studies [177], RIN values between the analyzed subgroups were similar. Of note, no differences in the performance in down-stream applications were observed between samples with lower and higher RIN values of the same subgroup. There is conflicting data regarding the potential influence of the cause of death on RNA quality, too. Studies have shown that near-death physiological stress in the agony phase altered the gene expression pattern [192]. Especially antemortem events with tissue hypoxia, such as coma, multiple organ failure or respiratory distress might be of relevance [193]. However, when working with postmortem tissue the parameter antemortem events can hardly be controlled or avoided. Most importantly, cause of death was demonstrated to have no influence on RIN in brain tissue [177].

Third, since previous studies revealed a huge variety of the most common reference genes among tissues, a project-specific search for adequate control genes is recommended [194-196]. In an extensive search for suitable reference genes, only three genes presented overall high expression stability.

Consistent with other studies *GAPDH* was also found to be the most stable gene in cerebellum in PD, AD and LBD [196] and in SN in PD cases [197]. Nevertheless, the gene stability measure M was slightly above the reference value in ctx-fg. The difficulty in finding suitable reference genes is consistent with other gene expression profiling studies in postmortem tissue. By using an inter-run calibration and optimal reference genes, the gene expression data was adequately normalized.

Fourth, critical consideration must be given to which brain region to examine. In contrast to other studies, the SN was not selected as target region for various reasons. The SN is known as key region in PD and an inhomogeneous tissue containing multiple cell types such as dopaminergic and non-dopaminergic cells [198]. At the point of clinical manifestations of PD, a large proportion of neurodegeneration has already occurred in the SN [199]. In general, postmortem brain studies face the difficulty of interpreting the significance of results. The question is raised whether changes in mRNA or protein levels are the primary cause of cell death or result of the ongoing pathology [133, 200]. Since PD pathology is a global process spreading in a distinct pattern throughout the brain it is a justified approach to study extrastriatal brain regions [200]. The fusiform gyrus merits the fact that the amount of neuronal cell loss is less extreme compared to SN, but there is still considerable Lewy body pathology present [25]. Another advantage is the greater availability of the fusiform gyrus in brain banks. This is relevant for *MAPT* genotyping, as a sufficiently large number of postmortem brain donors with available tissue was required to identify cases with the rarer *MAPT* H2/H2 haplotype.

"The ctx-cbl was chosen as reference region in accordance with former post mortem brain studies [93, 201, 202]. Even though LB pathology is typically not present in ctx-cbl, PD related changes have been reported previously indicating a possible involvement of the cerebellum in PD [203]. In turn, the disease-specific findings regarding α-syn in the target brain region confirmed the selection of brain tissue as a validated source for the analysis of *MAPT* haplotype-specific expression differences and the questionable association to PD" [1].

Fifth, only grey matter of the tissue samples was used in order to focus on neuronal enrichment. However, PD-related changes also occur in the white matter. It is assumed that astrocytes, for example, the most populous cell type of the glia, contribute to PD pathogenesis [204]. Differences in *MAPT* expression with *MAPT* mRNA and protein levels in white matter compared to neocortex have been revealed by a postmortem study conducted in healthy donors [96]. Hence, the investigation of white matter in this context is of interest in further studies. Sixth, gender related differences in alterations of gene expression associated with PD have been described. Therefore, gender matching was considered indispensable [133, 134], which was properly addressed in the selection of brain donors.

"With the stringent tissue quality process, we made the best efforts to identify a well-balanced study population in terms of demographic, clinical and neuropathologic parameters. The most important strength of our analysis lies in the fact that mRNA and protein extraction were performed

simultaneously from the very same tissue sample. Noteworthy, differences in methods (e.g. method of extraction or quantification) and in material (e.g. sample size, brain regions, types of pathologies) across postmortem brain studies limit the possibility of comparisons among them and with the presented study" [1].

5 Conclusion and outlook

In consistence with previous literature, the presented data suggests that haplotype-specific expression of genes within the *MAPT* haplotype block and the protein tau may play a role in sporadic PD. "These findings support the hypothesis that homozygosity for the H1/H1 *MAPT* haplotype predisposes to PD through increased mRNA expression of the *MAPT* gene. This in turn predisposes to increased aggregation of the tau protein, which catalyses the aggregation of α-syn. Regulation by long non-coding antisenses like *MAPT-AS1* and *KANSL1-AS1* on disease relevant genes like *MAPT and KANSL1* may be crucial in disease involvement or progression. This study demonstrated also the effect of the *MAPT* haplotype on gene expression within the *MAPT* locus. More data about function and possible implications in human brain in healthy and pathologic status of the differentially regulated genes is warranted. Future research should address the distinct functions of N- and C-terminal tau domains, the role of transcriptome regulating anti-senses and the remaining genes located at the 17q21.3 inversion locus in terms of expression, function and potential role in sporadic PD and tauopathies" [1].

To date, there is no approved disease-modifying or preventive therapy for synucleinopathies such as PD. A variety of strategies are being explored targeting different forms and conformational states of α-syn. Therapeutic approaches include blocking the misfolding or aggregation of α-syn or immunotherapies that lower the level of α-syn either by passive or active immunization [205, 206]. For instance, the antibody Prasenezumab directed against aggregated α-syn missed the primary efficacy outcome on clinical scores in the PASADENA study [207]. With positive signals on secondary endpoints, it is currently being evaluated in early PD patients in the PADOVA study (clinicaltrials.gov; No. NCT04777331). For tauopathies, disease modifying therapies targeting tau and ß-amyloid are being examined [208-210]. As example, the anti-tau antibody Semorinemab did not slow disease progression in patients with mild AD in a recent clinical trial [211]. With repeated findings of limited or no clinical benefit of immunotherapies, it is widely discussed if antibody-mediated reduction of extracellular protein pathology is a promising approach [212]. In contrast, so called oligonucleotide therapies including antisense oligonucleotides, small interfering RNA and microRNA can modify gene translation by binding with selected cellular RNA [213]. Antisense oligonucleotides have been shown to inhibit the production of all forms of α-syn by targeting *SNCA* RNA intracellulary [214] and to decrease human tau mRNA and protein in mice brain [215]. There are several ongoing trials for intrathecal applied antisense oligonucleotide therapy targeting *SNCA* in the synucleinopathy multiple system atrophy (NCT04165486) or *MAPT* in AD (NCT03186989), for instance. In conlusion, this study highlights the concept of *MAPT* haplotype- and disease-specific gene and protein expression in PD which potentially provides new directions for thinking about therapeutic strategies.

Acknowledgement

Eidesstattliche Versicherung/Affidavit

Hiermit versichere ich an Eides statt, dass ich die vorliegende Dissertation "Microtubule-associated protein Tau as risk factor for the idiopathic Parkinson syndrome - A postmortem brain study in PD patients and controls" selbstständig angefertigt habe, mich außer der angegebenen keiner weiteren Hilfsmittel bedient und alle Erkenntnisse, die aus dem Schrifttum ganz oder annähernd übernommen sind, also solche kenntlich gemacht und nach ihrer Herkunft unter Bezeichnung der Fundstelle einzeln nachgewiesen habe.

I hereby confirm that the dissertation "Microtubule-associated protein Tau as risk factor for the idiopathic Parkinson syndrome - A postmortem brain study in PD patients and controls" is the result of my own work and that I have only used sources or materials listed and specified in the dissertation.

München, den 11.November.2022   Unterschrift

Munich, 11 November 2022   Signature

Curriculum Vitae

Christina Tauber

Assistenzärztin der LMU Frauenklinik
christina.tauber@med.uni-muenchen.de
+4915774360417
* 21.02.1995

Schulische Ausbildung

2005-2012	Gymnasium Waldkraiburg Abiturnote 1.2

Studium

WS12/13 - SS14	**Vorklinik Humanmedizin** Ludwigs-Maximilians-Universität München (LMU) 1. Teil der ärztlichen Prüfung 2.0
WS14/15 – SS20	**Klinik Humanmedizin** Technische Universität München (TUM) 2. Teil der ärztlichen Prüfung 2.0 (86%) 3. Teil der ärztlichen Prüfung 1.0 Gesamtnote 1.66

Facharztausbildung

Seit Nov 2021	**Assistenzärztin** Klinik und Poliklinik für Frauenheilkunde und Geburtshilfe, LMU Klinikum München, Ludwigs-Maximilians-Universität München (LMU) Prof. Dr. Sven Mahner

Stipendien

Seit Okt 2016	Promotionsstipendium Translationale Medizin – TUM Graduate School gefördert durch Else-Kröner-Fresenius Stiftung
Seit April 2017	Max-Weber-Stiftung - Elite Netzwerk Bayern Mentor: Prof. Dr. Henningsen

Wissenschaftliches Arbeiten

Seit Okt 2016	**Experimentelle Doktorarbeit** "Microtubuli-associated protein tau as risk factor for idiopathic Parkinson syndrome" Translationale Medizin – TUM Graduate School Prof. Dr. Günter Höglinger Deutsches Neurodegeneratives Zentrum, München
Juni 2017	Tierversuchskurs in Theorie und Praxis (EU-Kategorie B, FELASA B)

Famulatur

Feb 2015	Gefäßchirurgie Universitätsklinikum Hamburg-Eppendorf
März 2015	Chirurgische Notaufnahme Klinikum Mühldorf am Inn
Aug 2016	Onkologie

Kaiser Franz-Josef-Spital, Wien

Feb 2018   Transplantationschirurgie
                  Universitätsklinikum Großhadern, LMU München

---

Praktisches Jahr

Mai – Juni 2019   Nephrologie & Allgemeinmedizin
                    Norwich & Norfolk University Hospital Norwich, England
                    Leitung: Dr. Karim

Juli – Aug 2019   Kardiologie
                    Deutsches Herzzentrum, TU München
                    Präsentation einer Publikation im Rahmen des Journal Clubs
                    Leitung Chest Pain Unit: Prof. Dr. Cassese

Sept – Dez 2019   Gynäkologie und Geburtshilfe
                    Klinikum rechts der Isar, TU München
                    Leitung: Prof. Dr. Kiechle

Jan – April 2020   Kinderchirurgie
                    Kantonspital Luzern
                    Leitung: Prof. Dr. Szavay

Erste Arbeitserfahrungen

2015 – 2017   Chirurgische Assistenz in Orthopädie & Unfallchirurgie
                    Barmherzige Brüder München
                    Leitung: Prof. Dr. Plötz

2017 - 2019   Chirurgische Assistenz in Plastischer Chirurgie
                    Villa Bella, München
                    Leitung: Dr. Meyer

2017-2018   Studienassistenz in klinischer Studie
                    Koordination von Studientagen, Erhebung von Mini-Mental-Status-Test
                    CAPIAS – Carotid Plaque Imaging in Acute Stroke
                    Neuro-Kopf-Zentrum, Neurologie, TU München
                    Leitung: Dr. Sepp, Prof. Dr. Wunderlich

Okt 2020 – Mai 2021 Unterstützung als Ärztin COVID-19-Pandemie
                     Gesundheitsamt München Land
                     Leitung: Dr. Schmitt

Nov 2020 – Nov 2021 Weiterbildungsassistentin in Allgemeinmedizin
                     Hausarztpraxis Dr. Tauber, Waldkraiburg
                     Leitung: Dr. Tauber

Wahlfach, Summer & Winter School

Wahlfächer   - Nephrologie
                    - International Case Discussion Rounds
                    - Genomische Medizin

Summer Schools
Juli 2017   The ageing brain
                    Universität Groningen, Niederlande

August 2018   International Case Discussion

TU München in Kooperation mit Weill Cornell Medical College
& Washington Universtiy School of Medicine

Aug 2019	Global Entrepreneurship Tongji Universität, China
Winter School Feb 2019	Global Health Center for Global Health, TU München

Soziales Engagement

Jan 2015-2016	Ehrenamtliche Workshops in Schulen Aufklärung gegen Tabak e.V. der LMU München
Nov 2016 – 2017	Ehrenamtliche Nachhilfe für Flüchtlinge in medizinischer Ausbildung In Via München e.V.
Mai 2017 - 2019	Head of Marketing Deutschland und Tanzania bei "Waterfilter" Verbesserung der lokalen Trinkwasserversorgung durch Wasserfilter in Kigoma, Tanzania durch Etablierung eines sozialen Businesskonzepts Enactus München e.V.

Interessen

Sprachen	C1 Englisch, B1 Spanisch, A2 Französisch, A1 Italienisch, A2 Dänisch
Freizeit	Universitätssegelverein Starnberg, Tennis, Cello

München, den 11.November.2022

References

1.   Tauber, C.V., et al., *Different MAPT haplotyes influence expression of total MAPT in postmortem human brain.* Acta neuropathologica communications, 2022. **Submitted publication, Review pending**.

2.   Rizek, P., N. Kumar, and M.S. Jog, *An update on the diagnosis and treatment of Parkinson disease.* Cmaj, 2016. **188**(16): p. 1157-1165.

3.   von Campenhausen, S., et al., *Prevalence and incidence of Parkinson's disease in Europe.* Eur Neuropsychopharmacol, 2005. **15**(4): p. 473-90.

4.   *Global, regional, and national burden of Parkinson's disease, 1990-2016: a systematic analysis for the Global Burden of Disease Study 2016.* Lancet Neurol, 2018. **17**(11): p. 939-953.

5.   Houlden, H. and A.B. Singleton, *The genetics and neuropathology of Parkinson's disease.* Acta Neuropathol, 2012. **124**(3): p. 325-38.

6.   Deng, H., P. Wang, and J. Jankovic, *The genetics of Parkinson disease.* Ageing Res Rev, 2018. **42**: p. 72-85.

7.   Neurologie, D.G.f.r., *DGN S3-Leitlinie Idiopathisches Parkinson-Syndrom.* Leitlinien für Diagnostik und Therapie in der Neurologie, 2016. **Extrapyramidale Störungen**.

8.   Deuschl, G., W. Oertl, and H. Reichmann, *Idiopathisches Parkinson-Syndrom.* Deutsche Gesellschaft fuer Neurologie, 2016. **Leitlinien für Diagnostik und Therapie in der Neurologie**.

9.   Sontheimer, H., *Chapter 5 - Parkinson Disease*, in *Diseases of the Nervous System*, H. Sontheimer, Editor. 2015, Academic Press: San Diego. p. 133-164.

10.   Lian, T.-H., et al., *Tremor-Dominant in Parkinson Disease: The Relevance to Iron Metabolism and Inflammation.* Frontiers in Neuroscience, 2019. **13**(255).

11.   Bonnet, A.M., et al., *Nonmotor Symptoms in Parkinson’s Disease in 2012: Relevant Clinical Aspects.* Parkinson’s Disease, 2012. **2012**: p. 15.

12.   Sveinbjornsdottir, S., *The clinical symptoms of Parkinson's disease.* J Neurochem, 2016. **139 Suppl 1**: p. 318-324.

13.   Hely, M.A., et al., *The Sydney multicenter study of Parkinson's disease: the inevitability of dementia at 20 years.* Mov Disord, 2008. **23**(6): p. 837-44.

14.   Stallworth, M. and R. King, *CHAPTER 50 - Parkinson's Disease*, in *Primary Care Geriatrics (Fifth Edition)*, R.J. Ham, et al., Editors. 2007, Mosby: Philadelphia. p. 591-600.

15.   Ishihara, L.S., et al., *Estimated life expectancy of Parkinson's patients compared with the UK population.* J Neurol Neurosurg Psychiatry, 2007. **78**(12): p. 1304-9.

16.   Delenclos, M., et al., *Biomarkers in Parkinson's disease: Advances and strategies.* Parkinsonism Relat Disord, 2016. **22 Suppl 1**: p. S106-10.

17.   He, R., et al., *Recent Advances in Biomarkers for Parkinson's Disease.* Front Aging Neurosci, 2018. **10**: p. 305.

18.   Wang, X., et al., *Detection of alpha-synuclein oligomers in red blood cells as a potential biomarker of Parkinson's disease.* Neurosci Lett, 2015. **599**: p. 115-9.

19.   Wang, Y., et al., *Phosphorylated alpha-synuclein in Parkinson's disease.* Sci Transl Med, 2012. **4**(121): p. 121ra20.

20.   Emamzadeh, F.N. and A. Surguchov, *Parkinson's Disease: Biomarkers, Treatment, and Risk Factors.* Front Neurosci, 2018. **12**: p. 612.

21.   Jellinger, K.A., et al., *Accuracy of clinical diagnosis of Parkinson disease: A systematic review and meta-analysis.* Neurology, 2016. **87**(2): p. 237-238.

22. Braak, H., et al., *Stages in the development of Parkinson's disease-related pathology.* Cell Tissue Res, 2004. **318**(1): p. 121-34.

23. Wakabayashi, K., et al., *The Lewy body in Parkinson's disease and related neurodegenerative disorders.* Mol Neurobiol, 2013. **47**(2): p. 495-508.

24. Shahmoradian, S.H., et al., *Lewy pathology in Parkinson's disease consists of crowded organelles and lipid membranes.* Nat Neurosci, 2019. **22**(7): p. 1099-1109.

25. Braak, H., et al., *Staging of brain pathology related to sporadic Parkinson's disease.* Neurobiol Aging, 2003. **24**(2): p. 197-211.

26. Del Tredici, K. and H. Braak, *Spinal cord lesions in sporadic Parkinson's disease.* Acta Neuropathol, 2012. **124**(5): p. 643-64.

27. Gelpi, E., et al., *Multiple organ involvement by alpha-synuclein pathology in Lewy body disorders.* Mov Disord, 2014. **29**(8): p. 1010-8.

28. Braak, H., et al., *Staging of Alzheimer disease-associated neurofibrillary pathology using paraffin sections and immunocytochemistry.* Acta Neuropathol, 2006. **112**(4): p. 389-404.

29. Fenyi, A., et al., *Detection of alpha-synuclein aggregates in gastrointestinal biopsies by protein misfolding cyclic amplification.* Neurobiol Dis, 2019. **129**: p. 38-43.

30. Klingelhoefer, L. and H. Reichmann, *Pathogenesis of Parkinson disease--the gut-brain axis and environmental factors.* Nat Rev Neurol, 2015. **11**(11): p. 625-36.

31. Lebouvier, T., et al., *The second brain and Parkinson's disease.* Eur J Neurosci, 2009. **30**(5): p. 735-41.

32. McCann, H., et al., *α-Synucleinopathy phenotypes.* Parkinsonism Relat Disord, 2014. **20 Suppl 1**: p. S62-7.

33. Burré, J., M. Sharma, and T.C. Südhof, *Cell Biology and Pathophysiology of α-Synuclein.* Cold Spring Harb Perspect Med, 2018. **8**(3).

34. Breydo, L., J.W. Wu, and V.N. Uversky, *Alpha-synuclein misfolding and Parkinson's disease.* Biochim Biophys Acta, 2012. **1822**(2): p. 261-85.

35. Del Tredici, K. and H. Braak, *Review: Sporadic Parkinson's disease: development and distribution of alpha-synuclein pathology.* Neuropathol Appl Neurobiol, 2016. **42**(1): p. 33-50.

36. Lashuel, H.A., et al., *The many faces of α-synuclein: from structure and toxicity to therapeutic target.* Nat Rev Neurosci, 2013. **14**(1): p. 38-48.

37. Toulorge, D., A.H. Schapira, and R. Hajj, *Molecular changes in the postmortem parkinsonian brain.* J Neurochem, 2016. **139 Suppl 1**: p. 27-58.

38. Schulz-Schaeffer, W.J., *Is Cell Death Primary or Secondary in the Pathophysiology of Idiopathic Parkinson's Disease?* Biomolecules, 2015. **5**(3): p. 1467-79.

39. Milber, J.M., et al., *Lewy pathology is not the first sign of degeneration in vulnerable neurons in Parkinson disease.* Neurology, 2012. **79**(24): p. 2307-14.

40. Jankovic, J., *Progression of Parkinson disease: are we making progress in charting the course?* Arch Neurol, 2005. **62**(3): p. 351-2.

41. Obeso, J.A., et al., *The basal ganglia in Parkinson's disease: current concepts and unexplained observations.* Ann Neurol, 2008. **64 Suppl 2**: p. S30-46.

42. Chaudhuri, K.R. and P. Odin, *The challenge of non-motor symptoms in Parkinson's disease.* Prog Brain Res, 2010. **184**: p. 325-41.

43. Braak, H., et al., *Pathology associated with sporadic Parkinson's disease--where does it end?* J Neural Transm Suppl, 2006(70): p. 89-97.

44. Connolly, B.S. and A.E. Lang, *Pharmacological treatment of Parkinson disease: a review.* Jama, 2014. **311**(16): p. 1670-83.

45.   Groiss, S.J., et al., *Deep brain stimulation in Parkinson's disease.* Ther Adv Neurol Disord, 2009. **2**(6): p. 20-8.

46.   Accolla, E.A. and C. Pollo, *Mood Effects After Deep Brain Stimulation for Parkinson's Disease: An Update.* Front Neurol, 2019. **10**: p. 617.

47.   Kalinderi, K., S. Bostantjopoulou, and L. Fidani, *The genetic background of Parkinson's disease: current progress and future prospects.* Acta Neurol Scand, 2016. **134**(5): p. 314-326.

48.   Kenborg, L., et al., *Lifestyle, Family History, and Risk of Idiopathic Parkinson Disease: A Large Danish Case-Control Study.* American Journal of Epidemiology, 2015. **181**(10): p. 808-816.

49.   Wirdefeldt, K., et al., *Heritability of Parkinson disease in Swedish twins: a longitudinal study.* Neurobiol Aging, 2011. **32**(10): p. 1923.e1-8.

50.   Rietdijk, C.D., et al., *Exploring Braak's Hypothesis of Parkinson's Disease.* Front Neurol, 2017. **8**: p. 37.

51.   Derkinderen, P., K.M. Shannon, and P. Brundin, *Gut feelings about smoking and coffee in Parkinson's disease.* Mov Disord, 2014. **29**(8): p. 976-9.

52.   *Single Nucleotide Polymorphism.* Nature Education 2014. **Scitable**

53.   Edwards, T.L., et al., *Genome-wide association study confirms SNPs in SNCA and the MAPT region as common risk factors for Parkinson disease.* Ann Hum Genet, 2010. **74**(2): p. 97-109.

54.   Simon-Sanchez, J., et al., *Genome-wide association study reveals genetic risk underlying Parkinson's disease.* Nat Genet, 2009. **41**(12): p. 1308-12.

55.   Nalls, M.A., et al., *Large-scale meta-analysis of genome-wide association data identifies six new risk loci for Parkinson's disease.* Nat Genet, 2014. **46**(9): p. 989-93.

56.   Lill, C.M., *Genetics of Parkinson's disease.* Mol Cell Probes, 2016. **30**(6): p. 386-396.

57.   Chang, D., et al., *A meta-analysis of genome-wide association studies identifies 17 new Parkinson's disease risk loci.* Nat Genet, 2017. **49**(10): p. 1511-1516.

58.   Grenn, F.P., et al., *The Parkinson's Disease GWAS Locus Browser.* bioRxiv, 2020: p. 2020.04.01.020404.

59.   Pascale, E., et al., *Genetic Architecture of MAPT Gene Region in Parkinson Disease Subtypes.* Front Cell Neurosci, 2016. **10**: p. 96.

60.   Lee, V.M., M. Goedert, and J.Q. Trojanowski, *Neurodegenerative tauopathies.* Annu Rev Neurosci, 2001. **24**: p. 1121-59.

61.   Guo, T., W. Noble, and D.P. Hanger, *Roles of tau protein in health and disease.* Acta neuropathologica, 2017. **133**(5): p. 665-704.

62.   Barbier, P., et al., *Role of Tau as a Microtubule-Associated Protein: Structural and Functional Aspects.* Frontiers in Aging Neuroscience, 2019. **11**(204).

63.   Tobin, J.E., et al., *Haplotypes and gene expression implicate the MAPT region for Parkinson disease: the GenePD Study.* Neurology, 2008. **71**(1): p. 28-34.

64.   Jadhav, S., et al., *A walk through tau therapeutic strategies.* Acta Neuropathol Commun, 2019. **7**(1): p. 22.

65.   Vasili, E., A. Dominguez-Meijide, and T.F. Outeiro, *Spreading of alpha-Synuclein and Tau: A Systematic Comparison of the Mechanisms Involved.* Front Mol Neurosci, 2019. **12**: p. 107.

66.   Goedert, M., et al., *Multiple isoforms of human microtubule-associated protein tau: sequences and localization in neurofibrillary tangles of Alzheimer's disease.* Neuron, 1989. **3**(4): p. 519-26.

67.   Höglinger, G.U., et al., *Differentiation of atypical Parkinson syndromes.* J Neural Transm (Vienna), 2017. **124**(8): p. 997-1004.

68.   Zhang, X., et al., *Tau Pathology in Parkinson's Disease.* Front Neurol, 2018. **9**: p. 809.

69.   Park, S.A., S.I. Ahn, and J.M. Gallo, *Tau mis-splicing in the pathogenesis of neurodegenerative disorders.* BMB Rep, 2016. **49**(8): p. 405-13.

70.   Silva, M.C. and S.J. Haggarty, *Tauopathies: Deciphering Disease Mechanisms to Develop Effective Therapies.* Int J Mol Sci, 2020. **21**(23).

71.   Horowitz, P.M., et al., *N-Terminal Fragments of Tau Inhibit Full-Length Tau Polymerization in Vitro.* Biochemistry, 2006. **45**(42): p. 12859-12866.

72.   Jeganathan, S., et al., *Global hairpin folding of tau in solution.* Biochemistry, 2006. **45**(7): p. 2283-93.

73.   Rosenberg, K.J., et al., *Complementary dimerization of microtubule-associated tau protein: Implications for microtubule bundling and tau-mediated pathogenesis.* Proceedings of the National Academy of Sciences of the United States of America, 2008. **105**(21): p. 7445-7450.

74.   Andreadis, A., *Tau splicing and the intricacies of dementia.* Journal of cellular physiology, 2012. **227**(3): p. 1220-1225.

75.   Baker, M., et al., *Association of an extended haplotype in the tau gene with progressive supranuclear palsy.* Hum Mol Genet, 1999. **8**(4): p. 711-5.

76.   Stefansson, H., et al., *A common inversion under selection in Europeans.* Nat Genet, 2005. **37**(2): p. 129-37.

77.   Zabetian, C.P., et al., *Association analysis of MAPT H1 haplotype and subhaplotypes in Parkinson's disease.* Ann Neurol, 2007. **62**(2): p. 137-44.

78.   Myers, A.J., et al., *The MAPT H1c risk haplotype is associated with increased expression of tau and especially of 4 repeat containing transcripts.* Neurobiol Dis, 2007. **25**(3): p. 561-70.

79.   Zhang, C.C., et al., *Meta-analysis of the association between variants in MAPT and neurodegenerative diseases.* Oncotarget, 2017. **8**(27): p. 44994-45007.

80.   Pennisi, E., *Genetics. 17q21.31: not your average genomic address.* Science, 2008. **322**(5903): p. 842-5.

81.   Hoglinger, G.U., et al., *Identification of common variants influencing risk of the tauopathy progressive supranuclear palsy.* Nat Genet, 2011. **43**(7): p. 699-705.

82.   Pastor, P., et al., *Further extension of the H1 haplotype associated with progressive supranuclear palsy.* Mov Disord, 2002. **17**(3): p. 550-6.

83.   Houlden, H., et al., *Corticobasal degeneration and progressive supranuclear palsy share a common tau haplotype.* Neurology, 2001. **56**(12): p. 1702-6.

84.   Kouri, N., et al., *Genome-wide association study of corticobasal degeneration identifies risk variants shared with progressive supranuclear palsy.* Nat Commun, 2015. **6**: p. 7247.

85.   Myers, A.J., et al., *The H1c haplotype at the MAPT locus is associated with Alzheimer's disease.* Hum Mol Genet, 2005. **14**(16): p. 2399-404.

86.   Wider, C., et al., *Association of the MAPT locus with Parkinson's disease.* Eur J Neurol, 2010. **17**(3): p. 483-6.

87.   Vandrovcova, J., et al., *Association of MAPT haplotype-tagging SNPs with sporadic Parkinson's disease.* Neurobiol Aging, 2009. **30**(9): p. 1477-82.

88.   Nalls, M.A., et al., *Identification of novel risk loci, causal insights, and heritable risk for Parkinson's disease: a meta-analysis of genome-wide association studies.* Lancet Neurol, 2019. **18**(12): p. 1091-1102.

89. Donnelly, M.P., et al., *The distribution and most recent common ancestor of the 17q21 inversion in humans.* Am J Hum Genet, 2010. **86**(2): p. 161-71.

90. Koolen, D.A., et al., *The Koolen-de Vries syndrome: a phenotypic comparison of patients with a 17q21.31 microdeletion versus a KANSL1 sequence variant.* Eur J Hum Genet, 2016. **24**(5): p. 652-9.

91. Simon-Sanchez, J., et al., *Genome-wide association study confirms extant PD risk loci among the Dutch.* Eur J Hum Genet, 2011. **19**(6): p. 655-61.

92. Caillet-Boudin, M.L., et al., *Regulation of human MAPT gene expression.* Mol Neurodegener, 2015. **10**: p. 28.

93. de Jong, S., et al., *Common inversion polymorphism at 17q21.31 affects expression of multiple genes in tissue-specific manner.* BMC Genomics, 2012. **13**: p. 458.

94. Caffrey, T.M., et al., *Haplotype-specific expression of exon 10 at the human MAPT locus.* Human Molecular Genetics, 2006. **15**(24): p. 3529-3537.

95. Caffrey, T.M., C. Joachim, and R. Wade-Martins, *Haplotype-specific expression of the N-terminal exons 2 and 3 at the human MAPT locus.* Neurobiol Aging, 2008. **29**(12): p. 1923-9.

96. Trabzuni, D., et al., *MAPT expression and splicing is differentially regulated by brain region: relation to genotype and implication for tauopathies.* Hum Mol Genet, 2012. **21**(18): p. 4094-103.

97. Lei, P., et al., *Tau deficiency induces parkinsonism with dementia by impairing APP-mediated iron export.* Nat Med, 2012. **18**(2): p. 291-5.

98. Colom-Cadena, M., et al., *Confluence of alpha-synuclein, tau, and beta-amyloid pathologies in dementia with Lewy bodies.* J Neuropathol Exp Neurol, 2013. **72**(12): p. 1203-12.

99. Ishizawa, T., et al., *Colocalization of tau and alpha-synuclein epitopes in Lewy bodies.* J Neuropathol Exp Neurol, 2003. **62**(4): p. 389-97.

100. Wills, J., et al., *Elevated tauopathy and alpha-synuclein pathology in postmortem Parkinson's disease brains with and without dementia.* Exp Neurol, 2010. **225**(1): p. 210-8.

101. Giasson, B.I., et al., *Initiation and synergistic fibrillization of tau and alpha-synuclein.* Science, 2003. **300**(5619): p. 636-40.

102. Kotzbauer, P.T., et al., *Fibrillization of alpha-synuclein and tau in familial Parkinson's disease caused by the A53T alpha-synuclein mutation.* Exp Neurol, 2004. **187**(2): p. 279-88.

103. Duka, V., et al., *Identification of the sites of tau hyperphosphorylation and activation of tau kinases in synucleinopathies and Alzheimer's diseases.* PLoS One, 2013. **8**(9): p. e75025.

104. Simone, R., *Antisense Long Non Coding RNA represses MAPT translation through an embedded MIR repeat* Alzheimer's & Dementia: The Journal of the Alzheimer's Association, 2017. **13**(7): p. P918.

105. Carrieri, C., et al., *Long non-coding antisense RNA controls Uchl1 translation through an embedded SINEB2 repeat.* Nature, 2012. **491**(7424): p. 454-7.

106. Coupland, K.G., et al., *Role of the Long Non-Coding RNA MAPT-AS1 in Regulation of Microtubule Associated Protein Tau (MAPT) Expression in Parkinson's Disease.* PLoS One, 2016. **11**(6): p. e0157924.

107. Koolen, D.A., et al., *Mutations in the chromatin modifier gene KANSL1 cause the 17q21.31 microdeletion syndrome.* Nat Genet, 2012. **44**(6): p. 639-41.

108. Jun, G., et al., *A novel Alzheimer disease locus located near the gene encoding tau protein.* Mol Psychiatry, 2016. **21**(1): p. 108-17.

109. Lin, M.K. and M.J. Farrer, *Genetics and genomics of Parkinson's disease.* Genome Medicine, 2014. **6**(6): p. 48.

110. Saeed, M., *Genomic convergence of locus-based GWAS meta-analysis identifies AXIN1 as a novel Parkinson's gene.* Immunogenetics, 2018. **70**(9): p. 563-570.

111. Ferrari, R., et al., *Genetic architecture of sporadic frontotemporal dementia and overlap with Alzheimer's and Parkinson's diseases.* J Neurol Neurosurg Psychiatry, 2017. **88**(2): p. 152-164.

112. O'Brien, H.E., et al., *Expression quantitative trait loci in the developing human brain and their enrichment in neuropsychiatric disorders.* Genome Biol, 2018. **19**(1): p. 194.

113. Elkouris, M., et al., *Long Non-coding RNAs Associated With Neurodegeneration-Linked Genes Are Reduced in Parkinson's Disease Patients.* Frontiers in Cellular Neuroscience, 2019. **13**(58).

114. Sündermann, F., M.-P. Fernandez, and R.O. Morgan, *An evolutionary roadmap to the microtubule-associated protein MAP Tau.* BMC Genomics, 2016. **17**(1): p. 264.

115. Del Fattore, A., et al., *A new heterozygous mutation (R714C) of the osteopetrosis gene, pleckstrin homolog domain containing family M (with run domain) member 1 (PLEKHM1), impairs vesicular acidification and increases TRACP secretion in osteoclasts.* J Bone Miner Res, 2008. **23**(3): p. 380-91.

116. Davis, A.A., et al., *Variants in GBA, SNCA, and MAPT influence Parkinson disease risk, age at onset, and progression.* Neurobiol Aging, 2016. **37**: p. 209.e1-209.e7.

117. Karic, A., et al., *Identifying candidate genes for Parkinson's disease by integrative genomics method.* Biochem Med (Zagreb), 2011. **21**(2): p. 174-81.

118. Liu, X., et al., *Genome-wide association study identifies candidate genes for Parkinson's disease in an Ashkenazi Jewish population.* BMC Med Genet, 2011. **12**: p. 104.

119. Mesika, R. and D. Reichmann, *When safeguarding goes wrong: Impact of oxidative stress on protein homeostasis in health and neurodegenerative disorders.* Adv Protein Chem Struct Biol, 2019. **114**: p. 221-264.

120. Robledinos-Ant, et al., *Activators and Inhibitors of NRF2: A Review of Their Potential for Clinical Development.* Oxidative Medicine and Cellular Longevity, 2019. **2019**: p. 20.

121. Brighina, L., et al., *Alpha-synuclein, pesticides, and Parkinson disease: a case-control study.* Neurology, 2008. **70**(16 Pt 2): p. 1461-9.

122. Gámez-Valero, A. and K. Beyer, *Alternative Splicing of Alpha- and Beta-Synuclein Genes Plays Differential Roles in Synucleinopathies.* Genes (Basel), 2018. **9**(2).

123. Landau, M., *Getting in charge of beta-synuclein fibrillation.* J Biol Chem, 2017. **292**(39): p. 16380-16381.

124. Beyer, K., et al., *The decrease of β-synuclein in cortical brain areas defines a molecular subgroup of dementia with Lewy bodies.* Brain, 2010. **133**(Pt 12): p. 3724-33.

125. Vargas, K.J. and S.S. Chandra, *Synucleins ☆,* in *Reference Module in Biomedical Sciences.* 2014, Elsevier.

126. Quinn, J.G., et al., *α-Synuclein mRNA and soluble α-synuclein protein levels in post-mortem brain from patients with Parkinson's disease, dementia with Lewy bodies, and Alzheimer's disease.* Brain Res, 2012. **1459**: p. 71-80.

127. Yamasaki, T.R., et al., *Parkinson's disease and multiple system atrophy have distinct α-synuclein seed characteristics.* J Biol Chem, 2019. **294**(3): p. 1045-1058.
128. Zhou, J., et al., *Changes in the solubility and phosphorylation of α-synuclein over the course of Parkinson's disease.* Acta Neuropathol, 2011. **121**(6): p. 695-704.
129. Westerlund, M., et al., *Cerebellar alpha-synuclein levels are decreased in Parkinson's disease and do not correlate with SNCA polymorphisms associated with disease in a Swedish material.* Faseb j, 2008. **22**(10): p. 3509-14.
130. Braak, H. and E. Braak, *Neuropathological stageing of Alzheimer-related changes.* Acta Neuropathol, 1991. **82**(4): p. 239-59.
131. Mirra, S.S., et al., *The Consortium to Establish a Registry for Alzheimer's Disease (CERAD). Part II. Standardization of the neuropathologic assessment of Alzheimer's disease.* Neurology, 1991. **41**(4): p. 479-86.
132. McKeith, I.G., et al., *Diagnosis and management of dementia with Lewy bodies: Fourth consensus report of the DLB Consortium.* Neurology, 2017. **89**(1): p. 88-100.
133. Greene, J.G., *Current status and future directions of gene expression profiling in Parkinson's disease.* Neurobiol Dis, 2012. **45**(1): p. 76-82.
134. Simunovic, F., et al., *Evidence for gender-specific transcriptional profiles of nigral dopamine neurons in Parkinson disease.* PLoS One, 2010. **5**(1): p. e8856.
135. Birbaumer, N., Schmidt R. , *Biologische Psychologie.* Springer-Lehrbuch, 2007. **7**: p. 89-91, 397, 408-410.
136. Braak, H. and K. Del Tredici, *Neuroanatomy and pathology of sporadic Parkinson's disease.* Adv Anat Embryol Cell Biol, 2009. **201**: p. 1-119.
137. Qiagen, *DNeasy Blood & Tissue Kit Handbook.* 2006. **07**(1037951).
138. Skipper, L., et al., *Linkage disequilibrium and association of MAPT H1 in Parkinson disease.* Am J Hum Genet, 2004. **75**(4): p. 669-77.
139. Rogers A., W.S., *Epidemiologic and population genetic studies.* Clinical and Translational Science, 2009. **Principles of Human Research**(Academic Press): p. 289-299.
140. Chomczynski, P. and K. Mackey, *Short technical reports. Modification of the TRI reagent procedure for isolation of RNA from polysaccharide- and proteoglycan-rich sources.* Biotechniques, 1995. **19**(6): p. 942-5.
141. Rodriguez-Lanetty, M., *Trizol/RNeasy Hybrid RNA extraction protocol.*
142. Bustin, S.A., et al., *The MIQE guidelines: minimum information for publication of quantitative real-time PCR experiments.* Clin Chem, 2009. **55**(4): p. 611-22.
143. Scientific, T., *T042-Technical Bulletin NanoDrop Spectrophotometers.* Technical Support, 2009. **Rev 3/09**.
144. Becker, C., et al., *mRNA and microRNA quality control for RT-qPCR analysis.* Methods, 2010. **50**(4): p. 237-43.
145. Schroeder, A., et al., *The RIN: an RNA integrity number for assigning integrity values to RNA measurements.* BMC Mol Biol, 2006. **7**: p. 3.
146. Sonntag, K.C., et al., *Limited predictability of postmortem human brain tissue quality by RNA integrity numbers.* J Neurochem, 2016. **138**(1): p. 53-9.
147. Weis, S., et al., *Quality control for microarray analysis of human brain samples: The impact of postmortem factors, RNA characteristics, and histopathology.* J Neurosci Methods, 2007. **165**(2): p. 198-209.
148. Spicakova, T., et al., *Expression and silencing of the microtubule-associated protein Tau in breast cancer cells.* Mol Cancer Ther, 2010. **9**(11): p. 2970-81.

149.   Strauß, T., et al., *iPS Cell-Based Model for MAPT Haplotype as a Risk Factor for Human Tauopathies Identifies No Major Differences in TAU Expression.* Front Cell Dev Biol, 2021. **9**: p. 726866.

150.   Hummon, A.B., et al., *Isolation and solubilization of proteins after TRIzol extraction of RNA and DNA from patient material following prolonged storage.* Biotechniques, 2007. **42**(4): p. 467-70, 472.

151.   Sigma-Aldrich. *RIPA Technical bulletin*. [Technical Bulletin] 2019 03/2019 [cited 03/19-1; Available from: https://www.sigmaaldrich.com/content/dam/sigma-aldrich/docs/Sigma/Bulletin/r0278bul.pdf.

152.   Weber, K. and D.J. Kuter, *Reversible denaturation of enzymes by sodium dodecyl sulfate.* J Biol Chem, 1971. **246**(14): p. 4504-9.

153.   Browning, M. *1% SDS is the lysis buffer of choice for most western blots*. Western Blot Techniques [Webpage] 2012 [cited 2019 28.07.2019]; Available from: https://www.phosphosolutions.com/2353-2/.

154.   Iovino, M., et al., *Early maturation and distinct tau pathology in induced pluripotent stem cell-derived neurons from patients with MAPT mutations.* Brain, 2015. **138**(Pt 11): p. 3345-59.

155.   Smith, B.J., *SDS Polyacrylamide Gel Electrophoresis of Proteins.* Methods Mol Biol, 1984. **1**: p. 41-55.

156.   Smith, P.K., et al., *Measurement of protein using bicinchoninic acid.* Anal Biochem, 1985. **150**(1): p. 76-85.

157.   Vandesompele, J., et al., *Accurate normalization of real-time quantitative RT-PCR data by geometric averaging of multiple internal control genes.* Genome Biol, 2002. **3**(7): p. Research0034.

158.   Hellemans, J., et al., *qBase relative quantification framework and software for management and automated analysis of real-time quantitative PCR data.* Genome Biol, 2007. **8**(2): p. R19.

159.   Imbeaud, S., et al., *Towards standardization of RNA quality assessment using user-independent classifiers of microcapillary electrophoresis traces.* Nucleic Acids Res, 2005. **33**(6): p. e56.

160.   Heinrich, M., et al., *Successful RNA extraction from various human postmortem tissues.* Int J Legal Med, 2007. **121**(2): p. 136-42.

161.   Sellin Jeffries, M.K., et al., *A comparison of commercially-available automated and manual extraction kits for the isolation of total RNA from small tissue samples.* BMC Biotechnology, 2014. **14**(1): p. 94.

162.   Jensen, P.S.H., et al., *Yield and Integrity of RNA from Brain Samples are Largely Unaffected by Pre-analytical Procedures.* Neurochem Res, 2021. **46**(3): p. 447-454.

163.   Ahlfen, v., *Effects of low A260/A230 ratios in RNA preparations on downstream applications.* Qiagen Gene Expression Newsletter, 2010(15/10): p. 7, 8.

164.   Chomczynski, P., *A reagent for the single-step simultaneous isolation of RNA, DNA and proteins from cell and tissue samples.* Biotechniques, 1993. **15**(3): p. 532-4, 536-7.

165.   *Laboratory of Thomas Ried.* BioTechniques, 2007. **42**(4): p. 415.

166.   Likhite, N. and U.M. Warawdekar, *A unique method for isolation and solubilization of proteins after extraction of RNA from tumor tissue using trizol.* J Biomol Tech, 2011. **22**(1): p. 37-44.

167.   Simões, A.E., et al., *Efficient recovery of proteins from multiple source samples after TRIzol(®) or TRIzol(®)LS RNA extraction and long-term storage.* BMC Genomics, 2013. **14**: p. 181.

168.   Wen, Y., et al., *High-yield skeletal muscle protein recovery from TRIzol after RNA and DNA extraction.* Biotechniques, 2020. **69**(4): p. 264-269.

169.   Kopec, A.M., et al., *Optimized solubilization of TRIzol-precipitated protein permits Western blotting analysis to maximize data available from brain tissue.* J Neurosci Methods, 2017. **280**: p. 64-76.

170.   Lee, C.R., et al., *Phosphorylation-Dependent Mobility Shift of Proteins on SDS-PAGE is Due to Decreased Binding of SDS.* Bulletin of Korean Chemical Society, 2013. **34**(7): p. Pages 2063-2066.

171.   Goedert, M., et al., *Tau proteins of alzheimer paired helical filaments: Abnormal phosphorylation of all six brain isoforms.* Neuron, 1992. **8**(1): p. 159-168.

172.   Hanger, D.P., et al., *The complex relationship between soluble and insoluble tau in tauopathies revealed by efficient dephosphorylation and specific antibodies.* FEBS Letters, 2002. **531**(3): p. 538-542.

173.   PhosphoSolutions.com, *Protein Dephosphorylation Methods.* Protocols, 2022.

174.   BIO-RAD, *Gel electrophoresis.* 2022.

175.   Yamaguchi, H., K. Hasegawa, and M. Esumi, *Protein from the fraction remaining after RNA extraction is useful for proteomics but care must be exercised in its application.* Exp Mol Pathol, 2013. **95**(1): p. 46-50.

176.   Ferrer, I., et al., *Brain banks: benefits, limitations and cautions concerning the use of post-mortem brain tissue for molecular studies.* Cell Tissue Bank, 2008. **9**(3): p. 181-94.

177.   Koppelkamm, A., et al., *RNA integrity in post-mortem samples: influencing parameters and implications on RT-qPCR assays.* Int J Legal Med, 2011. **125**(4): p. 573-80.

178.   Flynn, R.A. and H.Y. Chang, *Long noncoding RNAs in cell-fate programming and reprogramming.* Cell Stem Cell, 2014. **14**(6): p. 752-61.

179.   Soto-Beasley, A.I., et al., *Screening non-MAPT genes of the Chr17q21 H1 haplotype in Parkinson's disease.* Parkinsonism Relat Disord, 2020. **78**: p. 138-144.

180.   Brandt, R., M. Hundelt, and N. Shahani, *Tau alteration and neuronal degeneration in tauopathies: mechanisms and models.* Biochim Biophys Acta, 2005. **1739**(2-3): p. 331-54.

181.   Quinn, J.G., et al., *alpha-Synuclein mRNA and soluble alpha-synuclein protein levels in post-mortem brain from patients with Parkinson's disease, dementia with Lewy bodies, and Alzheimer's disease.* Brain Res, 2012. **1459**: p. 71-80.

182.   McKibben, K. and E. Rhoades, *Regulation of tau's proline rich region by its N-terminal domain.* bioRxiv, 2019: p. 633420.

183.   Simunovic, F., et al., *Gene expression profiling of substantia nigra dopamine neurons: further insights into Parkinson's disease pathology.* Brain, 2009. **132**(7): p. 1795-1809.

184.   Gründemann, J., et al., *Elevated alpha-synuclein mRNA levels in individual UV-laser-microdissected dopaminergic substantia nigra neurons in idiopathic Parkinson's disease.* Nucleic Acids Res, 2008. **36**(7): p. e38.

185.   Masliah, E., et al., *beta-amyloid peptides enhance alpha-synuclein accumulation and neuronal deficits in a transgenic mouse model linking Alzheimer's disease and Parkinson's disease.* Proc Natl Acad Sci U S A, 2001. **98**(21): p. 12245-50.

186. Robinson, A.C., et al., *Extended post-mortem delay times should not be viewed as a deterrent to the scientific investigation of human brain tissue: a study from the Brains for Dementia Research Network Neuropathology Study Group, UK.* Acta Neuropathologica, 2016. **132**(5): p. 753-755.

187. Zhu, Y., et al., *Systematic analysis of gene expression patterns associated with postmortem interval in human tissues.* Sci Rep, 2017. **7**(1): p. 5435.

188. Blair, J.A., et al., *Individual Case Analysis of Postmortem Interval Time on Brain Tissue Preservation.* PLoS One, 2016. **11**(3): p. e0151615.

189. Fleige, S. and M.W. Pfaffl, *RNA integrity and the effect on the real-time qRT-PCR performance.* Mol Aspects Med, 2006. **27**(2-3): p. 126-39.

190. Trabzuni, D., et al., *Quality control parameters on a large dataset of regionally dissected human control brains for whole genome expression studies.* J Neurochem, 2011. **119**(2): p. 275-82.

191. Fleige, S., et al., *Comparison of relative mRNA quantification models and the impact of RNA integrity in quantitative real-time RT-PCR.* Biotechnol Lett, 2006. **28**(19): p. 1601-13.

192. Durrenberger, P.F., et al., *Effects of antemortem and postmortem variables on human brain mRNA quality: a BrainNet Europe study.* J Neuropathol Exp Neurol, 2010. **69**(1): p. 70-81.

193. Tomita, H., et al., *Effect of agonal and postmortem factors on gene expression profile: quality control in microarray analyses of postmortem human brain.* Biological psychiatry, 2004. **55**(4): p. 346-352.

194. Rydbirk, R., et al., *Assessment of brain reference genes for RT-qPCR studies in neurodegenerative diseases.* Sci Rep, 2016. **6**: p. 37116.

195. Penna, I., et al., *Selection of candidate housekeeping genes for normalization in human postmortem brain samples.* Int J Mol Sci, 2011. **12**(9): p. 5461-70.

196. Coulson, D.T., et al., *Identification of valid reference genes for the normalization of RT qPCR gene expression data in human brain tissue.* BMC Mol Biol, 2008. **9**: p. 46.

197. Grunblatt, E., et al., *Gene expression profiling of parkinsonian substantia nigra pars compacta; alterations in ubiquitin-proteasome, heat shock protein, iron and oxidative stress regulated proteins, cell adhesion/cellular matrix and vesicle trafficking genes.* J Neural Transm (Vienna), 2004. **111**(12): p. 1543-73.

198. Agarwal, D., et al., *A single-cell atlas of the human substantia nigra reveals cell-specific pathways associated with neurological disorders.* Nature Communications, 2020. **11**(1): p. 4183.

199. Halliday, G.M. and H. McCann, *The progression of pathology in Parkinson's disease.* Ann N Y Acad Sci, 2010. **1184**: p. 188-95.

200. Lewis, P.A. and M.R. Cookson, *Gene expression in the Parkinson's disease brain.* Brain Res Bull, 2012. **88**(4): p. 302-12.

201. Chappell, S., et al., *Observations of extensive gene expression differences in the cerebellum and potential relevance to Alzheimer's disease.* BMC Res Notes, 2018. **11**(1): p. 646.

202. Negi, S.K. and C. Guda, *Global gene expression profiling of healthy human brain and its application in studying neurological disorders.* Sci Rep, 2017. **7**(1): p. 897.

203. Wu, T. and M. Hallett, *The cerebellum in Parkinson's disease.* Brain, 2013. **136**(Pt 3): p. 696-709.

204. Booth, H.D.E., W.D. Hirst, and R. Wade-Martins, *The Role of Astrocyte Dysfunction in Parkinson's Disease Pathogenesis.* Trends Neurosci, 2017. **40**(6): p. 358-370.

205. McFarthing, K. and T. Simuni, *Clinical Trial Highlights: Targetting Alpha-Synuclein.* J Parkinsons Dis, 2019. **9**(1): p. 5-16.

206. Jankovic, J., *Immunologic treatment of Parkinson's disease.* Immunotherapy, 2018. **10**(2): p. 81-84.

207. Pagano, G., et al., *Trial of Prasinezumab in Early-Stage Parkinson's Disease.* N Engl J Med, 2022. **387**(5): p. 421-432.

208. VandeVrede, L., A.L. Boxer, and M. Polydoro, *Targeting tau: Clinical trials and novel therapeutic approaches.* Neuroscience Letters, 2020. **731**: p. 134919.

209. Congdon, E.E. and E.M. Sigurdsson, *Tau-targeting therapies for Alzheimer disease.* Nat Rev Neurol, 2018. **14**(7): p. 399-415.

210. Pluta, R. and M. Ułamek-Kozioł, *Tau Protein-Targeted Therapies in Alzheimer's Disease: Current State and Future Perspectives*, in *Alzheimer's Disease: Drug Discovery*, X. Huang, Editor. 2020, Exon Publications

Copyright: The Authors.: Brisbane (AU).

211. Teng, E., et al., *Safety and Efficacy of Semorinemab in Individuals With Prodromal to Mild Alzheimer Disease: A Randomized Clinical Trial.* JAMA Neurol, 2022. **79**(8): p. 758-767.

212. Panza, F. and M. Lozupone, *The challenges of anti-tau therapeutics in Alzheimer disease.* Nature Reviews Neurology, 2022. **18**(10): p. 577-578.

213. Gagliardi, M. and A.T. Ashizawa, *The Challenges and Strategies of Antisense Oligonucleotide Drug Delivery.* Biomedicines, 2021. **9**(4).

214. Cole, T.A., et al., *α-Synuclein antisense oligonucleotides as a disease-modifying therapy for Parkinson's disease.* JCI Insight, 2021. **6**(5).

215. DeVos, S.L., et al., *Tau reduction prevents neuronal loss and reverses pathological tau deposition and seeding in mice with tauopathy.* Sci Transl Med, 2017. **9**(374).